HUMAN iPSC-BASED MODELING OF LATE-ONSET DISEASE VIA PROGERIN-INDUCED AGING

by

Justine Dana Miller

A Dissertation

Presented to the Faculty of the Louis V. Gerstner, Jr.

Graduate School of Biomedical Sciences,

Memorial Sloan-Kettering Cancer Center

in Partial Fulfillment of the Requirements for the Degree of

Doctor of Philosophy

New York, NY

May, 2014

_____ _____

Lorenz Studer, MD Date

Dissertation Mentor

DEDICATION

To my parents, for always believing in me and supporting me.

To my grandfather, for the blueberry muffins.

And to Philip, for always finding a way to make me laugh at myself.

ABSTRACT

Induced pluripotent stem cells (iPSCs) represent a powerful technology for modeling human disease in vitro. Our lab has previously demonstrated the use of iPSC technology for modeling early-onset disorders such as familial dysautonomia and herpes simplex encephalitis. Those studies led to novel insights into disease mechanisms and enabled the first high throughput drug screen in an iPSC-based disease model. Despite those early successes, there is a fundamental question as to how well iPSC-based approaches can model late-onset disorders such as Parkinson's disease (PD), which normally take decades to develop. Indeed current efforts using models of genetic or sporadic forms of PD show mild phenotypes and have not yet recreated the severe degenerative pathology characteristic of the disease.

We sought to investigate whether age, the most significant risk factor in PD, is maintained during in vitro reprogramming of patient-specific fibroblasts, and during the subsequent re-differentiation of iPSCs into somatic cells, including midbrain dopamine (mDA) neurons. Previous studies have suggested that the reprogramming process may reset the molecular clock of the cell, making aged cells appear young. We first defined a set of molecular markers capable of stratifying healthy fibroblasts according to donor age. Those markers, related to age-dependent changes in nuclear morphology, chromatin state, DNA repair, and mitochondrial function, were fully reset after reprogramming to pluripotency,

independent of fibroblast donor age. In addition, re-differentiation into iPSC-derived fibroblasts did not re-establish those age-related markers, further suggesting that age was permanently erased during the reprogramming process.

In order to address this reset to a young/embryonic cell state, we explored the use of synthetic mRNA technology to rapidly induce in vitro aging via progerin overexpression. Progerin, a nuclear scaffolding protein involved in a premature aging disease, re-induced the age-related signature in iPSC-derived fibroblasts, independent of fibroblast donor age. We next assessed the impact of our accelerated in vitro aging technology on iPSC-derived midbrain dopamine (mDA) neurons, the cell type responsible for key clinical symptoms in PD. While multiple phenotypes observed in “aged” iPSC-fibroblasts could be induced in “aged” iPSC-mDA neurons, mDA neurons also exhibited unique phenotypes suggestive of neuronal-specific decline, including dendrite degeneration. Finally, we applied progerin-induced aging to mDA neurons derived from several PD iPSC lines to model the late-onset aspects of the disease. The “aged” mDA neurons from PD iPSCs displayed AKT dysregulation and accelerated degeneration indicative of frank disease, phenotypes which were not observed in control-treated cells. When these mDA neurons overexpressing progerin were transplanted in vivo, age-related neuromelanin accumulation as well as PD mutation-specific mitochondrial swelling or inclusion formation were observed. Our study presents a first attempt at controlling cellular age in vitro in combination with the modeling of genetic disease susceptibility.

TABLE OF CONTENTS

LIST OF TABLES

LIST OF FIGURES

LIST OF ABBREVIATIONS

6-OHDA: 6-hydroxydopamine

AD: Alzheimer's disease

ALS: amyotrophic lateral sclerosis

CNS: central nervous system

CRISPR: clustered, regularly interspaced, short palindromic repeat

EC: embryonal carcinoma

FACS: fluorescence-activated cell sorting

FD: familial dysautonomia

FTI: farnesyl transferase inhibitor

GABA: gamma-aminobutyric acid

H3K9me3: tri-methylated lysine 9 on histone 3

HP1γ: heterochromatin protein 1 gamma

HGPS: Hutchinson-Gilford progeria syndrome

HSE: herpes simplex encephalitis

hSyn: human synapsin promoter

ICM: inner cell mass

iPSC: induced pluripotent stem cell

iPSC-fibroblast: pluripotent stem cell-derived fibroblast

iPSC-mDA neuron: pluripotent stem cell-derived midbrain dopamine neuron

lamin A/C: lamin A, progerin, and lamin C

LAP2α: lamin A-associated protein alpha

LB: Lewy body

LRRK2: leucine-rich repeat kinase 2

mDA: midbrain dopamine

MPTP: 1-methyl-4-phenyl-1,2,5,6-tetrahydropyridine

modified-RNA: synthetic mRNA

mtROS: mitochondrial reactive oxygen species

NOD-SCID: nonobese diabetic/severe combined immunodeficiency

OSKM: OCT4, SOX2, KLF4, c-MYC

PD: Parkinson's disease

RT-PCR: reverse transcription polymerase chain reaction

SA-β-Gal: senescence-activated β-galactosidase

SCNT: somatic cell nuclear transfer

SeV: Sendai virus

SMA: spinal muscular atrophy

TALEN: transcription activator-like effector nuclease

TEM: transmission electron microscopy

TH: tyrosine hydroxylase

CHAPTER ONE

Introduction

Parkinson's Disease

Definition and Characteristics

Parkinson's disease (PD) is a degenerative disorder of the central nervous system. The disease, which was first described in 1817 by James Parkinson (Parkinson, 1817), is characterized by severe motor deficits that progressively worsen over time, including slowness of movements and reflexes, rigidity, and resting tremor (**Figure 1.1**). Other non-motor symptoms such as depression can also manifest as the disease advances, indicating that multiple regions of the brain are ultimately affected. PD primarily occurs in individuals over the age of 50 (defined as late-onset); however, certain forms have been found to affect younger individuals as well.

The motor symptoms that define PD are the result of the loss of pigmented midbrain dopamine (mDA) neurons (Hassler, 1938), which are located in a defined region of the brain known as the substantia nigra pars compacta (**Figure 1.2**). The pigment found in mDA neurons consists of neuromelanin granules that accumulate and give the substantia nigra (or "black substance") its characteristic dark color (Schrerer, 1939). While the function of neuromelanin remains unclear, it is a defining feature of mDA neurons that may play a role in the selective

Figure 1.1 Man with Parkinson's disease. Depiction of the side and front view of a man with PD. The classical features include the forward tilt of the trunk, reduced arm swinging, rigidity, trembling of head and extremities, and short, shuffling gait.

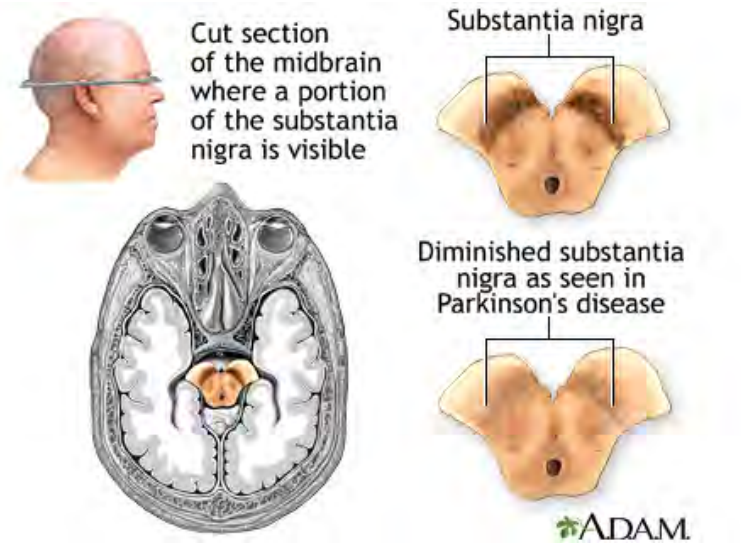

Figure 1.2 <u>The substanita nigra and Parkinson's disease.</u> PD involves the progressive loss of pigmented mDA neurons which are found in the substantia nigra region of the midbrain depicted here.

vulnerability of this specific population in PD (Hirsch et al., 1988). In addition, mDA neurons synthesize dopamine (Carlsson et al., 1957), which is a neurotransmitter that conducts signals to instruct movement via the basal ganglia motor circuit (**Figure 1.3**). The supply of dopamine to this circuit is continuously maintained by the spontaneous pacemaker activity of mDA neurons (Albin et al., 1989; Gonon and Bloch, 1998). The energy demand required to elicit this firing pattern may further contribute to the selective vulnerability of mDA neurons in PD as evidenced by the central role of mitochondrial dysfunction in both toxin-induced and genetic forms of the disease (discussed in the next section). When mDA neurons die in PD, reduced dopamine levels in the striatum shift the balance toward the indirect signaling pathway of the basal ganglia circuit, inhibiting stimulation of the motor cortex and reducing motor function (**Figure 1.3**). Of note, patients do not exhibit PD motor symptoms until 30-70% of their mDA neurons have been lost (Cheng et al., 2010), suggesting that a significant dopamine deficit is required to create the imbalance.

Pathological staging of PD described by Braak and colleagues (Braak et al., 2003) highlights another key hallmark of the disease: Lewy bodies (LBs). LBs are proteinaceous aggregates composed of an abnormal accumulation of ubiquitinated alpha-synuclein (Spillantini et al., 1997). LBs have a variety of morphological shapes, and the morphology appears to evolve over time (Shults, 2006). The classical LB morphology consists of granular material at the core surrounded by radiating fibrils or circular fibrillar material (Roy and Wolman,

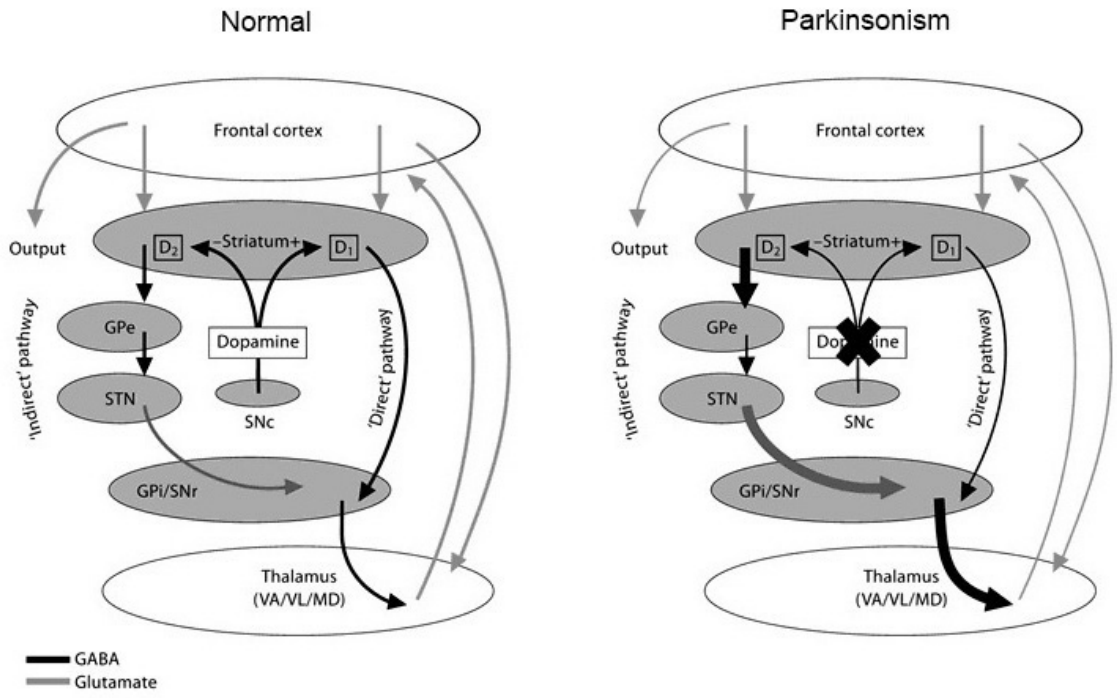

Figure 1.3 Basal ganglia motor circuit. Schematic diagram of the basal ganglia motor circuits in normal (*left*) and Parkinsonian (*right*) states. Dopamine from the substantia nigra pars compacta (SNc) excites D1 receptors, which sends an inhibitory signal to the globus pallidus internus (GPi) and reduces the inhibition of the thalamus. In contrast, dopamine inhibits D2 receptors, which inhibits the globus pallidus externus (GPe) and relieves the inhibition on the subthalamic nucleus (STN). The STN then transmits an excitatory signal to the GPi. Under normal conditions, the direct and indirect pathways are in balance to provide controlled excitation of the frontal motor cortex. In Parkinson's disease, the depletion of dopamine in the striatum causes an imbalance. While the direct pathway is shut down, there is reduced inhibition of D2 receptors, which increases the inhibitory signal to the thalamus and prevents stimulation of the motor cortex. Thickness of the arrows indicates the changes in activity of specific connections in Parkinsonism. GABA, inhibitory neurotransmitter; Glutamate, excitatory neurotransmitter; SNr, substantia nigra reticulate; VA, ventral anterior nucleus; VL, ventral lateral nucleus; MD, mediodorsal nucleus.

1969). Braak staging of sporadic PD delineates a defined, nonrandom pattern to the spread of LB formation, which progresses from the olfactory bulb and brainstem to the substantia nigra and finally the cortex (**Figure 1.4**). However, more recent observations suggest that the presence and distribution of LBs varies from patient to patient and that Braak staging does not predict the severity of a patient's disease (Burke et al., 2008). Nevertheless, the Braak staging scheme has gained renewed interest with the idea that PD may advance from cell to cell via prion-like transmission of misfolded alpha-synuclein (**Figure 1.5**). The prion hypothesis (Olanow and Prusiner, 2009) was first proposed following the observation that LBs had formed in healthy fetal mDA neuron grafts 10-20 years after transplantation into PD patients, a time point when the fetal neurons would have been too young to have naturally developed LBs on their own (Kemmerer et al., 2013; Kordower et al., 2008a; Kordower et al., 2008b; Li et al., 2008). Further investigation found that both wild-type and A53T mutant alpha-synuclein fibrils can act as seeds and oligomerize monomeric wild-type alpha-synuclein (Wood et al., 1999; Yonetani et al., 2009). In fact, several studies have now demonstrated the transmission of pathological alpha-synuclein both in cultured cells (Hansen et al., 2011; Luk et al., 2009) and in mice (Angot et al., 2012; Desplats et al., 2009; Luk et al., 2012a; Luk et al., 2012b) (**Figure 1.6**). However, it remains to be seen how well this phenomenon translates to human PD and whether it is specific to certain causes of the disease.

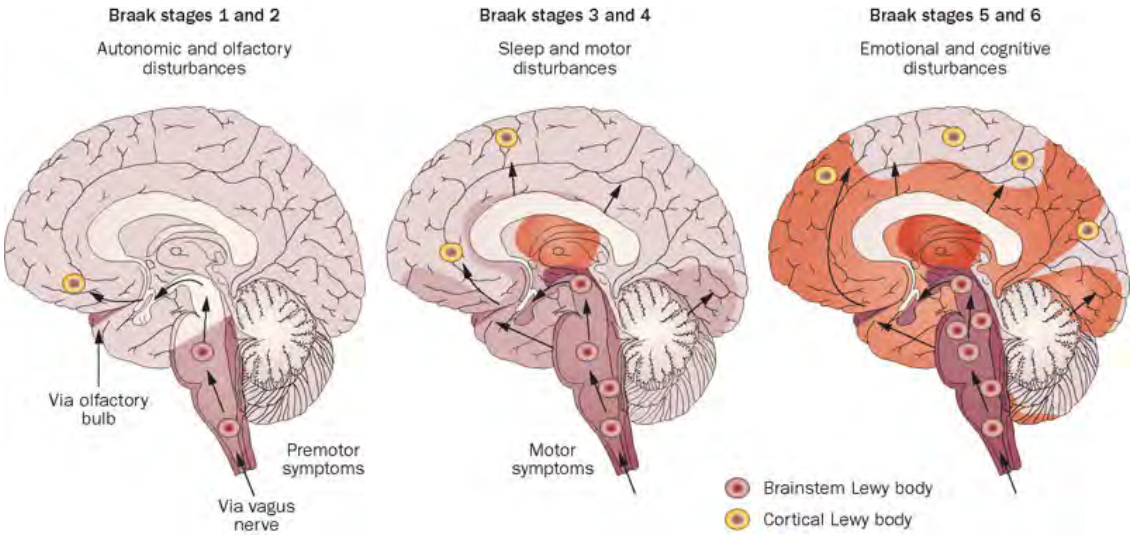

Figure 1.4 Braak staging of PD. Depiction of Braak staging, which is used to classify the degree of pathology in postmortem brans from patients with PD. Staging is based on the spread of ubiquitinated alpha-synuclein which aggregates into structures known as Lewy bodies. Initiation occurs in the olfactory bulb or the vagus nerve as indicated. The red shading signifies the spread of pathology.

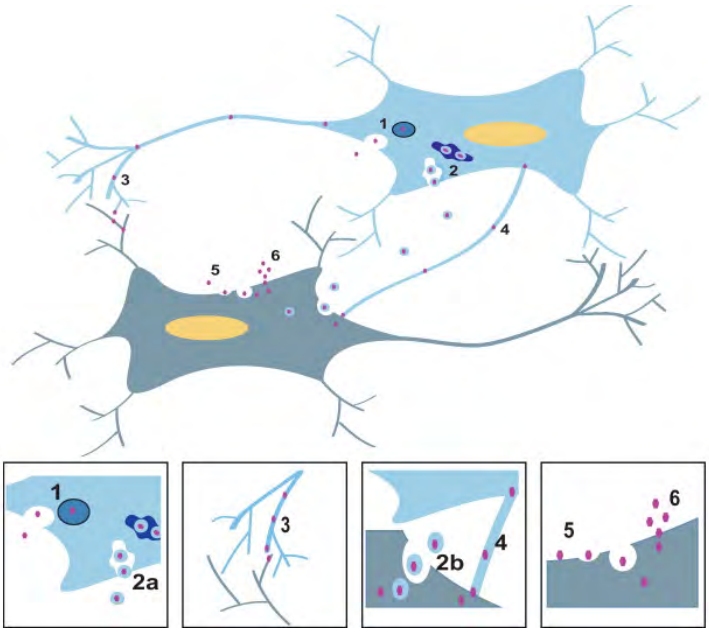

Figure 1.5 Mechanisms of alpha-synuclein cell-to-cell transfer. Schematic depicting the various ways alpha-synuclein (purple) has been proposed to transfer between cells. Alpha-synuclein could be released in both exocytotic vesicles (1) and exosomes (2a & 2b) or via direct cell-to-cell transmission through synapses (3) or possibly even tunneling nanotubes (4). It is unclear how α-synuclein is taken up by the host cell but could be by either endocytosis (5) or passive diffusion (6).

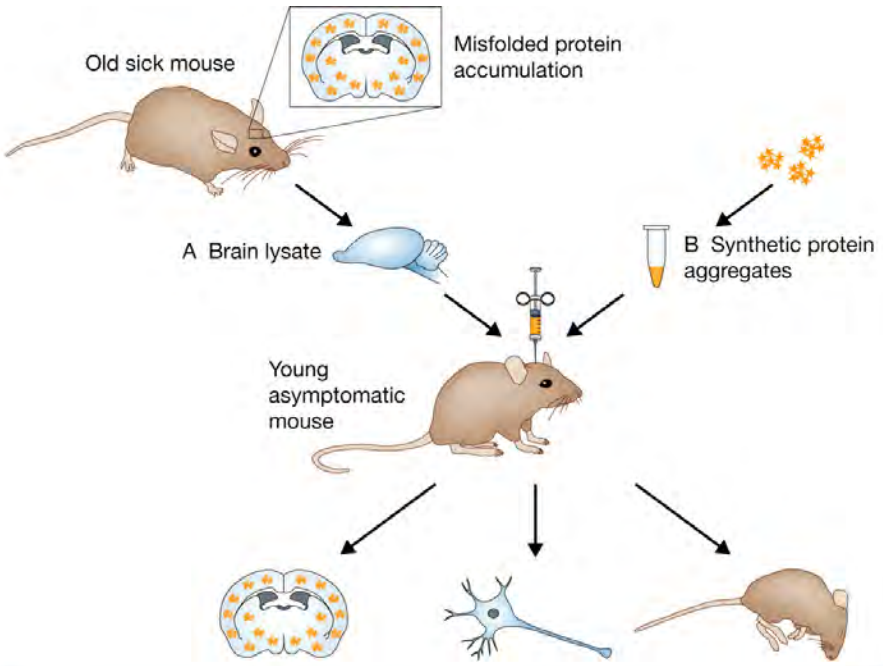

	Induction of aggregation		Neuronal loss		Fatal disease	
	Lysate	Synthetic	Lysate	Synthetic	Lysate	Synthetic
PrP^{Sc}	Yes[1]	Yes[2]	Yes[1]	Yes[2]	Yes[1]	Yes[2]
Aβ	Yes[3]	No[3]	Yes[3]	No[3]	No[3]	No[3]
α-synuclein	Yes[4,5]	Yes[5]	Yes[4,5]	Yes[5]	Yes[4,5]	Yes[5]
Tau	Yes[6]	n.d.	Yes[6]	n.d.	No[6]	n.d.

[1]Initially by Chandler 1961 and replicated by many; [2]Wang *et al*. 2010; [3]Meyer-Luehmann *et al*. 2006; [4]Mougenot *et al*. 2011; [5]Luk *et al*. 2012; [6]Clavaguera *et al*. 2009

Figure 1.6 Evidence for prion-like transmission of prion protein, Aβ, alpha-synuclein, and Tau. Depiction of the experimental paradigm used to replicate spreading of alpha-synuclein and other disease-related proteins by inoculating a recipient mouse with infectious aggregates derived in vivo from old disease mice (A) or in vitro using recombinant technology (B). The table summarizes the phenotype results in each case.

Etiology of PD: Environmental and Genetic Causes

PD most commonly occurs later in life with no known etiology, implicating a role for environmental factors. Reports that rural living increases the risk of developing PD (Barbeau et al., 1987; Gorrell et al., 1996) led to studies on pesticides such as rotenone (Caboni et al., 2004) and herbicides like paraquat (Corasaniti et al., 1992); however, the direct link between these factors and PD in human subjects has been inconclusive. Nevertheless, these studies point to the unifying theme of mitochondrial dysfunction and oxidative stress in PD, which was also suggested by the finding that a mitochondrial complex I inhibitor 1-methyl-4-phenyl-1,2,5,6-tetrahydropyridine (MPTP) caused PD-like symptoms when it was present as a contaminant in a designer drug (Langston et al., 1983).

While the majority of cases are idiopathic, about 10-15% of PD has a genetic cause (Payami et al., 1994). In fact, mutations have been identified in several genes (**Figure 1.7**). Dominantly inherited mutations can be found in *SNCA* (the gene that encodes alpha-synuclein) (Polymeropoulos et al., 1997) where a single point mutation or triplication causes buildup and aggregation and in *LRRK2* (Funayama et al., 2005; Paisan-Ruiz et al., 2004; Zimprich et al., 2004) where point mutations confer constitutive activation of the kinase, which may phosphorylate alpha-synuclein and thereby increase its fibrilization. Recessively inherited, loss-of-function mutations are observed in *PINK1 (Valente et al., 2004)*, *PARK2* (the gene that encodes Parkin) (Kitada et al., 1998), and *DJ-1* (Bonifati et al., 2003*)*. PINK1, Parkin, and DJ-1 protect cells against mitochondrial

Gene	Locus (chromosomal position)	Age of onset	Mutations	Clinical phenotype	Pathology	Comment
PINK1	PARK6 (1p35–p36)	20–40 years	Recessive missense and exon-deletion mutations	Parkinsonism that progresses slowly and is responsive to low doses of L-DOPA	Undetermined	Rare cause (~1–2%) of cases with onset at <50 years; haploinsufficiency might predispose to the disease
DJ1	PARK7 (1p36)	20–40 years	Recessively inherited; homozygous missense (Leu166Pro) and deletion (delEx1–5) mutations, and compound heterozygotes	Slowly progressive parkinsonism, occasionally with behavioural or psychiatric disturbance; rare compound heterozygotes documented with parkinsonism with dementia or amyotrophy	Undetermined	Rare cause (<1%) of cases with onset at <50 years
UCHL1	PARK5 (4p14)	55–58 years (ILe93Met)	Linkage for the Ile93Met substitution is equivocal	Sporadic PD	Undetermined for Ile93Met cases; UCHL1 protein is a prominent component of Lewy bodies	The Ser18Tyr association is supported by meta-analysis and functional data
		Late onset	Susceptibility to sporadic PD is associated with a Ser18Tyr polymorphism			
SNCA	PARK1 and PARK4 (4q21)	38–65 years (duplications); 24–48 years (triplications)	Dominant Ala30Pro, Glu46Lys and Ala53Thr substitutions; genomic duplications and triplications	Progressive L-DOPA responsive parkinsonism, associated with cognitive decline, autonomic dysfunction and dementia; progression is more rapid in SNCA triplication cases	Diffuse Lewy body disease, with prominent nigral and hippocampal (CA2–3) neuronal loss	Genetic and functional data indicate that common promoter and intronic variability are associated with sporadic PD
PARK2	PARK2 (6q25.2–q27)	~30 years on average (range 16–72)	Recessive homozygous and compound heterozygous missense (>57) and exonic deletion/duplication /triplication mutations	Parkinsonism, often presenting with dystonia, with diurnal fluctuations and sleep benefit; typically responsive to very low doses of L-DOPA	Predominantly nigral neuronal loss, although compound heterozygotes with Lewy bodies or tau pathology are described	Mutations account for ~50% of familial juvenile and early-onset parkinsonism, and ~18% of sporadic disease (<50 years at onset)
LRRK2	PARK8 (12p12)	Between 50 and 70 years (range 32–79)	Many dominant substitutions, notably Arg1441Cys/Gly/His, Tyr1699Cys, Ile2012Thr, Gly2019Ser and Ile2020Thr	Parkinsonism consistent with sporadic PD; dystonia, amyotrophy, gaze palsy and dementia occasionally develop	Predominantly Lewy body disease; rare cases have only neurofibrillary tangles and/or nigral neuronal loss	Common coding variation might affect risk in sporadic PD

LRRK2, leucine-rich repeat kinase 2; *PARK2*, the gene that encodes parkin; PD, Parkinson disease; *PINK1*, PTEN-induced kinase 1; *SNCA*, the gene that encodes α-synuclein; UCHL1, ubiquitin carboxyl-terminal esterase L1.

Figure 1.7 Genetics of Parkinson's disease. List of pathogenic mutations that have been identified in patients with PD. Information on associated clinical phenotypes and pathology is specified.

dysfunction. Although much is still unknown about the functions of these five proteins, further analysis suggests a common convergence on mDA neuron death through dysfunction of mitochondria and the ubiquitin-proteasome system (**Figure 1.8**).

Treatment of the Motor Symptoms of PD

Despite the identification of genetic drivers of PD, there is presently no cure for the disease. Rather, pharmacological and surgical therapies have been developed to mitigate the devastating motor symptoms. Soon after it was established that PD results in low striatal dopamine, Birkmayer and Hornykiewicz discovered that the precursor levodopa could be taken up by mDA neurons and converted to dopamine to replace the deficit (Birkmayer and Hornykiewicz, 1961). While levodopa treatment has been successful as a palliative therapy, it presents challenges due to long-term motor complications (Cotzias et al., 1969). The involuntary movements, or dyskinesias, are thought to result from the hypersensitivity of the basal ganglia circuit to dopamine following the dramatic loss of innervation, although the mechanism is still poorly understood (Cenci and Konradi, 2010; Halje et al., 2012). The difficulties with levodopa spurred the development of dopamine agonists as an alternative (Calne et al., 1974; Corrodi et al., 1973). However, while these dopamine agonists decrease the incidence of dyskinesias, the non-motor side effects, including psychiatric disturbances, nausea, and vomiting, are far more frequent.

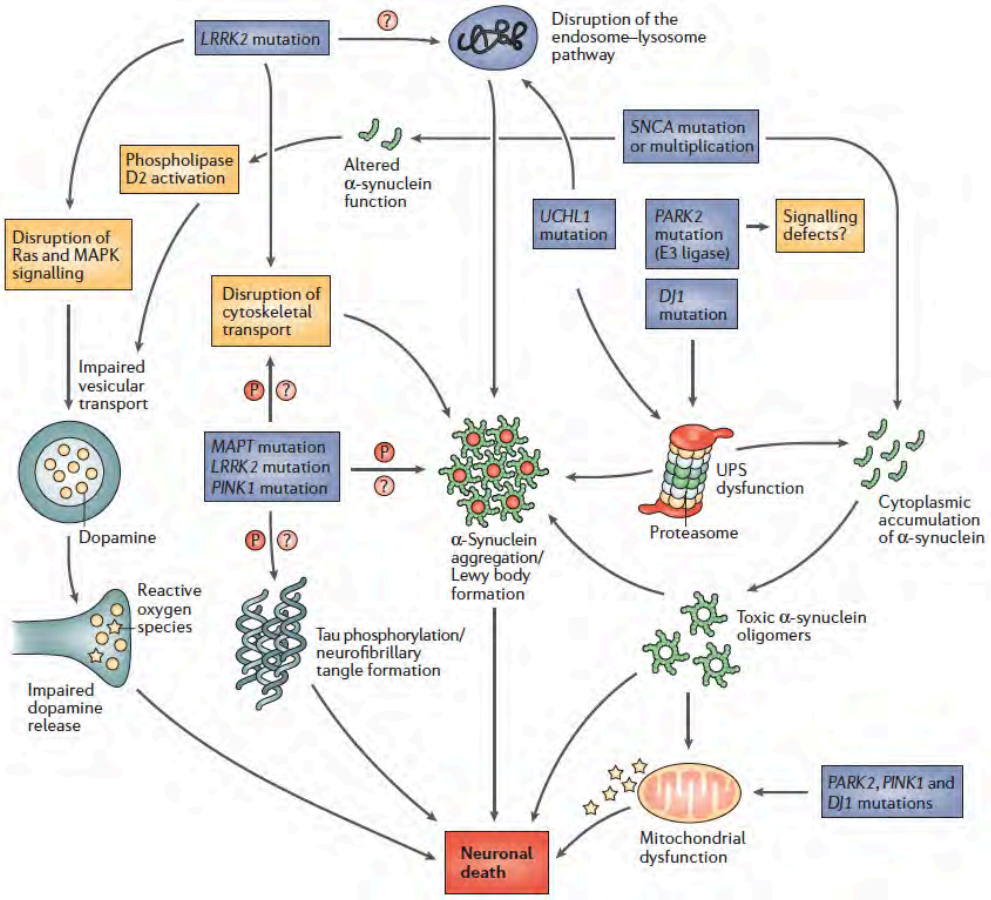

Figure 1.8 Converging pathways of Parkinson's disease. Schematic represents possible mechanisms that lead to PD through various disease-related mutations. Many of the proteins mutated in PD have functions that are still unclear. Nevertheless, it has been proposed that the deregulation in mDA neurons converges on mitochondrial dysfunction and impairment of the ubiquitin-proteasome and endosome-lysosome pathways, which result in neuronal death. The possible involvement of each mutant protein is indicated.

More recent advances have been made by taking a surgical approach. With the understanding of the basal ganglia circuitry (**Figure 1.3**), physicians have explored the use of electrodes to stimulate the subthalamic nucleus (Benabid et al., 1994; Limousin et al., 1995) or the globus pallidus internus (Siegfried and Lippitz, 1994) in a procedure known as deep brain stimulation (DBS). While the specific mechanism of action in DBS remains unclear, it has been shown to improve motor symptoms and to relieve some of the side effects caused by pharmacological agents.

Although levodopa and DBS have improved quality of life for PD patients, neither of these therapies counteracts the degeneration of mDA neurons. The reality of the massive cell death observed at diagnosis has stimulated the development of strategies for cell replacement. However, while efforts involving fetal transplants seemed promising at first (Lindvall et al., 1989; Madrazo et al., 1988), the extent of motor function improvement has been questioned (Smith et al., 2012) and the observation that LB pathology can be transmitted to the transplanted cells (Kemmerer et al., 2013; Kordower et al., 2008a; Kordower et al., 2008b; Li et al., 2008) raises concerns about the long-term health of grafted cells in PD patients. It now remains to be determined whether a new wave of cell therapies using stem cell-derived mDA neurons, improved transplantation techniques, and refined patient selection will result in a more consistent therapeutic benefit.

Animal Models of PD

While our understanding of PD has been greatly advanced over the last several decades, it is still unclear how mDA neurons are lost during the disease and whether protein aggregation is a driver or a passenger in the degeneration process. It is important to gain this knowledge, as late-onset neurodegenerative disorders such as PD are becoming a growing burden to society hastened by the gradual increase in life expectancy. The incidence of PD will likely continue to rise, as it is estimated that by 2050 21.8% of the projected world population (~2 billion people) will be over 60 years of age (Lutz et al., 2008).

In order to investigate the pathogenesis and pathophysiology of PD, researchers have attempted to make use of both toxin-induced and transgenic animal models of the disease. However, while the toxin- and genetic-based models have provided some insights into the basis of PD, they have failed to fully recapitulate many of the classical features of the human disease. For instance, systemic administration of MPTP in mice does not typically produce LBs, and the loss of mDA neurons across various models is inconsistent (Langston et al., 1983). Systemic administration of rotenone (Betarbet et al., 2000) or paraquat (Manning-Bog et al., 2002) selectively degenerates mDA neurons but LB formation is not reproducible. In contrast, local injection of 6-hydroxydopamine (6-OHDA) into the striatum robustly kills mDA neurons (Ungerstedt et al., 1974); however, degeneration occurs immediately and, therefore, does not mimic the progressive nature of PD. With the more recent genetic models such as a single

knockout of *PINK1 (Gautier et al., 2008)*, *PARK2 (Palacino et al., 2004)*, or *DJ-1* (Kim et al., 2005), there is no obvious phenotype. Finally, overexpression of wild-type or mutant alpha-synuclein or LRRK2 does not result in significant nigrostriatal degeneration. Modifications such as Thy-1-driven expression of alpha-synuclein (Sommer et al., 2000; van der Putten et al., 2000) and BAC-driven expression of LRRK2-G2019S (Li et al., 2010) have resulted in reduced striatal DA content; however, they still fall short of truly mimicking the human disease. The limitations of animal models suggest a requirement for additional components that may relate to a patient's background and/or environment exposure and has thus motivated the use of patient-derived pluripotent stem cells to attempt to model PD in a context-dependent manner.

Pluripotent Stem Cells

Embryonic Stem Cells: Derivation and Characteristics

The study of human disease has been restricted by the inability to model the same complexity in lower organisms and by the limitations involved with obtaining disease-relevant tissue from human subjects. Early work toward addressing these challenges arose from the identification of a population of cells known as the inner cell mass (ICM). Transplantation of the ICM from one blastocyst into another blastocyst demonstrated that these cells could contribute to the developing embryo (Gardner, 1968), suggesting that the ICM could be exploited to study development and, by association, disease. This work was further advanced by parallel studies on teratocarcinomas found in an inbred

strain of mice (Stevens and Little, 1954), which led to the identification and characterization of embryonal carcinoma (EC) cells. EC cells could not only recreate the germ cell tumors (Kleinsmith and Pierce, 1964) but could also contribute to the developing embryo (Brinster, 1974), demonstrating their functional equivalence to the ICM. Further work establishing culturing techniques for EC cells (Finch and Ephrussi, 1967) indicated that these stem-like properties could be maintained in vitro.

In 1981 cells of the ICM were successfully cultured in vitro and coined embryonic stem cells (ESCs) **(Figure 1.9**) (Evans and Kaufman, 1981; Martin, 1981). With adaptations to the culturing techniques, ESCs were also isolated using blastocysts from rhesus monkeys (Thomson et al., 1995) and eventually from humans (Thomson et al., 1998). Under the proper culture conditions, mouse, monkey, and human ESCs retain the pluripotent properties of the ICM. They have an unlimited capacity to self-renew (or continue to propagate in the undifferentiated state) and they can differentiate (or give rise to any cell type of the embryo) (**Figure 1.10**).

Derivation of differentiated cell types that comprise the three germ layers represented in the embryo (mesoderm, endoderm, and ectoderm) can be achieved using various methods. For instance, ESCs subjected to non-adherent conditions in the absence of self-renewal factors will spontaneously aggregate into embryoid bodies in an attempt to recreate the embryo and continue on with

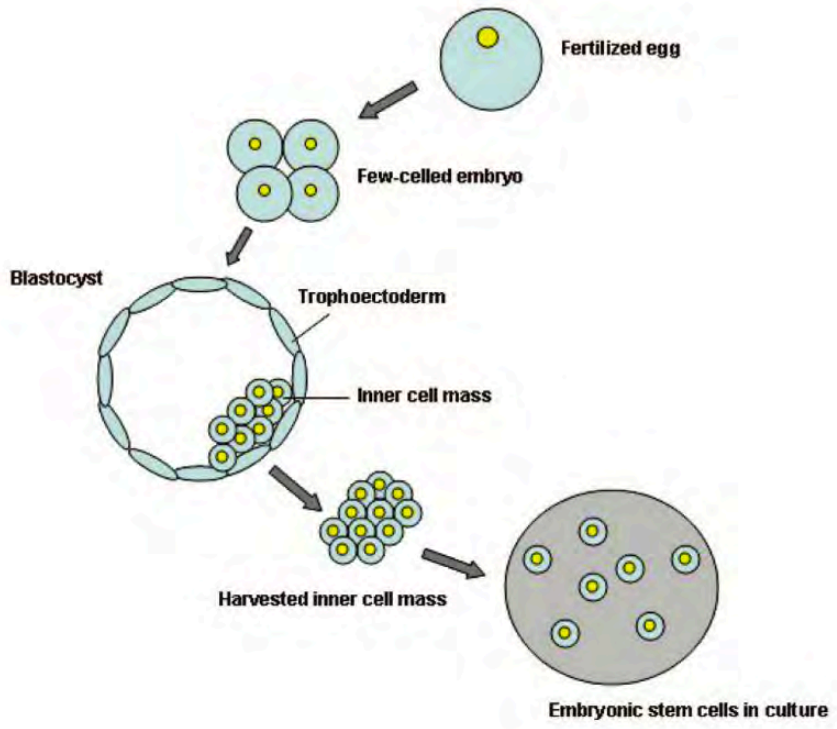

Figure 1.9 **Derivation of embryonic stem cells.** Illustration depicts a developing embryo from the point of fertilization of the egg to the blastocyst. The inner cell mass of the blastocyst can be replated in culture to give rise to pluripotent ESC colonies.

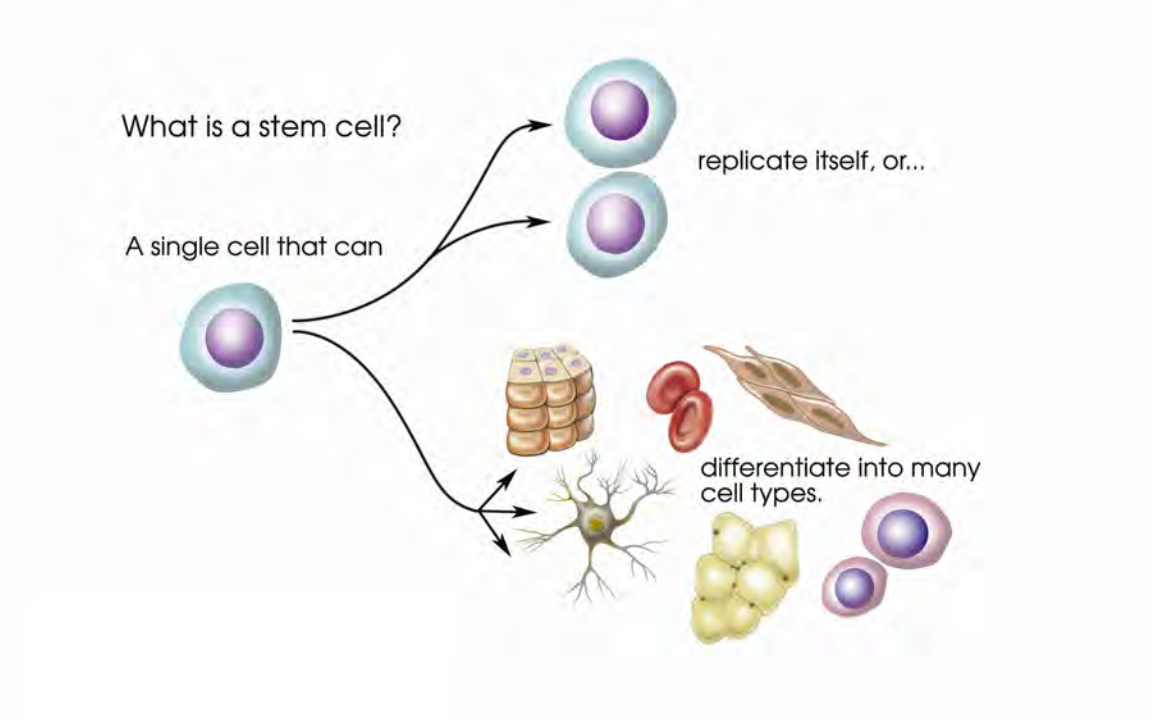

Figure 1.10 **Properties of embryonic stem cells.** ESCs have the ability to self-renew to regenerate themselves indefinitely. They also have the capacity to differentiate into potentially any cell type in the human body such as neurons, red blood cells, etc.

development (Doetschman et al., 1985; Itskovitz-Eldor et al., 2000). Over time, the upregulation of unique markers specifying each germ layer can be monitored by reverse transcription polymerase chain reaction (RT-PCR). For long-term analysis of spontaneous differentiation capacity, ESCs are subcutaneously transplanted into immunocompromised mice where they form a benign tumor, or teratoma, comprised of terminal cell types of multiple lineages (Thomson et al., 1998). More sophisticated techniques involve the directed differentiation of ESCs to a specific lineage by exposure to signaling molecules and/or by co-culture with feeder cells that supply the necessary signals (reviewed in (Keller, 2005)). Finally, chimeras and tetraploid complementation represent more stringent analyses that are limited to mouse ESCs. Mouse ESCs injected into a developing blastocyst at the proper stage will contribute in a mosaic pattern to various tissues of the recipient producing a chimera following transplantation into a pseudopregnant mother (Bradley et al., 1984). In tetraploid complementation (Nagy et al., 1990), a tetraploid embryo is generated by electrofusion of two embryos at the two-cell stage followed by injection of ESCs at the blastocyst stage. Although under debate (Eakin et al., 2005; Mackay and West, 2005), the tetraploid cells are thought to exclusively give rise to extraembryonic tissues due to their inability to form viable embryo tissue, resulting in an embryo comprised entirely of ESC derivatives.

Mouse and human ESCs have many distinct features (reviewed in (Nichols and Smith, 2009)). Although both mouse and human ESCs form colonies in culture,

these colonies have unique morphologies as well as different signaling requirements to maintain the pluripotent state. In fact, it has recently been determined that traditional mouse and human ESCs actually represent distinct developmental stages of the embryo (Brons et al., 2007; Tesar et al., 2007). While mouse ESCs are identical to ICM cells of a pre-implantation embryo ("the ground state"), human ESCs more closely resemble the post-implantation ("epiblast") stage (**Figure 1.11**). These findings have led to new classifications for ESCs as naïve or primed, respectively. In addition, derivation and in vitro culturing methods have been redefined to capture the desired ESC status (Gafni et al., 2013; Guo et al., 2009; Hanna et al., 2010).

Limitations of ESCs

The establishment of human ESCs has provided researchers with a valuable tool for understanding species-specific biology; however, the field has faced many controversies concerning the ethics of this practice (reviewed in (de Wert and Mummery, 2003)). Isolation of the inner cell mass indeed results in the destruction of the human embryo, but what is the moral status of the embryo and the resulting ESCs? Some would suggest that human life begins at conception and that any cell from which a human could be created (in principle) has a similar moral status. In fact, this belief has led to public policy, restricting the use of federal funds to a limited number of pre-approved human ESC lines. In an effort to continue such research, these ethical concerns with human ESCs have

Property	Ground State	Primed State
Embryonic tissue	early epiblast	egg cylinder or embryonic disc
Culture stem cell	rodent ESCs	rodent EpiSCs; primate "ESCs"
Blastocyst chimaeras	yes	no[a]
Teratomas	yes	yes
Differentiation bias	none	variable
Pluripotency factors	Oct4, Nanog, Sox2, Klf2, Klf4	Oct4, Sox2, Nanog
Naive markers[b]	Rex1, NrOb1, Fgf4	absent
Specification markers	absent	Fgf5, T
Response to Lif/Stat3	self-renewal	none
Response to Fgf/Erk	differentiation	self-renewal
Clonogenicity	high	low
XX status	XaXa	XaXi
Response to 2i	self-renewal	differentiation/death

[a] Not applied to primate cells.
[b] Representative examples.

Figure 1.11 Comparison of mouse and human ESCs. List of similarities and differences between the ground state and the primed state of pluripotent stem cells.

motivated alternative strategies, which we discuss below, aimed at exploiting the cellular plasticity of readily available adult human tissue.

Nuclear Reprogramming: Somatic Cell Nuclear Transfer

The transition of a cell from an uncommitted stage ("stem/precursor cell") to its final commitment ("differentiated cell") was originally thought to follow a path based on defined epigenetic alterations that irreversibly constrain a cell to a unique specification, similar to a ball rolling down a hill (**Figure 1.12**) (Waddington, 1957). In other words, it is not the genetic material itself but the *regulation* of the genetic material that progressively directs a cell toward a particular fate, exponentially restricting the available choices so that the hurdle of pushing the cell back up the hill is insurmountable. However, this dogma came into question with the discovery that a blastocyst-stage nucleus (Briggs and King, 1952) and even an older intestinal epithelial cell nucleus (Gurdon, 1962) could be "reprogrammed" following transplantation into an enucleated frog oocyte, giving rise to a viable organism genetically identical to the donor. This process, known as nuclear transfer, elucidated the plasticity of the nuclear material and the potential for a cell to become less committed.

Although animal cloning methods came into question over the following decades, nuclear transfer was eventually repeated using embryonic cell sources from sheep (Willadsen, 1986), cows (Prather et al., 1987), rabbits (Stice and Robl, 1988), pigs (Prather et al., 1989), mice (Kono et al., 1991), and monkeys

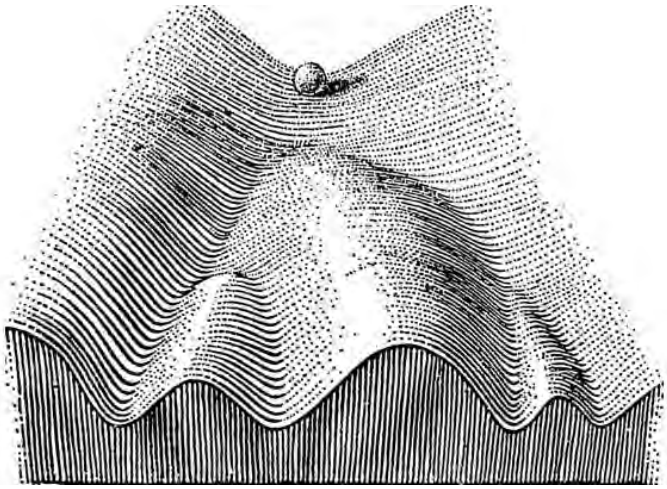

Figure 1.12 <u>Waddington's epigenetic landscape.</u> Differentiation of pluripotent stem cells is described as a ball rolling down a topographical hill. A stem cell (represented by the ball) has to make lineage commitment choices (represented by each bifurcation in the landscape) that are progressively restricted to a given fate (as represented by the hills between each endpoint).

(Tachibana et al., 2009). In 1997 Dolly was the first mammal to be cloned from an adult somatic cell nucleus (Wilmut et al., 1997) and several other species soon followed. However, despite these advances, somatic cell nuclear transfer (SCNT) efficiencies remain quite low (<1%). In fact, SCNT using human embryos was unsuccessful until just last year when nuclear transfer ESCs were established by minimizing oocyte donor age and by improving oocyte activation with caffeine treatment (Tachibana et al., 2013). Despite these advances, however, SCNT remains a technically challenging procedure that involves logistical and ethical concerns around the use of human oocytes for research purposes.

Nuclear Reprogramming: Transcription Factor Lineage Conversion

Research aimed at defining artificial methods to redirect cell fate began by accident when it was discovered that a fibroblast culture that had been treated with a new drug, 5-azacitidine, was not contaminated with mold but had converted to multinucleated muscle cells (Taylor and Jones, 1979). Confirming the epigenetic control of cell fate choice, 5-azacytidine was found to inhibit DNA methylation (Jones and Taylor, 1980) and relieve transcriptional silencing of *MyoD*. Indeed, it was later found that MyoD expression alone can confer muscle-inducing activity in fibroblasts (Davis et al., 1987). Furthermore, this phenomenon appeared to be more broadly true across multiple cell types when a subsequent study demonstrated that GATA-1 expression converts myeloblasts to megakaryocyte-erythrocyte precursors by not only activating a novel gene expression program but also by suppressing the program of the donor cell

(Kulessa et al., 1995). These data laid the groundwork for transcription factor-based lineage conversion.

The bold goal in the field was to use transcription factor-based lineage conversion to create a new source of pluripotent stem cells. Such methods could potentially bypass the practical and ethical challenges associated with human ESC and SCNT research. Toward this end, Takahashi and Yamanaka designed a screen to overexpress key ESC regulators via retroviruses in mouse fibroblasts. Using a nonessential pluripotency gene to drive resistance, they discovered that just four transcription factors (Oct4, Sox2, Klf4, and c-Myc) are sufficient to reprogram embryonic or adult mouse fibroblasts to cells termed induced pluripotent stem cells (iPSCs) that resemble ESCs by morphology, gene expression, and functional properties (Takahashi and Yamanaka, 2006). It was also demonstrated that these “Yamanaka factors” (Lowry et al., 2008; Park et al., 2008b; Takahashi et al., 2007) or an independently-derived combination of Oct4, Sox2, Lin28, and Nanog (Yu et al., 2007) can support the generation of human iPSCs. Furthermore, subsequent findings that iPSCs could be derived from patients with disease using readily available human tissue such as that obtained via a skin biopsy (Park et al., 2008a) or a routine blood draw (Ye et al., 2009) defined a new paradigm for disease modeling and reinvigorated hopes for cell replacement therapy.

iPSC-Based Modeling of Disease

Human iPSCs provide an unlimited population of patient-derived cells of a given background that can be differentiated into disease-relevant cell types. In addition to holding promise for functions in cell therapy as a source of replacement cells (Hanna et al., 2007), human iPSCs offer an unprecedented capacity to study disease mechanisms and to perform appropriate drug screens that could benefit individuals with disease (**Figure 1.13**). Furthermore, human iPSC-based models do not require knowledge of the genetic origin of the disease because the patient background is preserved through reprogramming and differentiation. This technology has enabled modeling of a variety of neurologic, hematopoietic, metabolic, and cardiovascular disorders (reviewed in (Unternaehrer and Daley, 2011)). A few examples of iPSC-based models of neuroligic diseases are discussed below.

An early successful example of iPSC-based modeling was the study of spinal muscular atrophy (SMA), a disease caused by a mutation in *SMN1*, which leads to reduced expression of SMN1 protein and loss of lower motoneurons. While iPSCs generated from a patient with SMA type 1 initially differentiated to motoneurons with a similar efficiency as iPSCs derived from an unaffected parent, analysis two weeks later showed a specific loss and reduction in size of SMA ChAT-positive motoneurons but not other neuronal subtypes. Using this model, it was further demonstrated that these SMA iPSC-derived neurons could be used to test candidate therapeutic drugs, which improved aggregation of

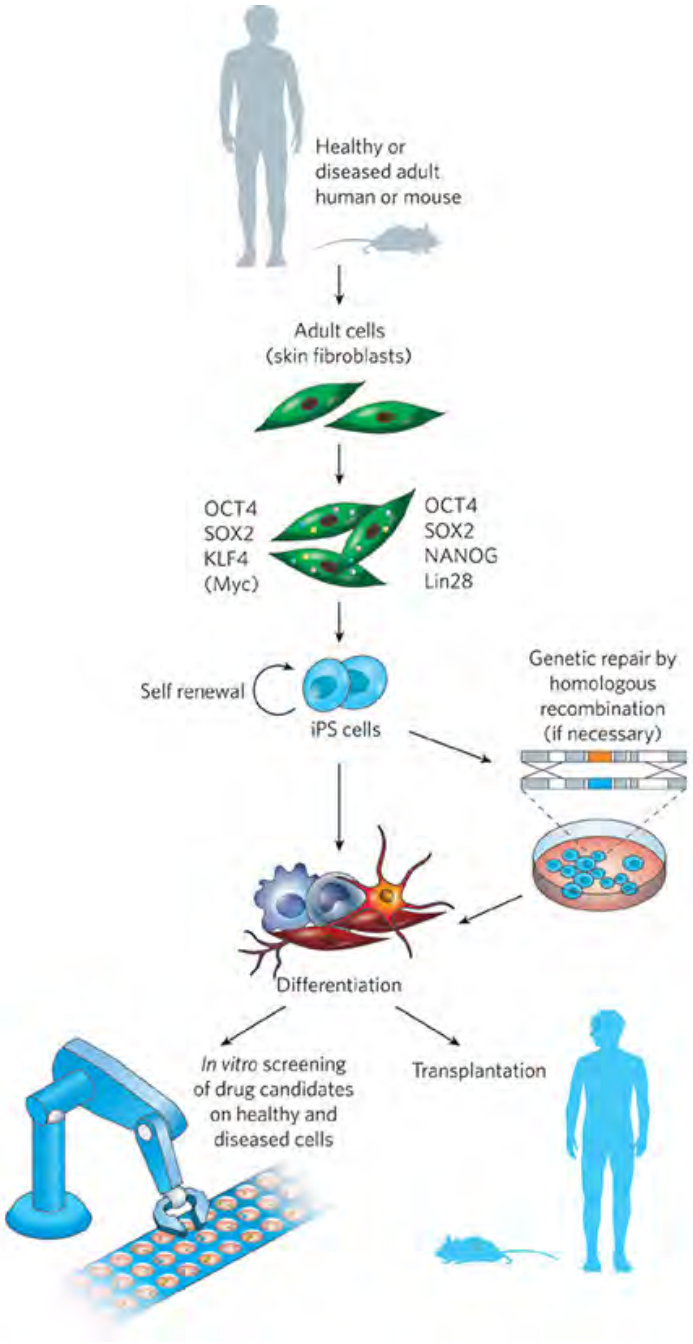

Figure 1.13 **Disease modeling paradigm.** Schematic representing the process of taking somatic cells from a healthy or diseased individual and reprogramming those cells back to the pluripotent state using overexpression of the Yamanaka factors (OCT4, SOX2, KLF4, and c-Myc) or the Thomson factors (OCT4, SOX2, NANOG, and Lin28). The resulting iPSCs can then be differentiated and used for in vitro drug screens to look for candidate therapeutics for patients with a particular disease, or they can be corrected of the disease mutation, differentiated, and given back to the patient to replace the diseased cells.

SMN1 protein into characteristic nuclear gems similar to that observed in healthy donor iPSC-derived neurons (Ebert et al., 2009), providing validation for the use of these cells in future drug screens.

Another example in support of iPSC-based models came from studying familial dysautonomia (FD), a monogenic disease caused by tissue-specific missplicing of *IKBKAP*. *IKBKAP* is a ubiquitously expressed gene involved in transcriptional elongation. Using iPSC technology it was possible to show that FD-specific missplicing of *IKBKAP* was particularly severe in neural crest lineages, suggesting a plausible mechanism to explain the specific disease symptoms in FD. While FD iPSCs differentiate to neural crest precursors with a similar efficiency as healthy donor-derived iPSCs, FD iPSC-derived neural crest show defects in migration and in neurogenic differentiation towards autonomic fates. The autonomic neuron defect in FD iPSC derivatives could be partially rescued by treatment with a known FD therapy, kinetin (Lee et al., 2009). A subsequent study used the same iPSC-based model to identify novel drug candidates that rescue *IKBKAP* expression in the neural crest lineage (Lee et al., 2012).

As another more resent example, human iPSC technology has also been used to model an infectious disease, herpes simplex encephalitis (HSE). Both UNC93B- and TLR3-deficient iPSC-derived neurons were found to be susceptible to HSV-1 infection but healthy donor iPSC-derived neurons were not, elucidating the

mechanism for HSV-1 spread to the brain in patients with the disease (Lafaille et al., 2012).

Limitations and Challenges of iPSCs

While iPSC technology has led to the establishment of many relevant disease models, several limitations to the current techniques remain to be addressed.

Yamanaka's original reprogramming method utilized individual retroviruses for each transgene that integrate into the genome (Takahashi et al., 2007; Takahashi and Yamanaka, 2006). While the retroviral transgenes are silenced following complete establishment of iPSCs, the integration sites (>20 on average) disrupt the integrity of the genome and increase the probability of transgene reactivation, complicating interpretation of disease phenotypes and potential use of these cells in clinical applications. Studies tackling these issues quickly emerged, employing improved methods of expression such as non-integrating adenoviruses (Okita et al., 2008; Stadtfeld et al., 2008), a polycistronic lentivirus (Sommer et al., 2009), inducible lentiviruses with loxP sites for Cre-mediated excision (Soldner et al., 2009), piggyback transposons (Woltjen et al., 2009), episomal vectors (Yu et al., 2009), synthetic mRNA (Warren et al., 2010), micro-RNA (Anokye-Danso et al., 2011), and small molecules (Ichida et al., 2009; Zhu et al., 2010). Even with these advances, the efficiency remains quite low (0.01-1%), which was once thought to be due to the stochastic nature of a reprogramming event. However, it has been proposed recently that

reprogramming can be induced in 100% of the donor cells by the addition of Mbd3 depletion (Rais et al., 2013), suggesting that the process can be triggered in every cell if the right obstacles are eliminated.

While there is hope that iPSCs may eventually obviate the need for ESCs, ongoing work continues to study the similarities and potential differences between these two cell types. For instance, studies report differences in methylation patterns (Doi et al., 2009) and genomic instability (Hussein et al., 2011; Laurent et al., 2011; Mayshar et al., 2010). In addition, it has been suggested that iPSCs retain an epigenetic memory of the cell they were derived from (Kim et al., 2010). However, many of these distinctions may be attributed to premature characterization of incomplete reprogramming (Polo et al., 2010) or to comparisons between iPSCs and ESCs derived in different labs and/or from different individuals (Newman and Cooper, 2010). In fact, many studies are unable to find significant differences between iPSCs and ESCs such as in the comparison of their global gene expression patterns (Guenther et al., 2010).

For applications in disease modeling, it is not only important to use iPSCs that are of sufficient passage number to ensure complete reprogramming, but it is also essential to carefully select controls. Defining disease phenotypes requires comparison between iPSC-derived populations of disease and non-disease origin, which can be derived from a variety of sources. Early studies of disease with iPSCs defined the gold standard for controls as healthy, age-matched

donors to minimize environmental diversity or as family members without disease to minimize genetic diversity. With the recent advances in genetic engineering using zinc-finger nucleases (Hockemeyer et al., 2009; Zou et al., 2009), transcription activation-like effector nucleases (TALENs) (Hockemeyer et al., 2011), or clustered, regularly interspaced, short palindromic repeat (CRISPR)/Cas9 technology (Cong et al., 2013; Mali et al., 2013), it is now theoretically possible to correct the disease-causing mutation in the patient iPSCs or to reciprocally introduce the mutation in healthy donor iPSCs so that we can study isogenic pairs for subtle differences attributable to the mutation alone. These technologies, however, are still in early phases of development, and precautions must be taken to limit off-target effects and ensure genomic integrity of the engineered iPSCs. It also remains to be determined whether these strategies will be suitable for modeling polygenic disease or late-onset disease with environmental components.

Recent studies have demonstrated that reprogramming resets at least some aspects of aging found in fibroblasts taken from old donors, potentially limiting the use of iPSCs to modeling early-onset disease (reviewed in (Freije and López-Otín, 2012; Liu et al., 2012a; Mahmoudi and Brunet, 2012)). For instance, aging in mitotic cells is typically associated with the shortening of telomeres to a critical point when the cell reaches Hayflick's limit and undergoes senescence (Hayflick, 1965). Surprisingly, telomerase is reactivated during reprogramming of fibroblasts to the pluripotent stage and telomeres elongate during early passages

of iPSCs (Agarwal et al., 2010; Marion et al., 2009). Furthermore, Lemaitre and colleagues have observed the loss of senescence-associated markers such as p16, p21, and senescence-activated β-galactosidase (SA-β-Gal) in iPSCs compared to the donor fibroblasts (Lapasset et al., 2011). The markers remain suppressed in newborn iPSC-derived fibroblast-like cells and are only reactivated after >50 passage doublings. Aging is also often associated with the accumulation of reactive oxygen species (ROS) as a result of reduced mitochondrial fitness. Following reprogramming, iPSC mitochondria are rejuvenated to an immature, healthy state regarding organelle morphology and distribution, expression of nuclear factors involved in mitochondrial biogenesis, content of mitochondrial DNA, intracellular ATP level, oxidative damage, and lactate generation (Prigione et al., 2010; Suhr et al., 2010). Taken together, these data suggest that fibroblasts from old donors are reset to a young-like state following reprogramming; however, additional markers will need to be analyzed before drawing firm conclusions.

In addition to the apparent loss of age-associated features at the iPSC stage, the directed differentiation of pluripotent stem cells (both ESCs and iPSCs) is known to yield immature, embryonic-like cell types that often require months of maturation to establish robust functional properties (reviewed in (Liu et al., 2012a; Saha and Jaenisch, 2009)). For example, while ESC-derived hematopoietic stem cells (HSCs) most closely align with definitive, adult-like HSCs by gene expression, they are functionally restricted to myeloid commitment

and lack a Notch signature (McKinney-Freeman et al., 2012), indicating incomplete specification. Differentiation of pluripotent stem cells to a cardiomyocyte fate results in cells with immature sarcomere organization, calcium handling, and electrophysiological properties (Dolnikov et al., 2006; Mummery et al., 2003; Zwi et al., 2009). Indeed, early-stage iPSC-derived cardiomyocytes demonstrate poor graft-host integration and lethal arrhythmias when transplanted to regenerate myocardium due to their immature nature (Khan et al., 2013; Zhang et al., 2002). As for pancreatic beta cells derived from human ESCs, they are not glucose-responsive in vitro (D'Amour et al., 2006) and only become responsive after several weeks of differentiation in vivo (Kroon et al., 2008). Similarly, human midbrain dopamine (mDA) neurons, the cell type predominantly affected in PD, require months of culture to develop mature physiological behaviors in vitro or months of in vivo maturation to rescue dopamine deficits in animal models of PD (Isacson and Deacon, 1997; Kriks et al., 2011). Furthermore, based on the BrainSpan: Atlas of the Developing Human Brain (http://www.brainspan.org), gene expression data from pluripotent stem cell-derived neural cells matches the transcriptome of first trimester embryos. These data argue for a species-specific, intrinsic "clocklike" mechanism that prevents the rapid generation of mature or aged cells, which poses a challenge for modeling adult- or late-onset disease using iPSCs.

iPSC-Based Models of Late-Onset Neurologic Diseases

Reprogramming of fibroblasts derived from patients with several different neurologic disorders has been demonstrated. However, while iPSC-based models of early-onset diseases such as FD (Lee et al., 2009) and spinal muscular atrophy (SMA) (Ebert et al., 2009) display disease-relevant phenotypes in a timely manner, models of late-onset diseases including amyotrophic lateral sclerosis (ALS), Alzheimer's disease (AD), and PD do not recapitulate the severe degeneration phenotypes (including protein aggregation and neuronal cell death) that occur later in life in these patients. In an early study, Eggan and colleagues showed that ALS iPSCs are capable of differentiation to a motoneuron cell fate, the lineage affected in the disease, but did not assess properties of those cells compared to motoneurons derived from healthy donor iPSCs (Dimos et al., 2008). ALS iPSCs from patients with a mutation in the vamp-associated protein B/C give rise to motoneurons with reduced vamp-associated protein B/C expression but without cytoplasmic aggregates, a key feature of ALS (Mitne-Neto et al., 2011). More recent reports on ALS iPSC models of TDP-43-mutant or sporadic disease are inconsistent with regard to observations of cytoplasmic aggregates, decreased survival, and altered neurite development in the patient-derived motoneurons (Bilican et al., 2012; Burkhardt et al., 2013; Egawa et al., 2012). Interestingly, few AD iPSC models have been described, which is likely attributable to the limited presentation of disease phenotypes. AD-associated phenotypes that have been reported are restricted to early events in the disease, such as accumulated Aβ peptide, increased tau phosphorylation, and endosomal

abnormalities, without cell death (Israel et al., 2012; Koch et al., 2012). Surprisingly, the earliest iPSC model of PD showed that PD iPSC-derived mDA neurons appear healthy and are even capable of rescuing motor asymmetry in a Parkinsonian animal model just like control iPSC-derived mDA neurons (Hargus et al., 2010). Similarly, additional PD models of LRRK2-G2019S (Cooper et al., 2012; Nguyen et al., 2011), PINK1-Q456X (Seibler et al., 2011), or alpha-synuclein-A53T (Chung et al., 2013) disease show only early biochemical phenotypes associated with dysfunctional mitochondria or endoplasmic reticulum stress. Decreased survival of the PD iPSC-derived mDA neurons is not observed until they are treated with mitochondrial toxins or oxidative stressors (Cooper et al., 2012; Nguyen et al., 2011; Seibler et al., 2011). These data suggest that conventional iPSC-derived neurons may be too young to give rise to late-onset phenotypes, necessitating strategies to accelerate the age of these cells.

Aging, Lamin A, and Progerin

Aging

Aging is a process involving the time-dependent accumulation of cellular damage, which further predisposes cells to cancer, neurodegenerative diseases, macular degeneration, and other age-related pathologies. Several candidate hallmarks of the aging process have been proposed, including genomic instability, telomere shortening, cellular senescence, epigenetic changes, loss of proteostasis, and mitochondrial dysfunction (reviewed in (Lopez-Otin et al., 2013)). These processes are characterized not only by their presence in normal

human aging but also by their ability to accelerate aging when aggravated or to prolong longevity when inhibited both in model organisms and in cell culture models.

The accumulation of DNA damage that triggers genomic instability has long been accepted as a key feature of the aging process (Szilard, 1959). DNA lesions arise in essential genes affecting key pathways that can, for instance, lead to over-proliferation and cancer or, conversely, senescence and absence of tissue renewal. The role of DNA damage in aging is also evidenced by the premature aging diseases caused by deficiencies in DNA damage repair such as Werner syndrome, Bloom syndrome, xeroderma pigmentosum, and Cockayne syndrome (Hoeijmakers, 2009; Murga et al., 2009). In contrast, overexpression of BubR1, a mitotic checkpoint protein, can ensure proper chromosome segregation, prolong cancer-free survival, and extend lifespan in mice (Baker et al., 2013).

Contrary to the random accumulation of DNA damage, telomeric regions of chromosomes are subjected to targeted loss during aging (Blackburn et al., 2006). Telomerase, the complex that elongates telomeres, is active in stem cells but is not expressed in differentiated somatic cells, resulting in the steady decline of telomere length with age. Age-related telomere shortening is observed in cultured mesenchymal cells, which inevitably reach a proliferative capacity and undergo senescence (Hayflick, 1965). However, this process can be reversed by overexpressing telomerase (Bodnar et al., 1998), thereby extending in vitro

lifespan. Systemic overexpression of telomerase also extends lifespan and cancer-free survival in wild-type mice (Bernardes de Jesus et al., 2012) while deletion of the RNA component of telomerase results in shortened lifespan and reduced capacity to respond to stresses (Herrera et al., 1999; Rudolph et al., 1999). More importantly, telomere shortening has been shown to occur during normal aging both in humans and in mice (Blasco, 2007).

Aging is also often associated with epigenetic changes that lead to the loss of heterochromatin and chromatin remodeling (Villeponteau, 1997). Increases in active histone marks (H4K16 acetylation, H4K20 trimethylation, and H3K4 trimethylation) as well as decreases in repressive marks (H3K9 methylation and H3K27 trimethylation) have been observed with age (Fraga and Esteller, 2007). These post-translational changes result in open chromatin and subsequent aberrant gene expression, which has been demonstrated both in mice (Bahar et al., 2006) and in humans (Penner et al., 2010). Further evidence suggests that this transcriptional noise may be responsible for the dysregulation of alternative splicing as seen in the human brain (Tollervey et al., 2011). Experimentally, reduction of H3K4 methylation in flies (Greer et al., 2010) and increases in H3K27 methylation in worms (Siebold et al., 2010) improve lifespan and the stress response. Manipulation of histone-modifying enzymes such as HP1α can also affect lifespan as shown in flies (Larson et al., 2012). Indeed, the link between aging and epigenetic changes has been solidified by the finding that overexpression of NAD-dependent histone deacetylases, known as sirtuins, can

extend health and/or lifespan in yeast (Kaeberlein et al., 1999; Kennedy et al., 1995), worms (Tissenbaum and Guarente, 2001), flies (Rogina and Helfand, 2004), and mice (Herranz et al., 2010). Interestingly, the effect with sirtuins can be mediated by caloric restriction and may not be limited to their activity on histones but may also extend to their role in directly targeting proteins for deacetylation. Whatever the mechanism, it is still unclear whether activation of sirtuins will positively influence health/lifespan in humans.

Proteostasis involves the control of proper protein folding and degradation. The role of this process in aging is evidenced by the accumulation of protein aggregates in the brain, which is accelerated in age-related neurodegenerative disorders such as AD and PD. Protein folding is controlled by chaperones. Deficiency of chaperones, including heat shock proteins, can be perturbed in mice to accelerate aging (Min et al., 2008), and increased levels of these proteins have been found in long-lived mice (Swindell et al., 2009). Both protein degradation pathways. the autophagy-lysosome pathway (reviewed in (Rubinsztein et al., 2011)) and the ubiquitin-proteasome pathway (reviewed in (Low, 2011)), are also involved in aging. For instance, activation of autophagy via inhibition of mTOR with rapamycin extends lifespan in yeast (Medvedik et al., 2007; Powers et al., 2006) and flies (Bjedov et al., 2010). While lifespan extension is also observed in mice (Harrison et al., 2009; Wilkinson et al., 2012), the effect of rapamycin in these cases may also be mediated through pathways downstream of mTOR that regulate translation. Increased expression of

components of the ubiquitin-proteasome pathway via EGF activation can increase lifespan in worms (Liu et al., 2011a). In addition, ubiquitylase inhibitors and other activators of the proteasome can extend longevity in yeast (Kruegel et al., 2011) and clear toxic proteins in human cultured cells (Lee et al., 2010).

The mitochondria free radical theory of aging suggests that the decline in function of the electron transport chain leads to the accumulation of reactive oxygen species (ROS) which can cause cellular damage (Harman, 1960). However, the experimental evidence to support this theory has been inconsistent. Unexpectedly, increases in ROS do not accelerate aging in mice (Van Remmen et al., 2003; Zhang et al., 2009) and may even reverse aging in yeast (Mesquita et al., 2010) and in worms (Doonan et al., 2008; Van Raamsdonk and Hekimi, 2009). However, an aging-related phenotype in mice deficient in DNA polymerase γ indicates that dysfunctional mitochondria may contribute to aging independently of ROS (Edgar et al., 2009; Trifunovic et al., 2004). Reduced efficiency of mitochondrial bioenergetics may also play a role in aging as evidenced by the resveratrol-mediated activation of PGC-1α, a transcriptional coactivator of energy metabolism, through SIRT1, the major mammalian sirtuin, during lifespan extension in mice (Lagouge et al., 2006). With the conflicting evidence, it still remains to be determined whether improving mitochondrial function will have an effect on reversing aging.

While these key features of aging have defined functions in their own right, it is clear that their contributions to the aging process are often interconnected and may be even more so in yet unidentified ways. In order to better understand these mechanisms, it will be important to do more human-based studies as the aging process is likely different than in lower organisms as has been noted for human muscle (Welle et al., 2001) and for brain tissue (Loerch et al., 2008).

Hutchinson-Gilford Progeria Syndrome

Because the human aging process still remains elusive, researchers have looked to accelerated aging disorders such as Hutchinson-Gilford progeria syndrome (HGPS). HGPS is a rare genetic disorder characterized by premature aging of various tissues resulting in early death (Hennekam, 2006). Most commonly, the disease is caused by a de novo point mutation in exon 11 of *LMNA*, the gene coding for the nuclear envelope protein lamin A. The c.1824C>T mutation results in the activation of a cryptic splice site, which produces a shorter transcript known as progerin (**Figure 1.14**) (Eriksson et al., 2003). Both lamin A and progerin undergo several posttranslational modifications in the nucleus. Following farnesylation of the C-terminus, this region is cleaved in lamin A. Conversely, progerin lacks the proper endoproteolytic cleavage site which is removed by the internal deletion so that the mature protein is permanently farnesylated (**Figure 1.15**). As a result, progerin aberrantly accumulates in the nuclear membrane, preventing at least some of the normal scaffolding functions

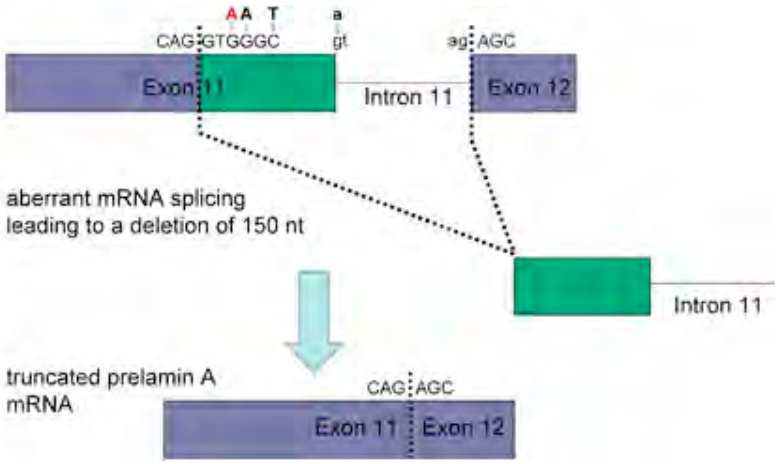

Figure 1.14 Alternative splicing of *LMNA*. In HGPS, a cryptic splice site in exon 11 of the *LMNA* gene is activated by a point mutation, removing 150 nucleotides (nt) of the mRNA.

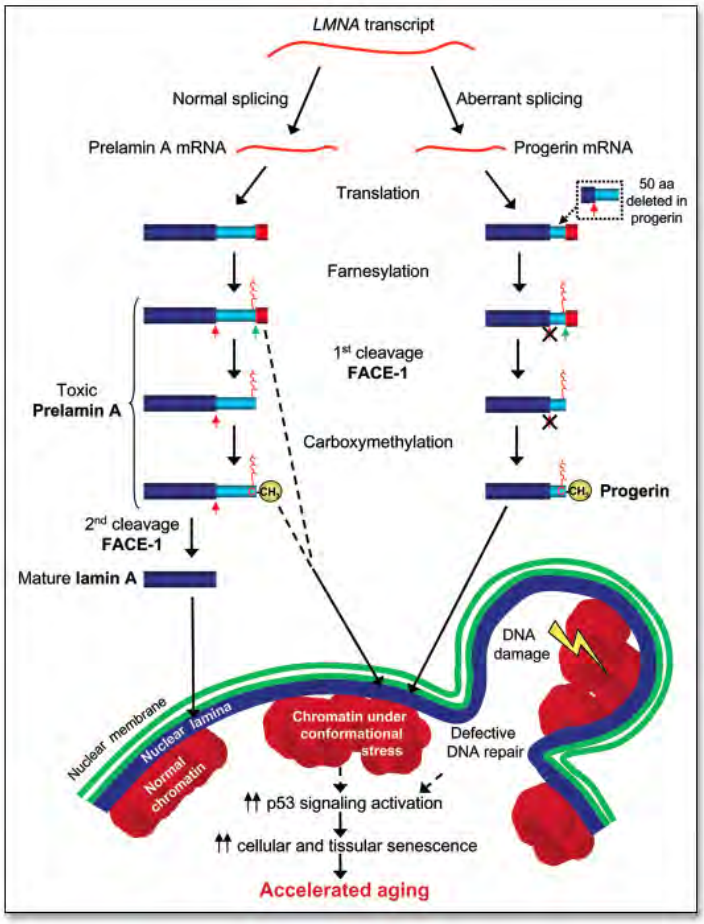

Figure 1.15 Posttranslational modification of lamin A and progerin results in mature proteins with different localizations and functions. Upon entering the nucleus, prelamin A is farnesylated on its C-terminal CaaX domain. It then undergoes a first cleavage event (*green arrow*) where the C-terminal domain is removed. After carboxymethylation of the C terminus, there is another cleavage event (*red arrow*) that removes the farnesyl group. Because of the 50 amino acid (aa) deletion in progerin, the farnesyl group is permanently attached. Unlike the normal incorporation of lamin A into the nuclear lamina, progerin accumulates in the nuclear envelope, inducing morphology changes as well as downstream effects that result in accelerated aging.

observed with lamin A in a dominant-negative fashion. Progerin's altered function in turn interferes with multiple processes in the nucleus including maintenance of nuclear morphology, heterochromatin formation, the DNA damage response, cell cycle, gene transcription and telomere maintenance (reviewed in (Dechat et al., 2008)). This nuclear dysfunction triggers scleroderma, stunted growth, alopecia, wrinkled skin, atherosclerosis, kidney failure, loss of eyesight, cardiovascular dysfunction, and shortened lifespan (reviewed in (Mazereeuw-Hautier et al., 2007)). Patients with HGPS are normal at birth and start to present phenotypes at 1 year of age. They typically do not live longer than 13 years of age due to cardiovascular problems caused by premature atherosclerosis. While we are beginning to understand the mechanisms involved in the disease, the direct link between progerin and accelerated aging is still unclear.

Understanding the nuclear processing machinery for converting precursor lamins (prelamins) into mature lamins has led to the identification of potential therapeutic intervention strategies for HGPS. Prior to the discovery of the HGPS p.G6086 mutation by Collins and colleagues (Eriksson et al., 2003), it was observed that mice lacking Zmpste24, the ortholog of human FACE-1, display severe growth retardation, hair loss, and decreased survival similar to mice lacking lamin A (Bergo et al., 2002; Pendas et al., 2002). These studies further showed that Zmpste24 impairs cleavage of the prelamin A farnesyl group, which corroborated its described role as a metallopeptidase involved in processing farnesylated proteins (Freije et al., 1999). Expanding on these studies, cell culture models

were established that demonstrated that the nuclear morphology defects are reversible using a farnesyl transferase inhibitor (FTI), suggesting its use as a therapeutic for HGPS (Capell et al., 2005; Glynn and Glover, 2005; Toth et al., 2005; Yang et al., 2005). However, treatment with FTIs could have a downside, resulting in alternative prenylation of progerin, which has been suggested with the use of FTIs to treat Kras-driven cancers (Whyte et al., 1997). Indeed, Lopez-Otin and colleagues confirmed the low efficacy of FTIs in progeroid mouse models shown previously (Rusinol and Sinensky, 2006) and demonstrated the alternative geranylgeranylation of progerin. They further explored a combinatorial treatment with pravastatin, which inhibits farnesyl synthesis, and zoledronate, which inhibits geranylgeranyl synthesis. These drugs prevent progerin prenylation, reverse the age-associated phenotypes in Zmpste24-null mice, and increase lifespan (Varela et al., 2008). Nevertheless, while this study and others made a strong argument against FTI treatment alone, a clinical trial showed improvement in at least one clinical outcome in all 25 patients treated for two years with the FTI lonafarnib (Gordon et al., 2012).

Cellular models of HGPS have further aided the characterization of progerin-induced phenotypes as well as the validation of other candidate therapeutics. Fibroblast models of HGPS have been shown to exhibit nuclear architecture changes and loss of peripheral heterochromatin, which alter the regulation of gene expression (Goldman et al., 2004). These phenotypes were used to test the efficacy of an antisense oligonucleotide that binds the *LMNA* cryptic splice site

and thereby inhibits transcription of progerin but not lamin A (Scaffidi and Misteli, 2005). The antisense oligonucleotide reverses nuclear abnormalities and restores levels of the nuclear organization protein LAP2α and the heterochromatin markers H3K9me3 and HP1γ. The antisense oligonucleotide strategy to block progerin transcription was also found to be effective in mice (Osorio et al., 2011) and may even be possible in humans (reviewed in (Sazani and Kole, 2003)). HGPS cells also display hyperproliferation, senescence, and increased apoptosis (Bridger and Kill, 2004) as well as genomic instability (Liu et al., 2005), which may be linked to a role for progerin in telomere-mediated induction of p53 (Benson et al., 2010). These studies led to the hypothesis that telomere dysfunction is solely responsible for the HGPS phenotype (Benson et al., 2010; Cao et al., 2011a). However, it remains to be determined whether shortened telomeres alone are sufficient to recapitulate HGPS. Another study suggests that the accelerated aging phenotype is associated with stem cell exhaustion via hyperactivation of Notch signaling (Scaffidi and Misteli, 2008). While there does not seem to be a consensus on progerin's most deleterious downstream effect, a recent report proposes a new strategy that targets progerin itself. Treatment of HGPS fibroblasts with the mTOR inhibitor rapamycin reverses proliferation defects and nuclear abnormalities by increasing autophagy-mediated degradation of progerin (Cao et al., 2011b).

Recently, iPSC-based models of HGPS have been established, allowing for study of the disease in multiple cell types beyond fibroblasts. For instance,

reprogramming of HGPS patient fibroblasts to iPSCs demonstrates a lack of disease-related phenotypes at the pluripotent stage (Liu et al., 2011b; Niedernhofer et al., 2011). While this finding is not surprising due to the known developmental regulation of lamin A and progerin expression (Röber et al., 1989), it shows that the iPSC model can mimic the onset of the disease, recapitulating the latency of the disease phenotypes observed in these patients. With differentiation of HGPS iPSCs, lamin A and progerin are upregulated to tissue-dependent levels. This upregulation rapidly triggers nuclear abnormalities, senescence, and general age-related dysfunction in mesenchymal stem cells, fibroblasts, and vascular smooth muscle cells but not in endothelial cells or neural stem cells, which led to the hypothesis that the segmental phenotype of HGPS is due to the low levels of progerin found in some tissues (Zhang et al., 2011).

Progerin and Normal Aging

HGPS recapitulates many of the hallmarks of aging, but it is still unclear exactly how closely HGPS mimics normal aging. Interestingly, the *LMNA* cryptic splice site is recognized even in the absence of the HGPS c.1824C>T mutation, giving rise to low levels of progerin in healthy individuals. In fact, a similar age-associated marker profile has been observed in fibroblasts from normally aged donors compared to HGPS donors (Cao et al., 2007; Scaffidi and Misteli, 2006). Whether these similarities result from age-related increases in progerin levels is uncertain due to inconsistent reports (Mcclintock et al., 2007; Rodriguez et al.,

2009; Scaffidi and Misteli, 2006). However, many of the age-associated phenotypes including nuclear morphology abnormalities and loss of heterochromatin appear to be progerin-dependent in fibroblasts from normally aged donors, for expression of an antisense oligonucleotide to block the progerin cryptic splice site reverts these phenotypes to a young-like state (Scaffidi and Misteli, 2006). Because of the differential expression of lamin A and progerin in different tissues, it remains to be determined whether progerin has relevance to aging in the brain and blood where expression levels are low (Chambers et al., 2007; Lin and Worman, 1997; Röber et al., 1989). Nevertheless, the potential universal link between progerin and normal aging warrants further study.

Thesis Aims

The objective of this study was to define an induced aging strategy to drive age-related markers in iPSC-derived somatic cells and to use this strategy in iPSC-based modeling of Parkinson's disease to reveal late-onset phenotypes.

In Chapter 3, we describe age-related markers that stratify young donor fibroblasts from old donor fibroblasts. We then establish induced pluripotent stem cells (iPSCs) from young donor fibroblasts, old donor fibroblasts, and HGPS patient fibroblasts using overexpression of *OCT4*, *SOX2*, *KLF4*, and *c-MYC* via Sendai virus. We reassess age-related markers in the iPSCs, and, similar to other reports but with a distinct set of markers, we demonstrate the rejuvenation of old donor fibroblasts to a young-like state.

In Chapter 4, we differentiate the iPSCs derived from young, old, and HGPS donors to a fibroblast-like cell type and reassess the set of age-related markers defined in Chapter 3. We demonstrate that differentiation of old iPSCs to fibroblasts is insufficient to reestablish the age-related markers that characterize the donor cells. In contrast, we find that HGPS iPSC-derived fibroblasts reestablish the age/disease-related markers that were erased at the iPSC stage, suggesting that the high upregulation of progerin during differentiation is sufficient to trigger these markers.

In Chapter 5, we define an induced aging strategy that uses synthetic mRNA (modified-RNA) to overexpress progerin in iPSC-derived fibroblasts. We demonstrate that short-term application of progerin modified-RNA is sufficient to induce age-related markers in both young and old iPSC-derived fibroblasts.

In Chapter 6, we differentiate young and old iPSCs to mDA neurons and describe the use of modified-RNA to overexpress progerin in these cells. We demonstrate that both young and old iPSC-derived mDA neurons express a subset of age-related markers following progerin overexpression that overlap with the results described in Chapter 5. We further define neuronal-specific age-related markers induced by progerin.

In Chapter 7, we differentiate iPSCs derived from healthy donors and donors with Parkinson's disease (PD) to mDA neurons. We establish that PD iPSC-derived mDA neurons appear highly similar to iPSC-derived mDA neurons from healthy donors and that progerin overexpression is necessary to reveal disease-related differences both in vitro and in vivo.

Our results offer a strategy that represents a first attempt towards establishing more relevant disease models of late-onset disorders.

CHAPTER TWO

Materials and Methods

Generation and Characterization of iPSCs

Fibroblasts were purchased from Coriell (Camden, NJ) and reprogrammed based on a protocol modified from Fusaki et al. (Fusaki et al., 2009) using CytoTune Sendai viruses expressing OCT4, SOX2, KLF4, and c-MYC (OSKM; Life Technologies, Carlsbad, CA). Briefly, fibroblasts were plated onto gelatin at 10,500 cells per cm^2 per well of a 12-well plate in Minimal Essential Medium Alpha (Life Technologies) supplemented with 15% fetal bovine serum (Life Technologies). CytoTune viruses were combined at an MOI of 10 and added to the fibroblasts on the following day (notated as day 0) as well as on day 2 in some cases. Medium was replaced approximately 16 hours after addition. On day 4 fibroblasts were harvested by trypsinization and reseeded at 10,500 cells per cm^2 onto mitomycin C-treated mouse embryonic fibroblasts (MEFs; Global Stem, Rockville, MD) in iPSC maintenance medium containing DMEM-F12, 20% knockout serum replacement (Life Technologies), L-glutamine, non-essential amino acids, β-mercaptoethanol, and 10 ng/ml FGF2 (R&D) supplemented with 10 μM Rho-kinase inhibitor (Y-27632; Tocris, Bristol, UK) to support attachment. The medium was replaced every other day thereafter. Valproic acid (Sigma, St Louis, MO) was added to the medium at a final concentration of 1 mM from day 6 to day 13 to enhance the reprogramming efficiency as described previously (Huangfu et al., 2008). In addition, the cells were cultured in 5% oxygen from 1 week prior to transduction through 2.5 weeks after transduction to further improve the likelihood of iPSC colony formation (Yoshida et al., 2009). HGPS fibroblasts were also treated with rapamycin (Sigma) at 680 nM from 1 week prior to transduction

until the first appearance of iPSC colonies in order to reduce HGPS phenotypes (Cao et al., 2011b), which can act as a barrier to reprogramming. Approximately 30 days after transduction, colonies resembling human embryonic stem cell colonies were mechanically isolated and replated onto MEFs in 24-well plates. iPSC clones were picked from separately transduced wells in order to ensure independent reprogramming events. At least 3 surviving colonies from each starting fibroblast line were subsequently maintained on MEF feeder layers in iPSC medium and passaged approximately every week using dispase (STEMCELL Technologies, Vancouver, BC). Karyotype analysis was performed by the MSKCC Molecular Cytogenetics core facility using standard G-banding procedures. Spontaneous differentiation via embryoid body formation was performed as described previously (Park et al., 2008b). Experiments using iPSCs were performed using 3 independent clones per fibroblast line. All cells (including those listed below) were regularly tested for mycoplasma every 2 to 4 weeks and found to be negative.

iPSCs for PD Modeling

PD iPSCs generated by retroviral overexpression of OSKM from patients with mutations in PINK1 (c.1366C>T, p.Q456XStop) or PARK2/Parkin (c.1072Tdel, p.V324fsX110) were generously provided by the D. Krainc lab (Massachusetts General Hospital, Boston, MA). Apparently healthy iPSCs (C1, age 36; C2, age 48) also established using pMIG retroviruses (OSK, no c-Myc) were obtained from the K. Eggan lab (Harvard University, Cambridge, MA). Additional iPSC clones were derived using Sendai virus from fibroblasts from a patient with a different mutation in PARK2/Parkin (c.924C>T, p.R275W). Young (here called C3) and old (here called C4) iPSCs listed above were used as controls because they were also derived using Sendai virus reprogramming factors.

Fibroblast Differentiation

Differentiation of iPSCs to fibroblast-like cells was based on a protocol from Park et al. (Park et al., 2008b). Briefly, iPSC clones were enzymatically passaged using dispase and plated as multi-cell clumps onto gelatin in iPSC maintenance medium that had been conditioned on MEFs for 24 hours and then supplemented with 10 ng/ml FGF2 and 10 μM Y-27632. The next day the medium was replaced with Minimal Essential Medium Alpha (Life Technologies) supplemented with 15% fetal bovine serum (Life Technologies) and continually changed every other day thereafter. The differentiating cells were carefully passaged every 5-6 days using Accutase (Innovative Cell Technology, San Diego, CA) for the first two weeks and then trypsinized subsequently. Y-27632 was added to the medium on the day of passaging to help support attachment. After four weeks fibroblast-like cells were sorted based on high expression levels of CD-13 and HLA-ABC prior to phenotype assessment and overexpression studies. Sorted cells were expanded in Minimal Essential Medium Alpha with 15% fetal bovine serum (no Y-27632) thereafter.

mDA Neuron Differentiation

A modified version of the dual-SMAD inhibition protocol was used to direct cells towards floor plate-based mDA neurons as described previously (Kriks et al., 2011) and schematized in **Figure 6.2A**. iPSC-derived mDA neurons were replated on day 30 of differentiation at 260,000 cells per cm^2 on dishes pre-coated with polyornithine (PO; 15 μg/ml)/ Laminin (1 μg/ml)/ Fibronectin (2 μg/ml) in Neurobasal/B27/L-glutamine-containing medium (NB/B27; Life Technologies) supplemented with 10 μM Y-27632 (until day 32) and with BDNF (brain-derived neurotrophic factor, 20 ng/ml; R&D), ascorbic acid (AA; 0.2 mM, Sigma), GDNF (glial cell line-derived neurotrophic factor, 20

ng/ml; R&D), TGFβ3 (transforming growth factor type β3, 1 ng/ml; R&D), dibutyryl cAMP (0.5 mM; Sigma), and DAPT (10 nM; Tocris,). One to two days after plating, cells were treated with 1 μg/ml mitomycin C (Tocris) for 1 hour to kill any remaining proliferating contaminants. iPSC-derived mDA neurons were fed every 2 to 3 days and maintained without passaging until the desired time point for a given experiment. PO, laminin and fibronectin were added to the medium every 7-10 days to prevent neurons from lifting off.

Synthetic mRNA (Modified-RNA) Cloning, Synthesis, and Use

Modified-RNA was generated using an in vitro transcription (IVT) protocol described previously (Mandal and Rossi, 2013; Warren et al., 2010). The ORF for progerin was obtained by PCR from HGPS fibroblasts. N-terminal GFP fusion was achieved by inserting the progerin ORF into pAcGFP1-C using InFusion® cloning technology (Clontech, Mountain View, CA). Nuclear GFP was templated from pAcGFP1-Nuc (Clontech). Phosphorylated ORFs were cloned into a backbone already containing generic 5' and 3' UTRs (provided by the D. Rossi lab; Harvard Medical School, Boston, MA). Tail PCR and IVT reactions were carried out as described previously (Mandal and Rossi, 2013). For overexpression experiments, modified-RNA was thawed on ice and adjusted to a working concentration of 100ng/μl. Modified-RNA and Lipofectamine RNAiMAX® (Life Technologies, 1 μg modified RNA:3 μl Lipofectamine) were initially prepared in Opti-MEM separately, gently mixed and incubated at room temperature for 10 minutes. The Lipofectamine mixture was then transferred to the tube containing the modified-RNA mixture, gently mixed and incubated for an additional 10 minutes. 1 μg of modified-RNA was added per 80,000 fibroblasts in a single 24-well. 200 ng of modified-RNA was added per 100,000 neurons in a single 96-well. The transfection mixture was

added dropwise to cells that had been pre-treated with 200 ng/ml of the interferon inhibitor B18R (eBioscience, San Diego, CA) for at least 4 hours prior to transfection. After 4 hours at 37°C, the entire suspension was replaced with fresh medium supplemented with B18R. Transfection of iPSC-derived fibroblasts was performed starting on day 50 of differentiation and repeated on 2 consecutive days thereafter. iPSC-derived mDA neurons were transfected starting on day 65 or day 120 of differentiation and repeated on 4 consecutive days thereafter. The additional 2 days of transfections were required in order to establish a progerin expression levels equivalent to the iPSC-derived fibroblasts. All cells were analyzed one day after the final transfection.

Immunostaining

Cells. Cells were fixed in 4% paraformaldehyde for 15 minutes. Blocking was performed in phosphate-buffered saline supplemented with 1% BSA, and 0.3% Triton X-100 for 30 minutes to 1 hour. Cells were stained overnight at 4°C with primary antibodies diluted in blocking buffer. A list of antibodies and concentrations is provided in **Table 2.1**. Following several washes, cells were stained with appropriate Alexa Fluor-labeled secondary antibodies (Molecular Probes, Carlsbad, CA) at 1:500 in blocking buffer for 30 minutes to 3 hours at room temperature. Cells were counterstained with 4′,6-diamidino-2-phenylindole (DAPI; Thermo Fisher, Rockford, IL) to visualize nuclei. Images were acquired with an Olympus IX81 microscope using a Hamamatsu ORCA CCD camera.

Human Cortex Tissue. 5 µm paraffin-embedded human cortex tissue sections obtained from the National Disease Research Interchange (Philadelphia, PA) were deparaffinized in a microwave and hydrated prior to antigen retrieval in 10 mM citrate buffer (pH 6.4) for 15 minutes. Sections were stained as above.

Antigen	Company	Host	Concentration
p-4EBP1	Cell Signaling	Rabbit	1:1000 (WB)
4EBP1 (total)	Cell Signaling	Rabbit	1:1000 (WB)
p-AKT	Cell Signaling	Rabbit	1:250 (WB)
AKT (total)	Cell Signaling	Rabbit	1:1000 (WB)
CD13-PE	BD		20 ul per 1 M cells (FC)
Cleaved caspase-3	Cell Signaling	Rabbit	1:100 (ICC)
FOXA2	Santa Cruz	Goat	1:200 (ICC)
GFP	Abcam	Chick	1:2000 (WB, IHC)
GFP	Aves	Chick	1:3000 (EM)
γH2AX	Millipore	Mouse	1:250 (ICC)
H3K9me3	Abcam	Rabbit	1:4000 (ICC)
HLA-ABC-APC	BD		20 ul per 1 M cells (FC)
HP1γ	Millipore	Mouse	1:200 (ICC)
Ki67	Dako	Mouse	1:100 (ICC)
Lamin A	Abcam	Rabbit	1:100 (ICC)
Lamin A/C (clone JOL2)	Abcam	Mouse	1:200 (ICC)
Lamin A/C (clone N-18)	Santa Cruz	Goat	1:100 (WB)
Lamin B2	Abcam	Mouse	1:500 (ICC)
Lamin C	Abcam	Rabbit	1:100 (ICC)
LAP2α	Abcam	Rabbit	1:500 (ICC)
LMX1A	Millipore	Rabbit	1:2000 (ICC)
MAP2	Sigma	Mouse	1:200 (ICC)
NANOG	R&D	Goat	1:50 (ICC)
Nestin	R&D	Mouse	1:300 (ICC)
NURR1	R&D	Mouse	1:1000 (ICC)
OCT4	Santa Cruz	Mouse	1:200 (ICC)
Sendai	MBL Int.	Rabbit	1:500 (ICC)
SSEA3-FITC	BD		20 ul per 1 M cells (FC)
SSEA4-PE	BD		20 ul per 1 M cells (FC)
Total AKT	Cell Signaling	Rabbit	1:500 (WB)
TUJ1	Covance	Mouse/Rabbit	1:500 (ICC)
Tyrosine hydroxylase (TH)	Pel-Freez	Rabbit	1:500 (ICC, IHC, WB)
TH	Immunostar	Mouse	1:2000 (EM)
p-ULK1	Cell Signaling	Rabbit	1:500 (WB)
ULK1 (total)	Cell Signaling	Rabbit	1:1000 (WB)
Vimentin-Cy3	Sigma		1:200 (ICC)

Table 2.1 Antibodies used for molecular analyses. Antibodies and their respective vendor information and concentration are listed. EM, electron microscopy; FC, flow cytometry; ICC, immunocytochemistry; IHC, immunohistochemistry; WB, western blot.

Mouse Brain Tissue. Three months after transplantation of human iPSC-derived mDA neurons, mice received overdoses of Pentobarbital intraperitoneally (50 mg/kg) to induce deep anesthesia and were perfused in 4% paraformaldehyde (PFA). Brains were extracted, post-fixed in 4% PFA then soaked in 30% sucrose solutions for 2-5 days. The tissue was sectioned (30 µm) on a cryostat after embedding in O.C.T. (Sakura-Finetek, Torrance, CA). For immunostaining of mouse tissue for electron microscopy, see below.

Immunostaining Quantification

In Vitro Cells. Images were acquired on an Operetta (PerkinElmer, Waltham, MA) using a 20X objective. Image processing was performed using Harmony high content analysis software (version 3.0). Passage-matched cells were scored from three independent experiments. Where necessary due to bias against progerin-positive cells, images were processed using ImageJ software (version 1.43u, NIH). In these cases, 50 cells per condition were assessed for each independent experiment. All data are presented as mean ± standard error of means (SEM).

In Vivo Mouse Brain Tissue. Cell counts were determined using the optical fractionator probe and the Cavalieri estimator using the Stereo Investigator software (MBF bioscience, Vermont) as described previously (Tabar et al., 2005). Cell counts were scored on every fifth section where a graft was identifiable using a randomized grid. Counts were determined from three animals per condition. Data are presented as estimated total cell number ± SEM.

Assessment of Senescence

Senescence-activated beta-galactosidase was assessed using the staining kit from Cell Signaling according to the manufacturer's instructions. Positive cell staining was manually assessed (2 replicates, 50 cells each).

Flow Cytometry

Cells were dissociated with Accutase and stained with directly conjugated antibodies (BD Biosciences, San Jose, CA) according to manufacturer-recommended concentrations for 1 hour on ice. Antibodies are listed in **Table 2.1**. Cell sorting was performed on a FACSAria (BD Biosciences).

Mitochondrial ROS Assessment

Cells were dissociated with Accutase and stained with MitoSOX Red mitochondrial superoxide indicator (Life Technologies) at a final concentration of 20 μM in cell culture medium. Staining was carried out in a 37°C incubator for 30 minutes. Cells were washed and resuspended in cell culture medium containing DAPI to exclude dead cells from the analysis. In order to prevent positive staining due to cell shock, all reagents used were pre-warmed to 37°C and samples were kept at 37°C until just prior to analysis on a FACSAria. Samples were always compared to untreated young donor fibroblasts/iPSC-derived firboblasts/iPSC-derived mDA neurons as well as the young donor cells treated with 20 μM carbonyl cyanide 3-chlorophenylhydrazone (CCCP; Sigma) for 48 hours to induce mitochondrial superoxide production. These controls helped to ensure that the reagent had not become oxidized over time and that the cells were not stressed during the staining protocol. Quantification of the percent of the population that oxidized the MitoSOX reagent was performed using FlowJo software (version 9.5.3; Tree Star) and

averaged for at least three independent clones or experiments per condition. All data from an individual experiment were excluded from analysis when the negative control sample gave an entirely positive reading by flow cytometry, suggesting that the conditions or the reagent itself were compromised.

DNA Extraction and Mutation Analysis

Genomic DNA was extracted from cell pellets using the DNeasy blood and tissue kit (Qiagen). A small region around the mutation was PCR amplified using HiFi Hotstart (KAPA Biosystems) per the manufacturer's instructions (for primers used see **Table 2.2**). PCR products were cleaned up using standard phenol/chloroform extraction and ethanol precipitation. DNA sequencing of PCR products was performed by the MSKCC DNA Sequencing core facility or GENEWIZ (South Plainfield, NJ).

RNA Extraction and Gene Expression Analysis

Cells were lysed directly in Trizol (Life Technologies). RNA was extracted using chloroform and ethanol precipitation and further cleaned using the RNeasy kit (Qiagen). Samples were stored at -80°C until further processing. Total RNA was reverse transcribed (Superscript, Life Technologies) and 50 ng of RNA was used to template each RT-PCR reaction. For analysis of progerin expression levels, total RNA was hydrolyzed by 0.1X volume 5 M NaOH for 30 minutes at room temperature followed by 0.1X volume 5 M HCl (Scaffidi and Misteli, 2006). Quantitative RT–PCR was performed using the Mastercycler RealPlex2 (Eppendorf, Hauppauge, NY) platform following the manufacturer's instructions. Expression levels were normalized to cyclophillin A or 18S (housekeeping gene controls) as noted. For RNA-seq, total RNA was isolated from two independent experiments and processed by the MSKCC Genomic core facility. Paired-

Name	Application	Sequence (5' → 3')	Reference
cyclophilin A	qRT-PCR (SYBR)	F: GTCAACCCCACCGTGTTCTT R: CTGCTGTCTTTGGGACCTTGT	
GFP-progerin ORF	Modified RNA cloning	F: P-TGGTGAGCAAGGGCGCCGAGCTG R: P-TTACATGATGCTGCAGTTCTG	
lamin A	qRT-PCR (SYBR)	F: GCTCTTCTGCCTCCAGTGTC R: ACATGATGCTGCAGTTCTGG	
lamin C	qRT-PCR (SYBR)	F: CTCAGTGACTGTGGTTGAGGA R: AGTGCAGGCTCGGCCTC	
LMNA	Mutation sequencing	F: CTGAGCCTTGTCTCCCTTCC R: none	
LMNA exons 9-12	RT-PCR	F: GTGGAAGGCACAGAACACCT R: GTGAGGAGGACGCAGGAA	(Scaffidi and Misteli, 2006)
nuclear-GFP ORF	Modified RNA cloning	F: P-TGGTGAGCAAGGGCGCCGAGCTG R:P-TTATCTAGATCCGGTGGATCCTACC	
Parkin (c.1366C>T)	Mutation sequencing	F: GAAACTGGTTAAGCAAGAAATCC R: none	
PINK1 (c.1072delT)	Mutation sequencing	F: TGTGCAGGACATGAAAAGGT R: none	
progerin	qRT-PCR (SYBR)	F: GCGTCAGGAGCCCTGAGC R: GACGCAGGAAGCCTCCAC	
progerin ORF	Cloning into pAcGFP1-C	F:aaggcctctgtcgacAGCAGTCTCTGTCCTTCGACCC R:agaattcgcaagcttCTTCCACCTCCCACCTCATTCC	
Tail PCR	Modified RNA cloning	F:TTGGACCCTCGTACAGAAGCTAATACG	(Warren et al., 2010)

		R:(Tx120)CTTCCTACTCAGGCTTTATTC AAAGACCA	

Table 2.2 Sequences of primers used for sequencing, PCR analysis and RNA generation. Primers were synthesized by Sigma.

end 75 base pair RNA-sequencing libraries were sequenced on an Illumina HiSeq2000. Reads were mapped to the human genome (Hg19) using STAR 2.3.0e (Dobin et al., 2013) with default mapping parameters and read counts were assessed using HTSeq. Principal component analysis was completed in R (v2.15.2) using the base "stats" package. Differentially expressed genes were identified with limma voom (Smyth, 2004). A conservative approach was taken to account for low coverage in the sequencing library; a low read count filter was used such that all samples must contain non-zero read counts for a gene to be assessed in limma. Differentially expressed genes were identified using a fold change cut off of +/- 2 and a Bonferroni adjusted p value of 0.05. A hypergeometric test was used to assess the similarity in response to progerin overexpression in young donor and old donor iPSC-derived mDA neurons. Gene ontology analysis was completed using iPAGE (Goodarzi et al., 2009) with the fold change between nuclear-GFP and GFP-progerin expressing iPSC-derived mDA neurons as a continuous variable across 10 bins. Venn-diagrams, barplots, and PCA plots were generated in R (v2.15.2) using the base R 'ggplot2' graphics packages (Wickham, 2009). Raw data are available on Gene expression omnibus http://www.ncbi.nlm.nih.gov/geo/ (GSE52431).

Protein Isolation and Western Blot Analysis

Cells were collected with a cell lifter (Corning, Tewksbury, MA) in ice-cold phosphate-buffered saline without calcium or magnesium (PBS-/-). Cell pellets were rapidly frozen on ethanol and dry ice and stored at -80°C. Cell pellets were thawed on ice and resuspended in 50-200 µl RIPA lysis buffer (50 mM Tris-HCl pH 8.0, 120 mM NaCl, E mM EDTA, 0.5% NP-40) with 1% sodium dodecyl sulfate (SDS). Cell suspensions were vortexed at 15-minute intervals during a 45-minute incubation on ice. Lysates were

isolated following a 10,000 rpm spin for 10 minutes at 4°C. 20-40 µg samples were further diluted with 4X Laemmli sample buffer, boiled for 5 minutes at 95°C, and loaded onto a NuPAGE 4-12% Bis-Tris precast gel (Life Technologies). Gel electrophoresis was performed at 100 V for 2 hours. Gels were transferred to a methanol-activated PVDF membrane using the XCell II Blot Module (Life Technologies) according to the manufacturer's instructions. Blots were blocked in 3% bovine serum albumin (BSA) in Tris-buffered saline plus 0.1% Tween-20 (TBS-T) for 45 minutes at room temperature. Blots were incubated in primary antibodies overnight at 4°C on shaker (see **Table 2.1** for a list of antibodies used). Following several washes with TBS-T, blots were incubated in appropriate HRP-labeled secondary antibodies (Jackson ImmunoResearch, West Grove, PA) for 1 hour at room temperature. Visualization of protein bands was performed using Western Lightning Plus-ECL (PerkinElmer, Melville, NY) according to the manufacturer's instructions and developed on an SRX-101A x-ray film processor (Konica Minolta, Wayne, NJ). Densitometry quantification was performed using ImageJ on blots from three independent experiments.

Neurite Quantification

Following immunostaining with MAP2 to label dendrites, randomly chosen images of GFP+ cells were manually acquired on an Olympus IX81 microscope using a Hamamatsu ORCA CCD camera using a 40X objective. Dendrite lengths were measured using ImageJ to trace each labeled neurite extending from GFP+ nuclei. Cells with only perinuclear MAP2 staining were given a zero. GFP+ nuclei without MAP2 staining as well as cells with condensed GFP+ nuclei were not scored. Fifty cells per condition were assessed for each of three independent differentiations.

In Vivo Assessment

Transplantation. Animal procedures were performed following NIH guidelines and were approved by the local Institutional Animal Care and Use Committee (IACUC), the Institutional Biosafety Committee (IBC) as well as the Embryonic Stem Cell Research Committee (ESCRO). Six-week-old *NOD-SCID IL2Rgc*-null mice (20–35 g; Jackson Laboratory, Bar Harbor, ME) were anesthetized with Ketamine (90 mg/kg; Akorn, Decatur, IL) and Xylazine (4 mg/kg Fort Dodge, IA). 10 µg 6- hydroxydopamine (6-OHDA (Sigma-Aldrich) was injected stereotactically into the striatum of 6-week-old mice at the following coordinates (in millimeters): AP, 0.5 (from bregma); ML, -2.0; DV, -3.0 (from dura). Two weeks after lesioning, mice were tested twice (1 week apart) for rotational behavior (see below). Animals were divided into six groups so that those demonstrating high/low rotations were evenly distributed among the groups and then randomly assigned to a particular group. Y.M.G. was blind to the naming of the experimental groups. An initial sample size of 5 animals per condition was chosen to allow for analysis of at least 3 animals per group at the 3-month time point. Control (C1) and PD mutant (PINK1-Q456X, Parkin-V324A) iPSC-derived mDA neurons were infected with lentiviral vectors expressing either *hSyn::GFP-progerin* or *hSyn::nuclear-GFP* (based on an *hSyn::YFP* plasmid kindly provided by the K. Deisseroth lab) on day 21 of differentiation and transplanted on day 30 (animals approximately 2.5-months-old at time of transplantation). A total of 200 x 10^3 cells were injected in a volume of 2 µl into the striatum at the following coordinates (in mm): AP, 0.5; ML, -1.8; DV, 3.2.

Rotation testing. Amphetamine-induced rotation testing was performed before transplantation and 12 after transplantation. Rotation behavior in mice was recorded 10 min after i.p. injection of d-amphetamine (10 mg/kg, Sigma) and recorded for 30 minutes. The data were presented as the average number of rotations per minute.

Electron Microscopy

All procedures were performed according to (Milner et al., 2011). Briefly, six months following transplantation of human iPSC-derived mDA neurons, mice were overdosed with 150 mg/kg sodium pentobarbital intraperitoneally. The brains were fixed by aortic arch perfusion sequentially with normal saline (0.9%) containing 1000 units /ml of Heparin, 50 ml of 3.75% acrolein and 2% paraformaldehyde in 0.1 M phosphate buffer (PB, pH 7.4), and 200 ml of 2% PFA in PB. The brains were removed and post-fixed with 1.87% acrolein/2% PFA in PB for 30 minutes at room temperature. Coronal tissue blocks were sectioned (40 µm) on a vibrating microtome (Leica Microsystems, Deerfield, IL). Selected sections containing the xenograft were pretreated in 1% sodium borohydride. Non-specific binding was blocked with 0.5% BSA 0.1 M Tris-saline (TS, pH 7.6). Primary antibodies (see **Table 2.1**) were diluted in 0.1% BSA in TS and incubated overnight at 4°C. Sections were incubated with a biotinylated secondary antibody (Jackson ImmunoResearch, West Grove, PA) for 30 minutes at room temperature. Peroxidase labeling was performed using the Vectastain ABC kit (Vector Laboratories, Burlingame, CA) followed by incubation with diaminobenzidine for 7 minutes. Sections were then incubated in gold-conjugated secondary antibody (Electron Microscopy Sciences (EMS), Fort Washington, PA) overnight at 4°C. Sections were post-fixed in 2% glutaraldehyde, washed in 0.2M citrate buffer (pH 7.4), and silver intensified using the Silver IntenSE M kit (GE Healthcare, Piscataway, NJ). Following several washes, sections were fixed in 2% osmium tetroxide for 1 hr, dehydrated through an ascending ethanol series, and placed in propylene oxide/EMBed 812 (EMS) overnight. Sections were then embedded in EMBed 812 between two sheets of Aclar plastic at 60°C for 4 days. Selected sections containing the graft were glued on Beem capsules and cut on an ultramicrotome (Ultracut) using a glass knife (Leica). Ultrathin sections were collected on grids and counterstained with uranyl acetate and Reynold's lead citrate. Final

preparations were examined and photographed using a Phillips C10 transmission electron microscope. The number of TH-immunogold particles per μm^2 in 25 dendrites per group and the area (μm^2) quantification of 25 mitochondria per group were performed using ImageJ.

Statistical Analysis

Frequency distribution plots display the fluorescence intensity quantification of 100 cells (fibroblasts) or 50-100 cells from each of 3 independent experiments (all others) binned by 50 or 100 arbitrary unit increments. Distributions were compared by statistical analysis of corresponding cumulative distributions using Kolmogorov-Smirnov tests to analyze the difference between different ages or treatments. Arbitrary units for frequency distributions of different cell types should not be compared because staining was performed at different times. Bar graphs are plotted as mean ± SEM and represent 3 biological replicates except where noted. Technical replicates were averaged prior to being included in statistical analysis (i.e. average of technical replicates for 1 experiment = 1 biological replicate). Two-group comparisons were analyzed using Student t-tests. Multiple group comparisons against a control were analyzed using an ANOVA with Dunnett's test. Prism (version 6.0a, GraphPad) was used for data presentation and analysis.

CHAPTER THREE

Reprogramming Rejuvenates Old Donor Fibroblasts by Erasing Age-Related Markers

Introduction

In order to reconcile the lack of disease-related phenotypes in iPSC-based models of late-onset disease despite the presence of the disease-causing mutation, we hypothesized that the iPSC-derived cells were simply too young to mimic the disease. In fact, it has been suggested that fibroblasts from aged donors may be reset to a young-like state following reprogramming (reviewed in (Freije and López-Otín, 2012; Liu et al., 2012a; Mahmoudi and Brunet, 2012)). However, these data were limited to increased telomere length (Agarwal et al., 2010; Marion et al., 2009), improved mitochondrial fitness (Prigione et al., 2010; Prigione et al., 2011; Suhr et al., 2010), and loss of senescence markers (Lapasset et al., 2011).

A key problem in addressing global aspects of aging and rejuvenation during cell reprogramming is the identification of markers that reliably measure age in vitro. Candidate age-related cellular markers have been described in fibroblasts derived from prematurely aged Hutchinson-Gilford progeria syndrome (HGPS) patients where disease is caused by high levels of progerin expression (Goldman et al., 2004; Scaffidi and Misteli, 2005, 2006). These markers define nuclear morphology and organization, heterochromatin, DNA damage, and mitochondrial

dysfunction. Interestingly, low levels of progerin are expressed in healthy individuals, and a similar age-associated profile has been observed in fibroblasts from normally aged donors compared to HGPS patient fibroblasts (Cao et al., 2007; Scaffidi and Misteli, 2006).

Results

Defining an Age Marker Profile in Donor Fibroblasts

In order to validate a marker profile that could be followed during reprogramming and re-differentiation, we compared 12 passage-matched fibroblast populations from apparently healthy young donors (age 11), middle-aged donors (ages 31-55), old donors (ages 71-96), and prematurely aged donors with HGPS (ages 3-14) (**Table 3.1**). We observed a significant correlation of donor fibroblast age with age-associated markers (**Figure 3.1**), including markers previously described in HGPS fibroblasts (Scaffidi and Misteli, 2006). Furthermore, fibroblasts from old donors resembled HGPS fibroblasts rather than young donor fibroblasts (**Figure 3.2**), supporting previous findings by Misteli and colleagues (Scaffidi and Misteli, 2006). More specifically, old donor fibroblasts showed nuclear morphology abnormalities (i.e. folding and blebbing), loss of the nuclear lamina-associated protein LAP2α, global loss of the heterochromatin markers trimethylated H3K9 (H3K9me3) and heterochromatin protein 1 gamma (HP1γ) (**Figure 3.1 and Figure 3.2A**), as well as an increase in DNA damage and mitochondrial reactive oxygen species (mtROS) levels (**Figure 3.2B**) when compared to fibroblasts from younger donors. These data suggest that these age-associated markers can

Mutation status	Age	Coriell ID	Sex	Source
Young				
Apparently healthy	11 YR	GM01652	Female	Forearm skin
Apparently healthy	11 YR	GM02036	Female	Unspecified
Apparently healthy	11 YR	GM01864	Male	Unspecified
Middle-Aged				
Apparently healthy	31 YR	AG16146	Male	Arm skin
Apparently healthy	40 YR	GM02153	Female	Unspecified
Apparently healthy	55 YR	GM00967	Male	Arm skin
Old				
Apparently healthy	71 YR	GM01680	Female	Arm skin
Apparently healthy	81 YR	GM04204	Male	Unspecified
Apparently healthy	82 YR	GM01706	Female	Arm skin
HGPS				
HGPS (c.1824C>T)	3 YR	AG06917	Male	Arm skin
HGPS (c.1824C>T)	4 YR	AG06297	Male	Thigh
HGPS (c.1824C>T)	14 YR	AG11498	Male	Thigh

Table 3.1 Summary of apparently healthy and HGPS patient-specific fibroblasts. Fibroblasts were obtained from Coriell Cell Repositories. Donor information was provided by Coriell.

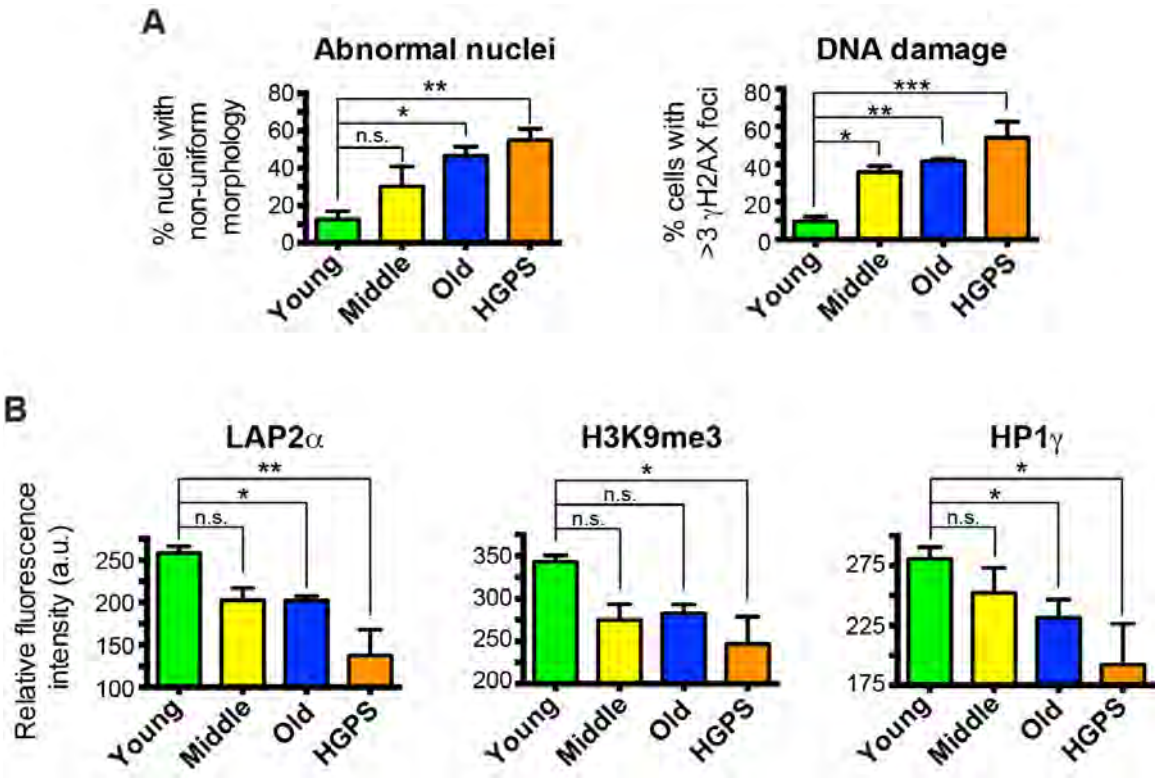

Figure 3.1 An age-associated marker profile that correlates with donor age of fibroblasts. (A and B) Quantification of immunocytochemical analysis of markers associated with aging in fibroblasts obtained from Coriell demonstrates (A) increases in abnormal nuclei and DNA damage and (B) decreases in lamina-associated protein (LAP2α) and markers of heterochromatin (H3K9me3, HP1γ) with age. Young, all 11 years of age; Middle, 31-55 years of age; Old, 71-82 years of age; HGPS (Hutchinson-Gilford progeria syndrome), 3-14 years of age. n= 3 independent donors per group. See Table 3.1 for additional fibroblast donor information.

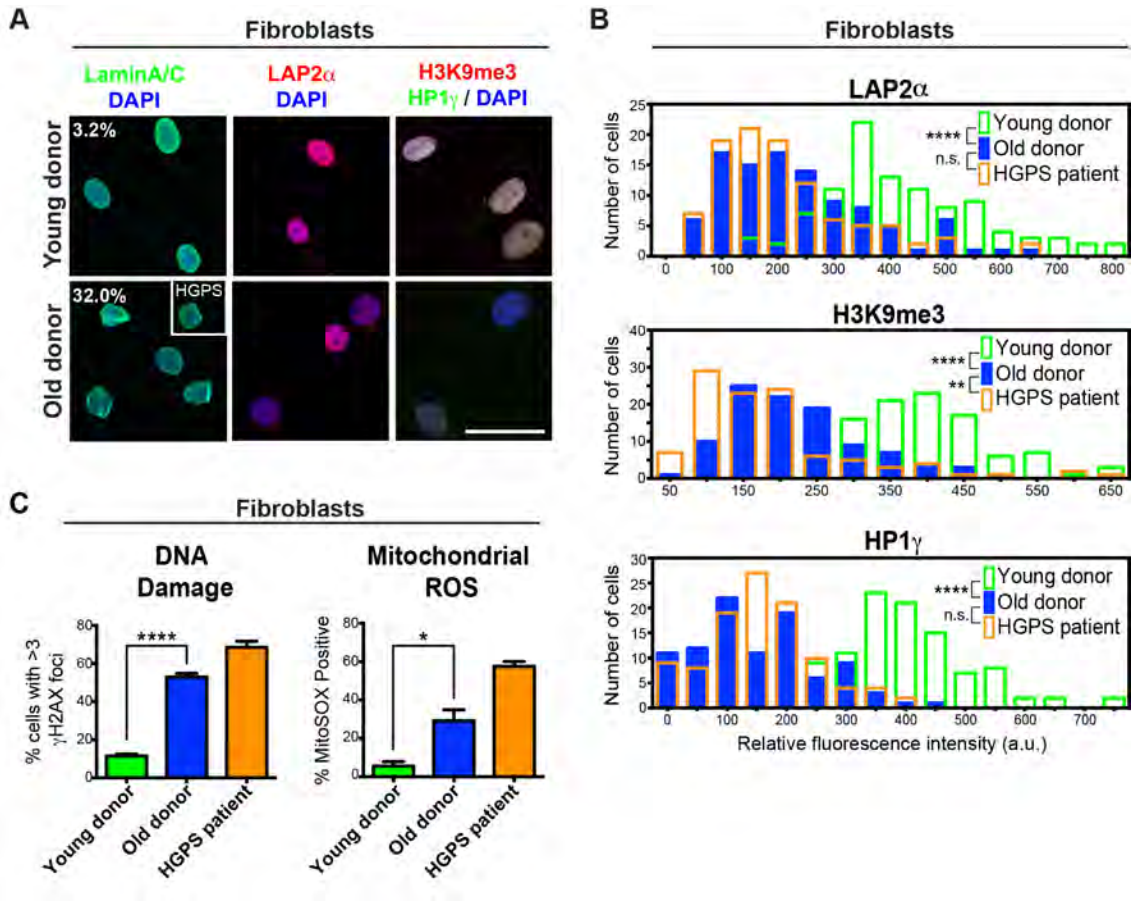

Figure 3.2 Old donor fibroblasts resemble HGPS fibroblasts according to several age-related markers. (A) Immunocytochemistry for markers identifying the nuclear lamina (Lamin A/C), a lamina-associated protein (LAP2α) and heterochromatin (H3K9me3, HP1γ) in young fibroblasts (11-year-old donor) compared to old fibroblasts (82-year-old donor). Percentages indicate the proportion of cells with folded and/or blebbed nuclear morphologies. *Inset:* Example of HGPS fibroblast nuclear morphology. (B) Quantification of the markers depicted in (A) demonstrates the ability of the selected age-associated markers to stratify young versus old donor fibroblasts and the similarity of old donor fibroblasts to HGPS patient fibroblasts. The data are plotted as frequency distributions of relative fluorescence intensity for 100 cells from single fibroblast lines that were passage-matched. a.u., arbitrary units. (C) Similar to HGPS patient fibroblasts, old donor fibroblasts have higher levels of DNA damage (measured by γH2AX immunocytochemistry) and higher levels of mitochondrial reactive oxygen species (ROS; measured by flow cytometry using the superoxide indicator MitoSOX) than young donor fibroblasts. n= 3 independent experiments. n.s. not significant, *p<0.05, **p<0.01, ****p<0.0001 according to Kolmogorov-Smirnov tests (B) or Student's t tests (C). Bar graphs represent mean ± SEM. Scale bar: 50 μm.

faithfully stratify young versus old donor fibroblasts. Importantly, however, phenotypic similarities between old donor and HGPS fibroblasts could not be explained by progerin levels because non-disease old donor fibroblasts expressed very low levels of progerin similar to young donor fibroblasts (**Figure 3.3**).

Reprogramming and Reassessment of Age-Related Markers

To address the effects of reprogramming on markers of cellular age, we selected fibroblasts from young (age 11), old (age 82), and HGPS (age 14) donors and transduced them with Sendai viruses (SeV) individually expressing OCT4, SOX2, KLF4 and c-MYC (OSKM) (Fusaki et al., 2009) (**Figure 3.4**). The use of the cytoplasmic RNA viruses allowed for the derivation of integration-free iPSCs by 25-40 days post transduction. For HGPS patient fibroblasts, it was necessary to treat the cells with rapamycin (**Figure 3.4**), which reduced the negative effects of progerin on proliferation (Cao et al., 2011b), in order to establish iPSC colonies.

From each donor fibroblast line, at least three iPSC clones were picked based on embryonic stem cell-like morphology and subjected to analysis for pluripotent properties following further expansion. At early passages, a few iPSC clones continued to express OSKM exogenously (as indicated by immunocytochemistry for SeV) (**Figure 3.5A**). However, as previously reported (Fusaki et al., 2009), all iPSC clones were free of SeV and endogenously expressing OCT4 by passage

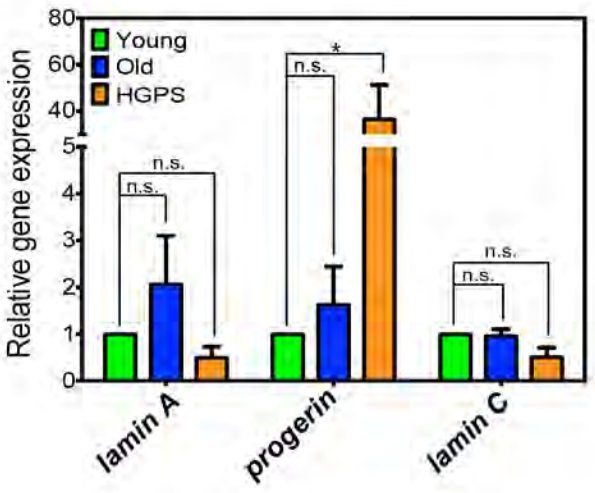

Figure 3.3 Analysis of *LMNA* isoform expression in donor fibroblasts. qRT-PCR for relative lamin A, progerin, and lamin C mRNA transcript levels in young (11-years-old), old (82-years-old), and HGPS (14-years-old) fibroblasts. Expression levels were normalized to those levels observed in the young fibroblasts. Bar graphs represent mean ± SEM. n= 3 independent experiments. n.s. not significant, *p<0.05 according to Student's t tests.

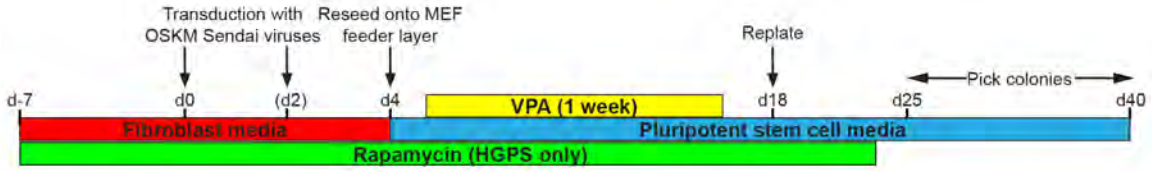

Figure 3.4 Reprogramming schematic. Fibroblasts from young, old, and HGPS donors were reprogrammed using overexpression of OCT4, SOX2, KLF4, and c-MYC (OSKM). Four days after transduction, cells were replated on mouse embryonic fibroblasts (MEFs) in pluripotent stem cell media to promote iPSC formation. Valproic acid (VPA) was added to enhance the reprogramming efficiency as reported (Huangfu et al., 2008). HGPS patient fibroblasts required rapamycin treatment to establish iPSCs.

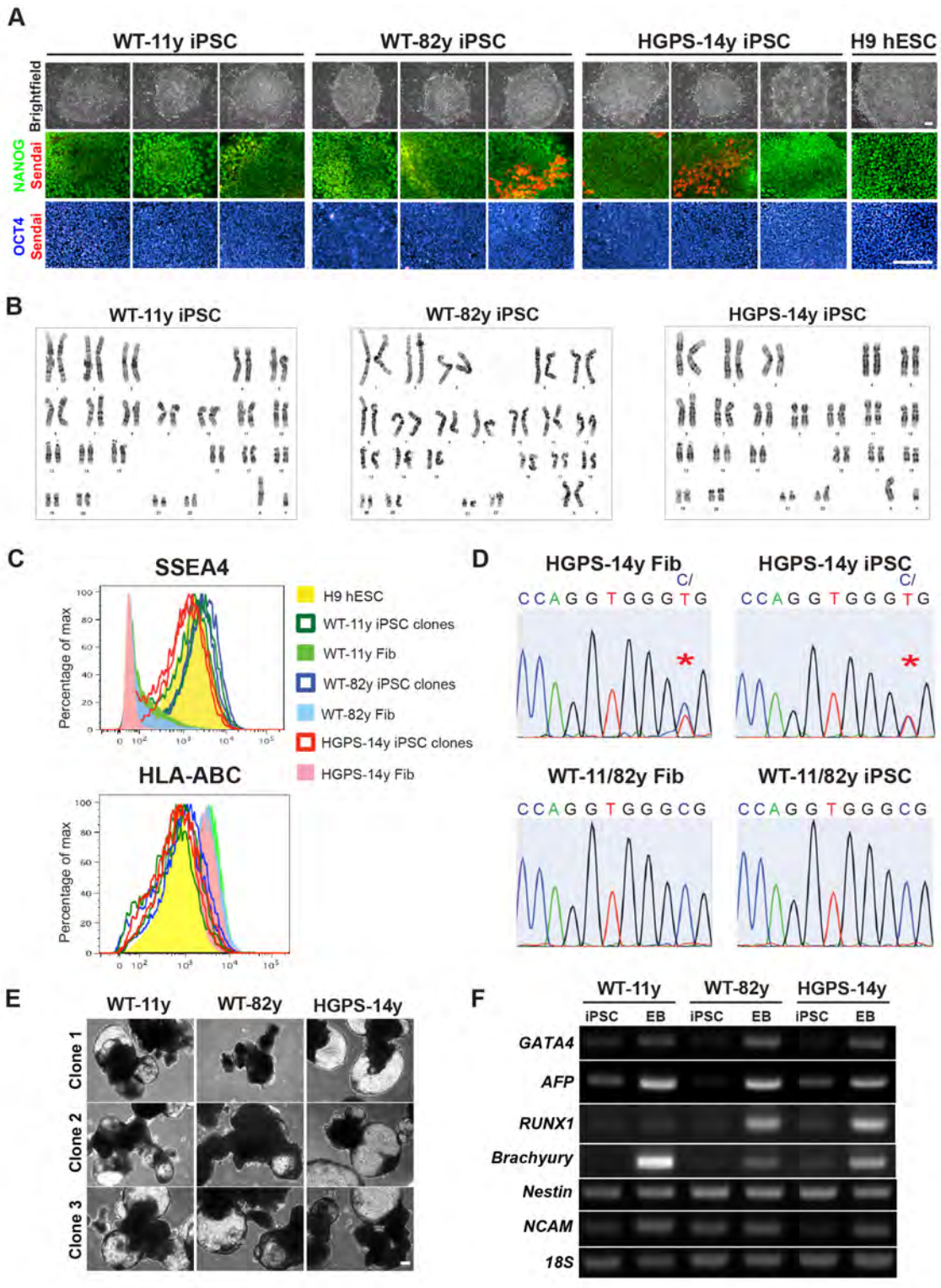

Figure 3.5 Characterization of iPSCs. (A) iPSC clones demonstrated expression of the pluripotency markers NANOG and OCT4 similar to H9 human embryonic stem cells

(hESCs) as well as no signs of residual Sendai expression by passage 10. (B) Karyotype analysis of representative iPSC clones. (C) Flow cytometry analysis of the cell surface markers SSEA-4 and HLA-ABC. (D) Sequencing analysis of the HGPS 1824C>T heterozygous mutation. (E) All iPSC clones are capable of forming embryoid bodies (EBs) upon suspension culture and addition of serum. (F) Gel analysis of RT-PCR for markers indicating the presence of endoderm (*GATA4, AFP*), mesoderm (*RUNX1, Brachyury*), and ectoderm (*Nestin, NCAM*). Scale bars: 200 μm.

10 (**Figure 3.5A**). In addition, iPSC clones demonstrated a normal karyotype (**Figure 3.5B**) as well as increased expression of the cell surface marker SSEA-4 and decreased expression of HLA-ABC compared to the donor fibroblasts (**Figure 3.5C**). iPSCs derived from HGPS patient fibroblasts also maintained the disease mutation (**Figure 3.5D**). Finally, upon suspension culture and addition of serum to the culture medium, all iPSC clones formed embryoid bodies (**Figure 3.5E**) which upregulated markers of the three germ layers (**Figure 3.5F**).

We next reassessed the age-associated molecular markers shown above to distinguish between young and old fibroblasts. iPSCs were not assessed prior to passage 10 to ensure stability of each clone as indicated by loss of SeV expression (**Figure 3.5A**). Following reprogramming, iPSCs which were derived from old donor fibroblasts were indistinguishable from young donor-derived iPSCs with respect to expression of lamin A, LAP2α, H3K9me, and HP1γ (**Figure 3.6A and B**). Furthermore, all iPSCs displayed minimal levels of DNA damage or mtROS (**Figure 3.6C**), suggesting a reset of phenotypic age. However, the age-associated signature could be dependent on progerin expression (Scaffidi and Misteli, 2006) and absence of an age-related phenotype in iPSCs may simply reflect the fact that pluripotent cells do not express A-type lamins including progerin (Constantinescu et al., 2006). Immunocytochemical analysis for all A-type lamin isoforms showed expression restricted to cells undergoing spontaneous differentiation at the periphery of iPSC colonies (**Figure 3.6A**, *left column*). Thus, even HGPS iPSCs demonstrated a comparable loss of age-

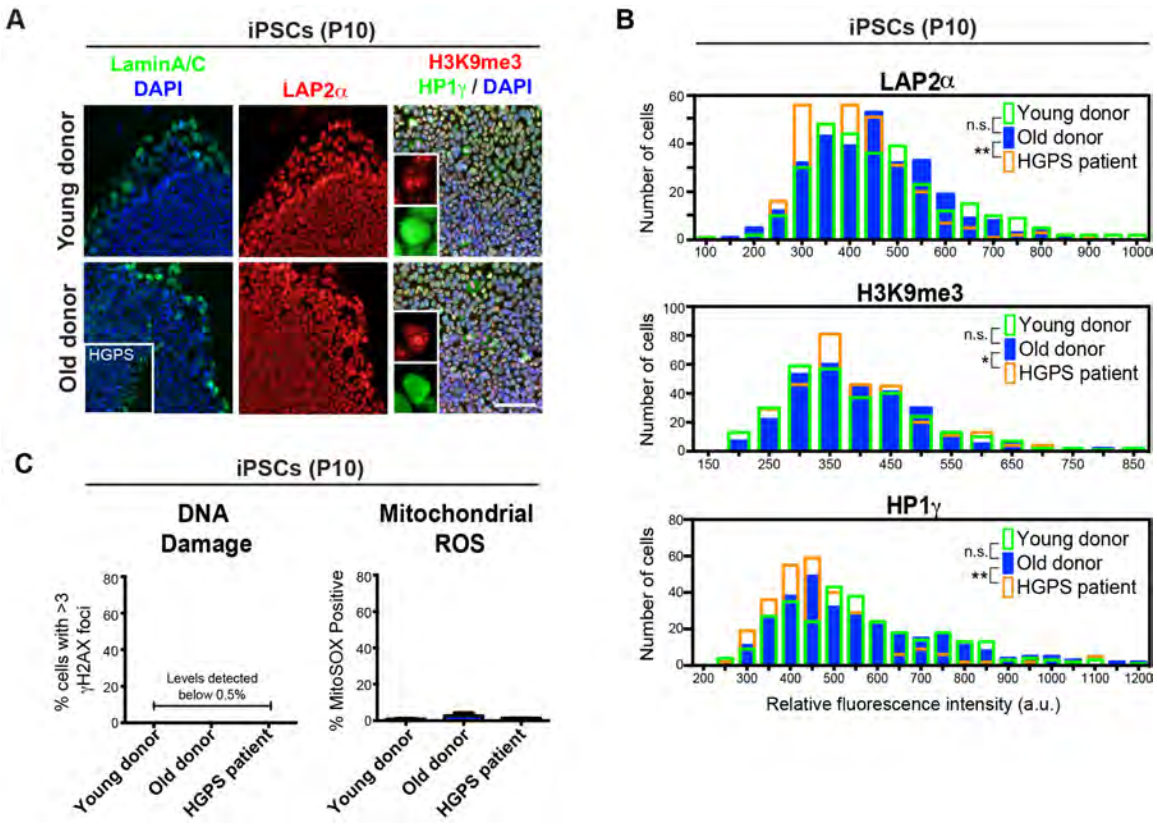

Figure 3.6 Old donor fibroblasts lose age-associated markers following reprogramming to the pluripotent state. (A) Immunocytochemistry for age-associated markers in passage 10 (P10) iPSCs derived from the young and old donor fibroblasts. *Inset*: Example of lamin A/C staining in HGPS iPSCs and zoomed in view of H3K9me3 and HP1γ staining. (B) Quantification of staining in (A) indicates loss of age-associated markers after reprogramming in old donor-derived iPSCs (similar to HGPS-derived iPSCs). n= 300 cells each (100 cells from 3 independent iPSC clones). (C) DNA damage and mitochondrial superoxide levels are reset upon reprogramming. n= 3 independent clones. n.s. not significant, *p<0.05, **p<0.01 according to Kolmogorov-Smirnov tests (B) or Student's t tests (C). Bar graphs represent mean ± SEM. Scale bar: 100 μm.

associated markers at the pluripotent stage (**Figure 3.6B and C**). These results demonstrate that iPSCs, independent of donor age or HGPS status, lack expression of several age-associated markers.

Discussion

We have defined a set of cellular markers that correlate with the chronological age of donor fibroblasts, including markers of nuclear organization, heterochromatin, DNA damage and mitochondrial stress. We also demonstrate a loss of these age-associated markers upon reprogramming, suggesting that the return to pluripotency does not maintain cellular age.

Defining Age-Related Markers

A critical requirement for our study was the identification of markers that predict fibroblast donor age and that can be used to monitor cellular age. While our set of selected age-related markers is not exhaustive, it offers a unique complement to previous studies which had first suggested this reprogramming phenomenon (Agarwal et al., 2010; Lapasset et al., 2011; Marion et al., 2009; Prigione et al., 2010; Suhr et al., 2010). In future studies it will be interesting to consider additional candidate markers, such as methylation levels at particular CpG sites that have been reported to predict donor age across multiple tissues (Hannum et al., 2013; Koch and Wagner, 2011) or methylation patterns reported to reflect epigenetic memory in iPSCs of donor cell fate (Kim et al., 2010; Polo et al., 2010), to determine whether the reset of age occurs uniformly.

Addressing Rejuvenation in the Reprogrammed Cell

Despite the loss of age-related markers in iPSCs derived from old donor fibroblasts, our data do not rule out the possibility that reprogramming selects for cells with low levels of age-related marker expression (a “young” cell) among the heterogeneous old donor fibroblasts rather than truly re-setting age. Interestingly, clonal growth of primary donor fibroblasts resulted in cultures that reestablished a distribution of age-related markers comparable to the original fibroblast population within two weeks (data not shown), suggesting an intrinsic mechanism that maintains donor age. Therefore, it was not possible to obtain fibroblast populations homogeneous in the expression of age-related markers. More elegant lineage tracing methods will need to be considered in order to further address the phenotype of the cell that is reprogrammed. Nevertheless, even though we do not yet understand the mechanism for rejuvenation, it appears that *conventional* reprogramming methods erase at least some aspects of donor age.

CHAPTER FOUR

Memory of Age is Not Triggered by Differentiation of iPSCs Derived from Old Donors

Introduction

Assessment of age-related markers in two highly distinct cell types (donor fibroblasts and their matched iPSCs) may not be a suitable comparison to accurately measure age status. We hypothesized that memory of donor age could simply be suppressed at the pluripotent stage through absence of lamin A and/or progerin expression or through other mechanisms and would thus require differentiation to be revealed. Therefore, proper determination of whether old donor cells indeed retain a memory of their age following reprogramming necessitates comparing cellular age in similar cell fates.

Results

Differentiation of iPSCs to Fibroblast-Like Cells

In order to achieve a cell population that resembled the donor fibroblasts, iPSCs were fed with serum-containing medium and continually passaged until the cells had transitioned to a mesenchymal cell morphology (approximately 30 days) (**Figure 4.1A**). The fibroblast-like cells were then purified by fluorescence-activated cell sorting (FACS) for the fibroblast marker CD13 (Verlinden, 1981) and high expression of HLA-ABC (Papapetrou et al., 2009) (**Figure 4.1B**). $CD13^{+}$/

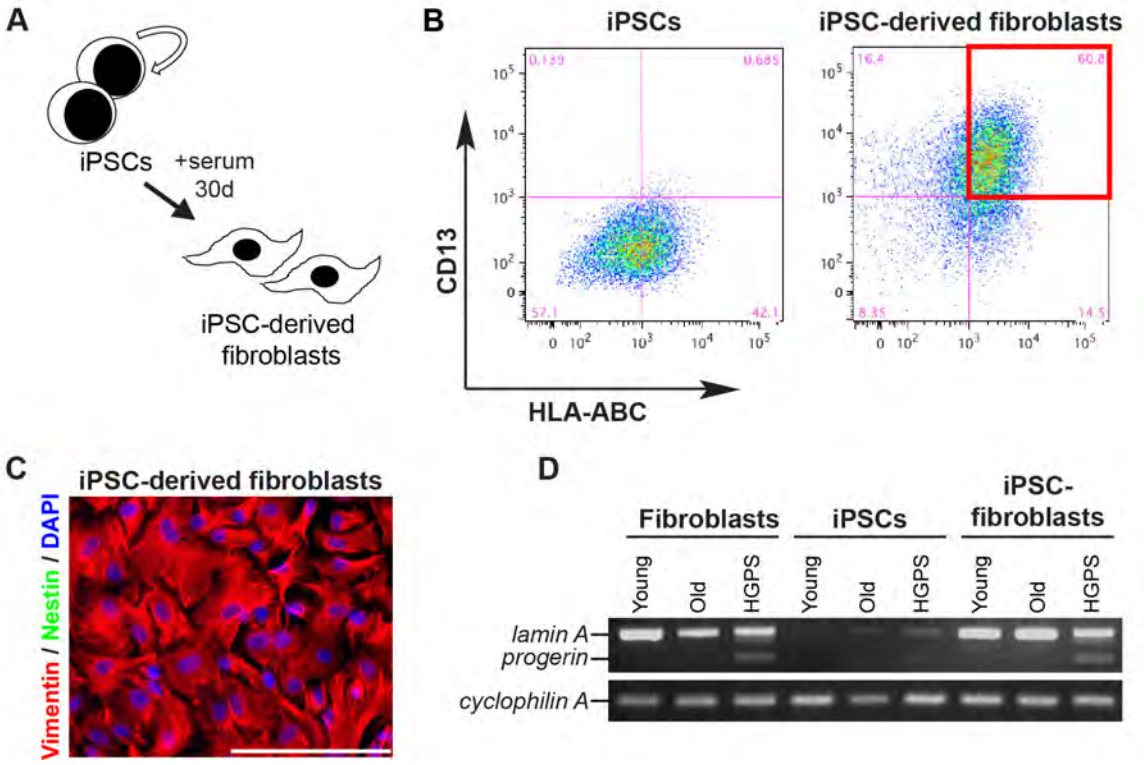

Figure 4.1 **Differentiation of iPSCs to fibroblast-like cells.** (A and B) iPSCs were differentiated to fibroblast-like cells in serum-containing medium for 30 days (A) and sorted by flow cytometry (B) for high levels of expression of the fibroblast marker CD13 and high HLA-ABC (red box) as compared to iPSCs. (C) iPSC-derived fibroblasts after sorting display fibroblast-like morphologies and expression of vimentin but no nestin (a neural marker) by immunocytochemistry. (D) RT-PCR for lamin A and progerin transcripts show upregulation in iPSC-derived fibroblasts (iPSC-fibroblasts) to similar levels observed in the donor fibroblasts. Scale bar: 200 μm.

HLA-ABC^{hi} cells were further expanded for an additional 30 days prior to characterization. iPSC-derived fibroblasts (iPSC-fibroblasts) demonstrated expression of the fibroblast marker vimentin and absence of the neural precursor marker nestin (**Figure 4.1C**). Furthermore, iPSC-fibroblasts showed expression of lamin A and progerin at levels similar to those observed in primary donor fibroblasts (**Figure 4.1D**).

Assessment of Age-Related Markers in iPSC-Fibroblasts

In order to determine whether cells derived from old donors had reestablished their age, we reassessed our panel of age-related markers in the iPSC-fibroblasts. Surprisingly, differentiation did not reestablish the age-associated marker profile in old donor iPSC-fibroblasts. In fact, old donor iPSC-fibroblasts closely matched the profile of passage-matched young donor iPSC-fibroblasts, displaying uniform nuclear morphologies (**Figure 4.2A**) as well as high levels of LAP2α, H3K9me, and HP1γ (**Figure 4.2A and B**). Furthermore, old donor iPSC-fibroblasts showed rare evidence of DNA damage and mitochondrial dysfunction (**Figure 4.2C**). Importantly, cellular age was evaluated in the young and old iPSC-fibroblasts following several passages to reduce the possibility that old donor iPSC-fibroblasts appeared young simply due to being newly established. These data demonstrate that age-associated markers in primary fibroblasts from aged, apparently healthy donors are reset following reprogramming and are not reestablished upon differentiation into iPSC-fibroblasts.

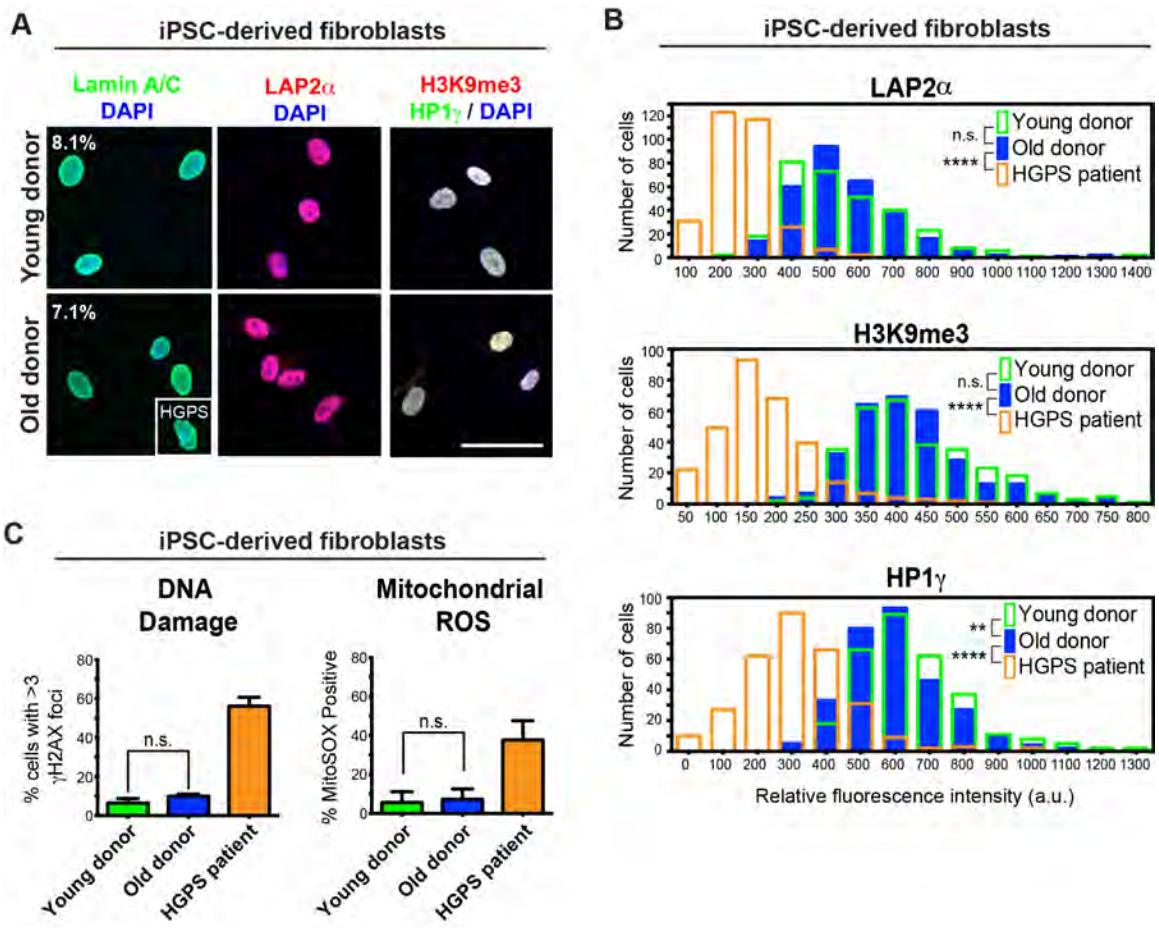

Figure 4.2 iPSC-Fibroblasts from Old Donors Do Not Regain Age-Associated Markers. (A) Immunocytochemistry for age-associated markers. Percentages indicate the proportion of cells with folded and/or blebbed nuclear morphologies. *Inset:* Example of HGPS iPSC-fibroblast nuclear morphology. (B) Quantification of the markers shown in (A) indicates the high degree of overlap between iPSC-derived fibroblasts (iPSC-fibroblasts) from young and old donors compared to HGPS iPSC-fibroblasts, which reestablish an age-like phenotype. (C) Analysis of DNA damage (left) and mitochondrial superoxide (right) further show that iPSC-fibroblasts from old donors have been reset to a "young"-like state. n.s. not significant, **p<0.01, ****p<0.0001 according to Kolmogorov-Smirnov tests (B) or Student's t tests (C). n= 3 differentiations of independent iPSC clones performed at different times. Bar graphs represent mean ± SEM. Scale bar: 50 μm.

In contrast, HGPS iPSC-fibroblasts spontaneously reestablished high progerin expression (**Figure 4.1D**) as well as abnormal nuclear folding and blebbing (**Figure 4.2A**, *inset*) and expression of age-associated markers upon differentiation (**Figure 4.2B and C**) as reported in other iPSC-based models of HGPS (Liu et al., 2011b; Zhang et al., 2011). This data suggests that cues such as high levels of progerin expression (**Figure 4.1D**) can return iPSC-fibroblasts to an aged-like state.

Discussion

We have differentiated iPSCs from young, old, and HGPS donors with high efficiency to a mesenchymal cell type that resembles a fibroblast-like cell similar to the donor population. By assessing molecular markers associated with aging, we demonstrate that old donor iPSC-fibroblasts maintain the young-like state established following reprogramming as described in Chapter 3.

Additional Considerations for Evaluating Cellular Age

While our study provides additional support for previous claims that cellular age is reset following reprogramming (reviewed in (Freije and López-Otín, 2012; Mahmoudi and Brunet, 2012)), there are several additional parameters that could be addressed in future studies. In addition to the inclusion of an even broader set of age-related markers as mentioned in Chapter 3, it will be interesting to determine whether any of these phenotypes transition to an age-like state with further in vitro culturing of either young donor or old donor iPSC-fibroblasts or

whether replicative senescence and aging are uncoupled. Furthermore, it will be important to assess cells derived from young and old donors that more fully represent the spectrum of diverse ethnicities as primarily Caucasian backgrounds were considered in this study. Finally, alternative differentiation protocols to generate fibroblast-like cells along with global expression analysis should be considered to better determine the appropriate fibroblast characteristics that best capture the primary donor fibroblast cells which are often procured from a variety of sources (e.g. arm, thorax, lung).

Implications of the Reprogramming-Induced Age Reset

Reprogramming and re-differentiation eliminate at least several key age-related markers and give rise to phenotypically young iPSC-fibroblasts (as determined by the specific set of age-related markers used herein) that may require years of in vitro culture to reestablish age. In addition to posing problems for modeling age-related diseases in a timely manner, the young-like state of old donor iPSC-fibroblasts suggests that the low levels of progerin in both young and old donor-derived healthy newborn cells (**Figure 4.1D**) is insufficient to induce aging over the course of the 60-day differentiation (**Figure 4.2**). In contrast, progerin at high levels (**Figure 4.1D**) is capable of inducing age in newborn cells (as in the case of HGPS iPSC-fibroblasts (**Figure 4.2B and C**)). Nevertheless, progerin at low levels may still play an important role over time as it has been shown to be necessary to *sustain* age-related markers in old donor cells (Scaffidi and Misteli, 2006). Finally, in the context of our in vitro culture system, it will be interesting in

future studies to determine whether the status of a cell's natural defense mechanisms against aging play a role in susceptibility to low levels of progerin as may be the difference between young and old donor fibroblasts.

CHAPTER FIVE

Acute Progerin Overexpression Reestablishes Age-Related Markers in iPSC-Derived Fibroblasts

Introduction

Whether a hierarchy of events in normal aging exists is unknown; however, it is clear that the process is complex. Therefore, devising a strategy for inducing age in cultured cells necessitates the consideration of manipulating not just one but several pathways in an attempt to mimic this complexity. However, in order to minimize the toxic effects of such a strategy, it would be ideal to target a single protein that can then trigger many downstream effects related to aging. To this end, we explored a strategy using overexpression of progerin, an isoform of *LMNA* that induces age-associated phenotypes because of its altered nuclear scaffolding function compared to lamin A. While no one has used progerin overexpression in iPSC-derived somatic cells to our knowledge, it was previously reported that progerin overexpression in apparently healthy normal human fibroblasts induced nuclear abnormalities (Glynn and Glover, 2005) and defects in mitosis (Cao et al., 2007) as well as aberrant nuclear morphologies, loss of LAP2α, and increased DNA damage (Scaffidi and Misteli, 2008). Furthermore, these studies demonstrated the use of a GFP tag that allowed for real-time visualization of progerin expression and nuclear morphology changes without interfering with the protein's normal localization and function. Finally, the practical application of an induced aging strategy in a dish requires that the method be

efficient, allow for easy manipulation of the amount and duration of expression, and trigger its effects rapidly without modifying the genome. To satisfy these criteria, we used synthetic mRNA technology (Kariko et al., 2005; Warren et al., 2010), which has been successfully used to reprogram fibroblasts to iPSCs and to differentiate iPSCs to a myogenic cell fate (Warren et al., 2010).

Results

Progerin Overexpression and Evaluation of Age-Related Markers

In order to determine whether progerin overexpression is sufficient to induce age-associated markers in apparently healthy young or old donor iPSC-fibroblasts, we used synthetic mRNA (termed modified-RNA) (Kariko et al., 2005; Warren et al., 2010) to overexpress either GFP fused to progerin (GFP-progerin) or a nuclear-localized GFP control (nuclear-GFP) (**Figure 5.1A**). Daily transfection of modified-RNA for three days (**Figure 5.1B**) induced progerin expression to levels similar or higher than those in HGPS iPSC-fibroblasts (**Figure 5.1C**). Strikingly, overexpression of GFP-progerin but not nuclear-GFP in young and old donor iPSC-fibroblasts induced nuclear morphology abnormalities, loss of LAP2α expression, formation of DNA double strand breaks (γH2AX), and loss of heterochromatin markers (H3K9me3 and HP1γ) (**Figure 5.2A and B**). Progerin also elicited increased levels of mtROS (**Figure 5.2C**) in iPSC-fibroblasts. All progerin-induced changes in iPSC-fibroblasts were independent of donor age.

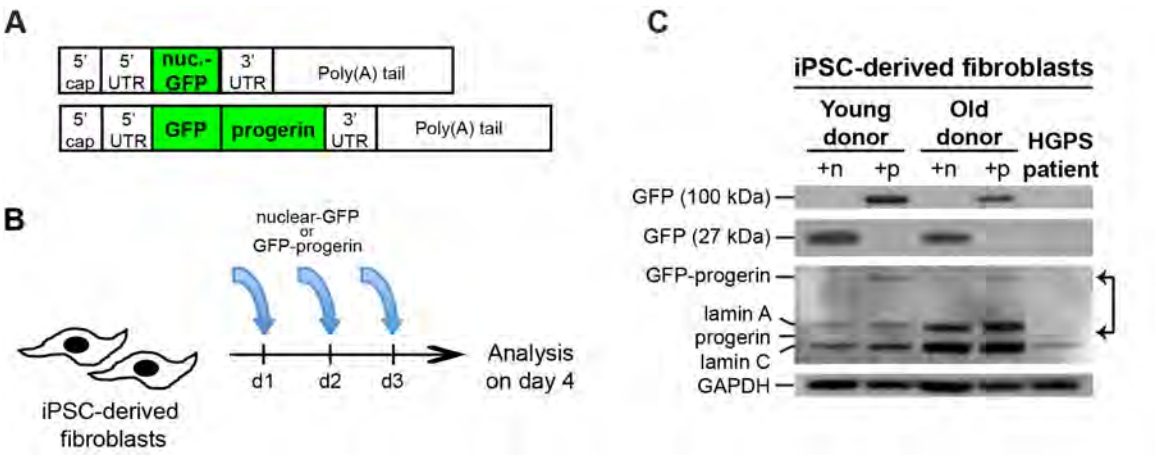

Figure 5.1 Modified-RNA expression in iPSC-Fibroblasts. (A) Modified-RNA was designed to express either nuclear-localized green fluorescent protein (nuclear-GFP) as a control or progerin fused to GFP (GFP-progerin). The addition of generic 5' and 3' UTRs as well as a PolyA tail and 5' cap structure facilitated the in vitro transcription reaction (B) Modified-RNA was transfected into iPSC-fibroblasts on three consecutive days prior to analysis on day 4. (C) Western blot analysis of transgene expression. n, nuclear-GFP; p, GFP-progerin. Analysis of detection using a lamin A/C antibody (N-18) revealed that progerin overexpression induces levels higher than the endogenous progerin level observed in HGPS iPSC-derived fibroblasts (arrows).

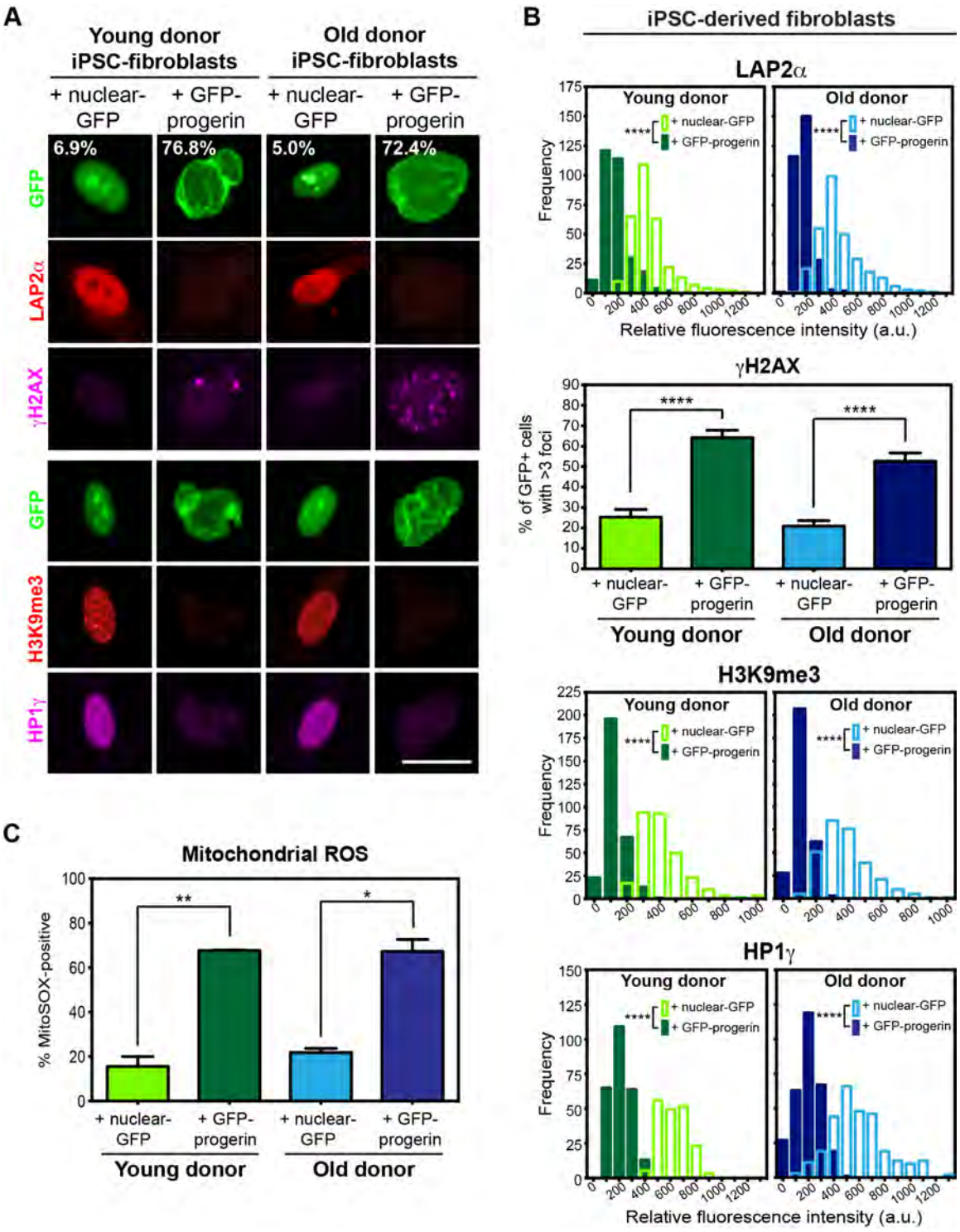

Figure 5.2 Progerin Overexpression Induces Age-Associated Changes in iPSC-Fibroblasts Regardless of Donor Age. (A) Overexpression of progerin (GFP-progerin) in iPSC-fibroblasts causes changes in nuclear morphology (as seen by GFP), expression of the lamina-associated protein (LAP2α), levels of DNA damage (γH2AX),

and chromatin organization (H3K9me3; HP1γ), which were not observed with overexpression of a nuclear-localized GFP control (nuclear-GFP). Percentages indicate the proportion of cells with folded and/or blebbed nuclear morphologies. (B) Quantification of data shown in (A). Frequency distribution plots represent the fluorescence intensity of 100 cells from 3 independent RNA transfections of iPSC-fibroblasts derived from independent iPSC clones. (C) Flow cytometry analysis of the mitochondrial superoxide indicator MitoSOX suggests a dramatic increase in mitochondrial dysfunction with progerin overexpression. n= 3 independent RNA transfections of iPSC-fibroblasts derived from independent iPSC clones. *$p<0.05$, **$p<0.01$, ****$p<0.0001$ according to Kolmogorov-Smirnov tests (LAP2α, H3K9me3, HP1γ) or Student's t-tests (γH2AX, MitoSOX). Bar graphs represent mean ± SEM. Scale bar: 25 μm.

Furthermore, these progerin-induced features were indistinguishable from those observed in primary fibroblasts from aged donors (**Figure 3.2**).

Aging in mitotic cells is also typically associated with the shortening of telomeres to a critical point when the cell reaches Hayflick's limit and undergoes senescence (Hayflick, 1965). Therefore, we measured telomere lengths using quantitative fluorescence in situ hybridization (Canela et al., 2007) in transfected iPSC-fibroblasts to determine whether progerin can induce telomere shortening. Following progerin overexpression, iPSC-fibroblasts demonstrated a decrease in overall telomere length (**Figure 5.3A**) and an increase in the percentage of short telomeres (**Figure 5.3B**). This result was further corroborated by an increase in senescence-activated β galactosidase (SA-β-Gal) staining (**Figure 5.3C**).

Discussion

We have established an efficient method to rapidly trigger age-related markers in iPSC-derived fibroblasts in just three days. The use of modified-RNAs allowed for high levels of progerin expression without significant toxicity, providing a viable, non-integrating tool to direct age.

Our study addresses the ability to measure and manipulate age in cells differentiated from iPSCs, which represents a fundamental challenge in pluripotent stem cell research that has remained unresolved to date. There has

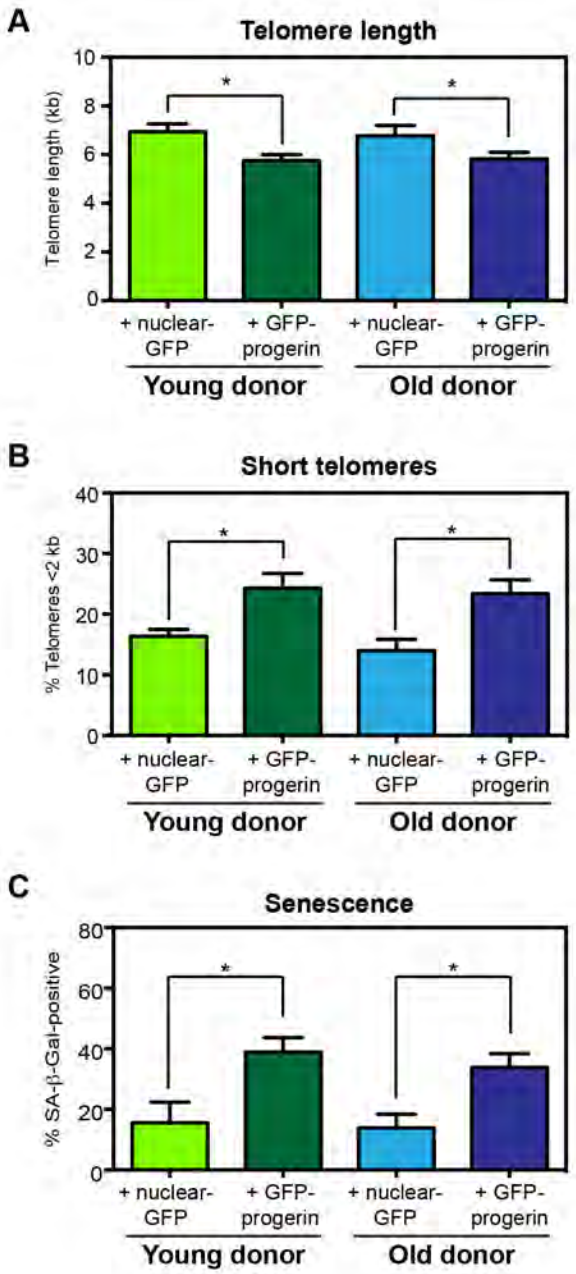

Figure 5.3 Progerin induces telomere shortening in iPSC-derived fibroblasts. (A and B) Quantification of telomere length (A) and the percentage of telomeres less than 2 kilobases (kb) in length (B) by Q-FISH. n= 4 replicate wells. (B) Assessment of the senescence marker senescence-activated beta-galactosidase (SA-β-Gal). n= 2 replicate wells. *p<0.05 according to Student's t-tests. Bar graphs represent mean ± SEM.

been considerable progress in directing cell fate into the various derivatives of all three germ layers; however, there has been no technology to switch the age of a given cell type on demand from embryonic to neonatal, adult or aged status. This has remained a major impediment in the field as illustrated by the persistent failure to generate hiPSC-derived adult-like hematopoietic stem cells (McKinney-Freeman et al., 2012), fully functional cardiomyocytes (Sheng et al., 2012), or mature pancreatic islets (Blum et al., 2012), and the general inability to derive aged cell types stage-appropriate for modeling late-onset diseases.

Our aging strategy represents a first attempt at inducing age-associated markers in a dish, and thus it remains to be determined how well progerin overexpression truly phenocopies aging. Future work involving extensive profiling of iPSC-fibroblasts overexpressing progerin compared to normally aged fibroblasts and evaluation of the timeline of events will be beneficial to resolving this issue. Furthermore, it will be interesting in future studies to investigate other strategies to induce aging, including but not limited to telomerase inhibition, DNA damage induction, SIRT1 knockdown, p16 overexpression, or NF-κB pathway activation. It may be that an alternative method can complement or replace progerin overexpression to better mimic the normal aging process (see Chapter 8 for further discussion). Finally, It will be interesting to see whether progerin overexpression will be applicable to other cell types or whether different cell types will require a unique set of induced aging factors (although our results in Chapter 6 suggest that progerin may also be applicable to aging mDA neurons).

CHAPTER SIX

Progerin is Expressed in the Human Brain and Induces Neuronal Aging Phenotypes in iPSC-Derived mDA Neurons

Introduction

Validation of a broadly applicable induced aging strategy requires testing in multiple iPSC-derived cell types. An important question is whether the effects of progerin expression are limited to proliferative cell types (e.g. fibroblasts) or whether age-related markers can be induced via progerin in all cells of the body including post-mitotic cells (e.g. neurons). In fact, neural cells in general warrant further investigation as the levels of progerin expression are thought to be low in the central nervous system (CNS) and thus may be insufficient to trigger a neurological phenotype during the lifespan of an HGPS patient. Previous reports found that low CNS levels are due to the brain-specific expression of miR-9, which targets lamin A and progerin but not lamin C (Jung et al., 2012; Nissan et al., 2012). Fong and colleagues demonstrated that lamin A and progerin expression are lower in the mouse CNS compared to other tissues but did not address progerin levels in the *human* brain or potential changes in expression during aging (Jung et al., 2012). In contrast, Peschanski and colleagues rescued the effects of progerin on nuclear abnormalities in HGPS iPSC-derived mesenchymal stem cells but did not address whether increasing the levels of progerin in HGPS iPSC-derived neural stem cells or neurons could induce nuclear changes (Nissan et al., 2012).

Results

Analysis of LMNA and miR-9 in the Human Brain

To address the levels of progerin expression in the aged human brain we obtained samples of human cortex from donors ranging from 35-years-old to 89-years-old (**Table 6.1**). We measured transcript levels for each *LMNA* isoform and observed marked increases in lamin A and progerin but not lamin C expression in donors over 70 years of age despite unchanged miR-9 levels (**Figure 6.1A**). We also observed parallel increases in the ratio of $MAP2^+$ cells immunoreactive for all *LMNA* isoforms (lamin A/C, *left*) in contrast to the loss of lamin C expression (*right)* (**Figure 6.1B**), indirectly indicating the expression of lamin A and progerin at later ages. Finally, $MAP2^+$ neurons in the human cortex tissue exhibited age-dependent changes in heterochromatin organization and nuclear size (**Figure 6.1C**) that may also be reflective of changes in lamin A and progerin. Our results suggest that lamin A and progerin are in fact present in the aged human brain and therefore could potentially contribute to neuronal aging.

mDA Neuron Differentiation and Progerin Overexpression

We addressed next whether progerin overexpression would be a suitable tool to induce in vitro aging of iPSC-derived neurons. We differentiated young and old donor iPSCs into midbrain dopamine (mDA) neurons, a neuronal subtype affected in PD, using our previously established protocol (Kriks et al., 2011) (**Figure 6.2A**). Within 13 days, differentiated iPSCs had downregulated the pluripotency marker OCT4 and converted to LMX1A/FOXA2-double positive

NDRI#	Age	Race	Recovery Time (hr)	Cause of Death
0068458	35	C	6.5	Liver disease
0067837	44	C	6.1	Liver disease
0067941	58	C	5.3	Anoxia
0067549	71	C	6.5	Cardiac arrest
0067720	82	C	7.9	Respiratory arrest
0067515	89	C	4.1	GI bleed

Table 6.1 Summary of postmortem human cortex tissue. Matched frozen tissue samples and paraffin tissue sections were obtained from the National Disease Research Interchange (NDRI). Donor information was provided by NDRI. hr, hours postmortem.

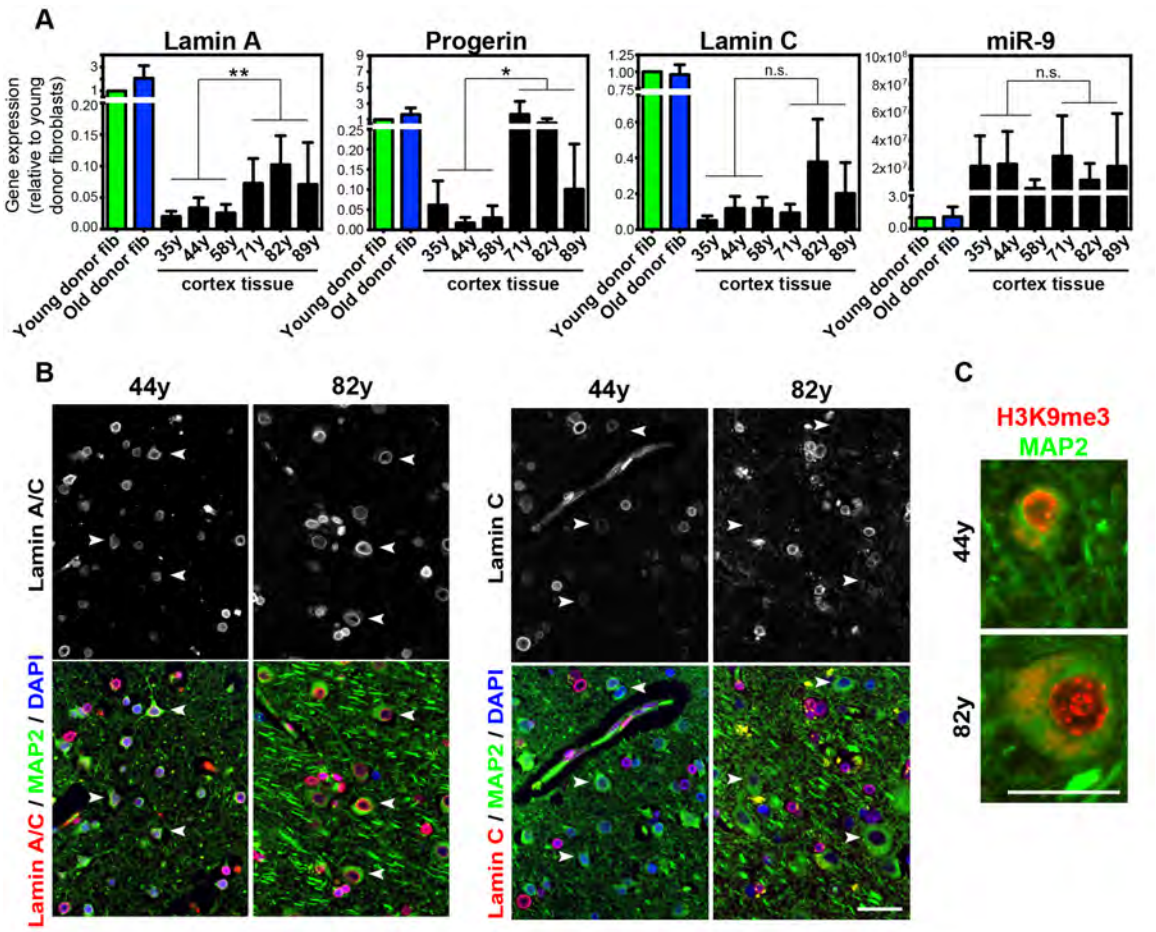

Figure 6.1 Analysis of human cortex tissue reveals an age-associated increase in lamin A and progerin expression. (A) Quantitative RT-PCR analysis of expression of the *LMNA* isoforms (Lamin A, Progerin, Lamin C) and miR-9 (far right) show a specific increase in lamin A and progerin mRNA in human cortex tissue from aged donors. *p<0.05, **p<0.01, n.s., not significant according to Student's t-tests. Data are presented as mean ± SEM; n=3 independent RNA extractions. (B) Immunohistochemistry for total A-type lamins (Lamin A/C; left) and lamin C only (right) within paraffin-embedded human cortex tissue demonstrates an age-dependent decrease in lamin C protein specifically in neurons ($MAP2^+$ cells) while no gross changes in the level of total A-type lamins were observed. Arrowheads indicate examples of $MAP2^+$ neurons. (C) Immunohistochemistry for the heterochromatin marker H3K9me3 reveals differences in heterochromatin organization and nuclear size in $MAP2^+$ neurons with age. Scale bars: 50 μm (B), 25 μm (C).

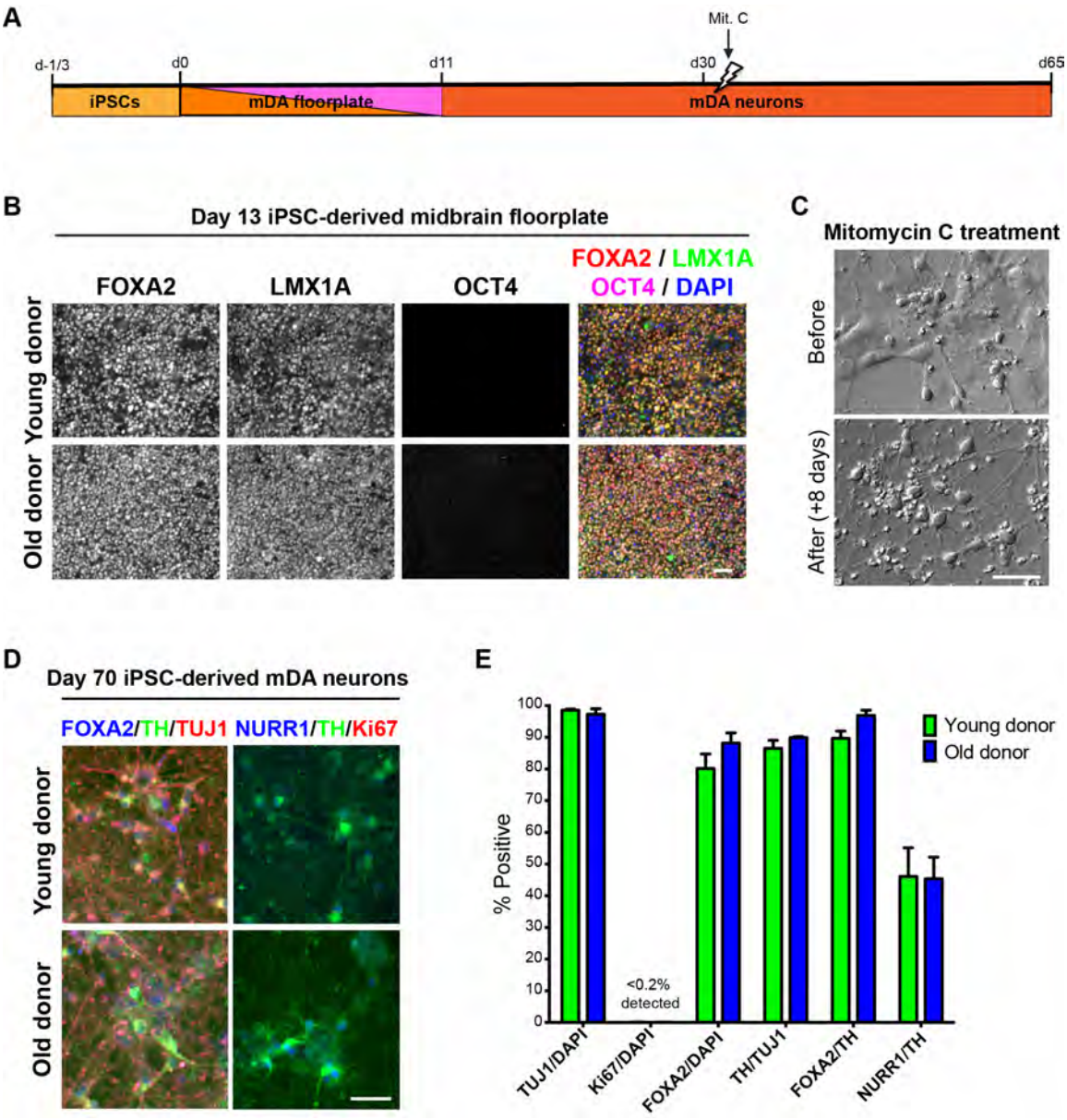

Figure 6.2 Differentiation of iPSCs to mDA neurons. (A) Schematic illustration of the differentiation timeline for the derivation of mDA neurons from iPSCs. Mit. C, mitomycin C. (B) Immunocytochemistry at day 13 of differentiation for FOXA2 (red), LMX1A (green) and OCT4 (pink). (C) Mitomycin C treatment 2 days following the final day 30 replating helped to eliminate the remaining proliferating cells (post-mitotic neurons unaffected). (D and E) Immunocytochemistry (D) and quantification (E) demonstrate that almost 100% of the remaining cells at day 70 of differentiation were post-mitotic neurons ($TUJ1^+/Ki67^-$) and that greater than 80% of those neurons expressed mDA-specific markers ($FOXA2^+/TH^+$). As previously reported (Kriks et al., 2011) approximately 40% of the TH^+ neurons also express the more mature mDA marker NURR1. n= at least 3 independent differentiations of independent iPSC clones. Bar graph represents mean ± SEM. Scale bars: 50 μm.

midbrain floorplate precursors, an early stage of mDA neuron development (**Figure 6.2B**). Immature mDA neurons at day 32 of differentiation were transiently treated with mitomycin C to eliminate the remaining proliferating progenitors and/or contaminants (**Figure 6.2C**). iPSC-mDA neurons that were matured for an additional five weeks (65 days of differentiation in total) continued to express mDA markers such as FOXA2 and tyrosine hydroxylase (TH) at high purity in all iPSC clones independent of donor age (**Figure 6.2D and E**). Interestingly, iPSC-mDA neurons spontaneously showed evidence of low level nuclear folding (**Figure 6.3A**) similar to $FOXA2^+$ cells found in the substantia nigra of a 1-month-old mouse (**Figure 6.3B**), which may simply reflect a cell type-specific nuclear morphology. The nuclear folding occurred in iPSC-mDA neurons concomitant with the onset of endogenous lamin A expression (**Figure 6.3A**).

To achieve similar expression levels of progerin in iPSC-mDA neurons as in the iPSC-fibroblasts, we extended modified-RNA exposure to 5 days (**Figure 6.4A**), which induced progerin levels that exceeded the levels of endogenous lamin A (**Figure 6.4B**, *arrows*). Following progerin overexpression, GFP-positive cells showed evidence of enhanced nuclear folding and blebbing and accumulation of DNA damage (**Figure 6.4C**) as well as increased production of mtROS (**Figure 6.4D**). However, in contrast to iPSC-fibroblasts (**Figure 5.2**), we did not observe significant changes in LAP2α, H3K9me3 or HP1γ in neurons (**Figure 6.4E**). Positive SA-β-Gal staining, a marker of senescence, was also not detected in iPSC-mDA neurons (data not shown). These data demonstrate both shared and

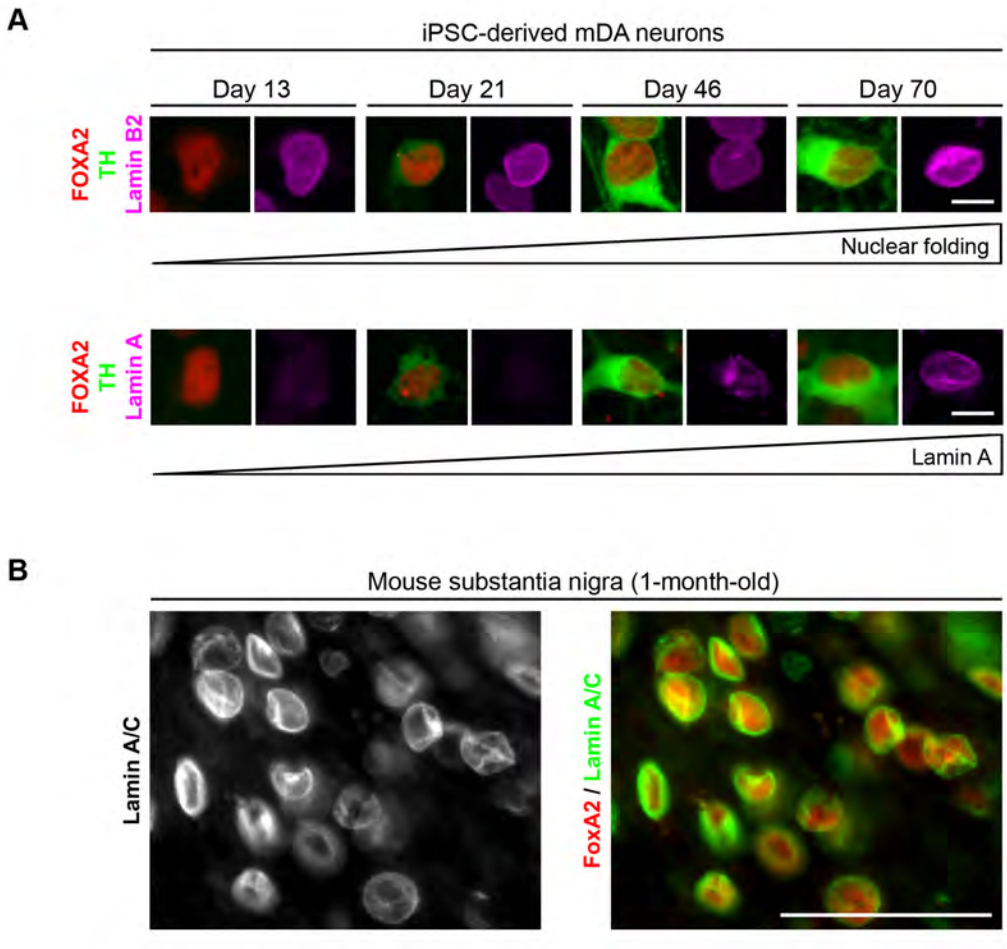

Figure 6.3 Nuclear folding in iPSC-derived mDA neurons resembles morphology of substantia nigra cells in the mouse brain. (A) Representative immunocytochemistry for lamin A and lamin B2 during mDA neuron differentiation of both young and old donor iPSCs shows nuclear folding with similar timing to endogenous upregulation of the lamin A isoform. (B) Immunohistochemistry for all A-type lamins (lamin A/C) in mouse brain tissue show similar nuclear folding in FoxA2^{+} cells. Scale bars: 50 μm.

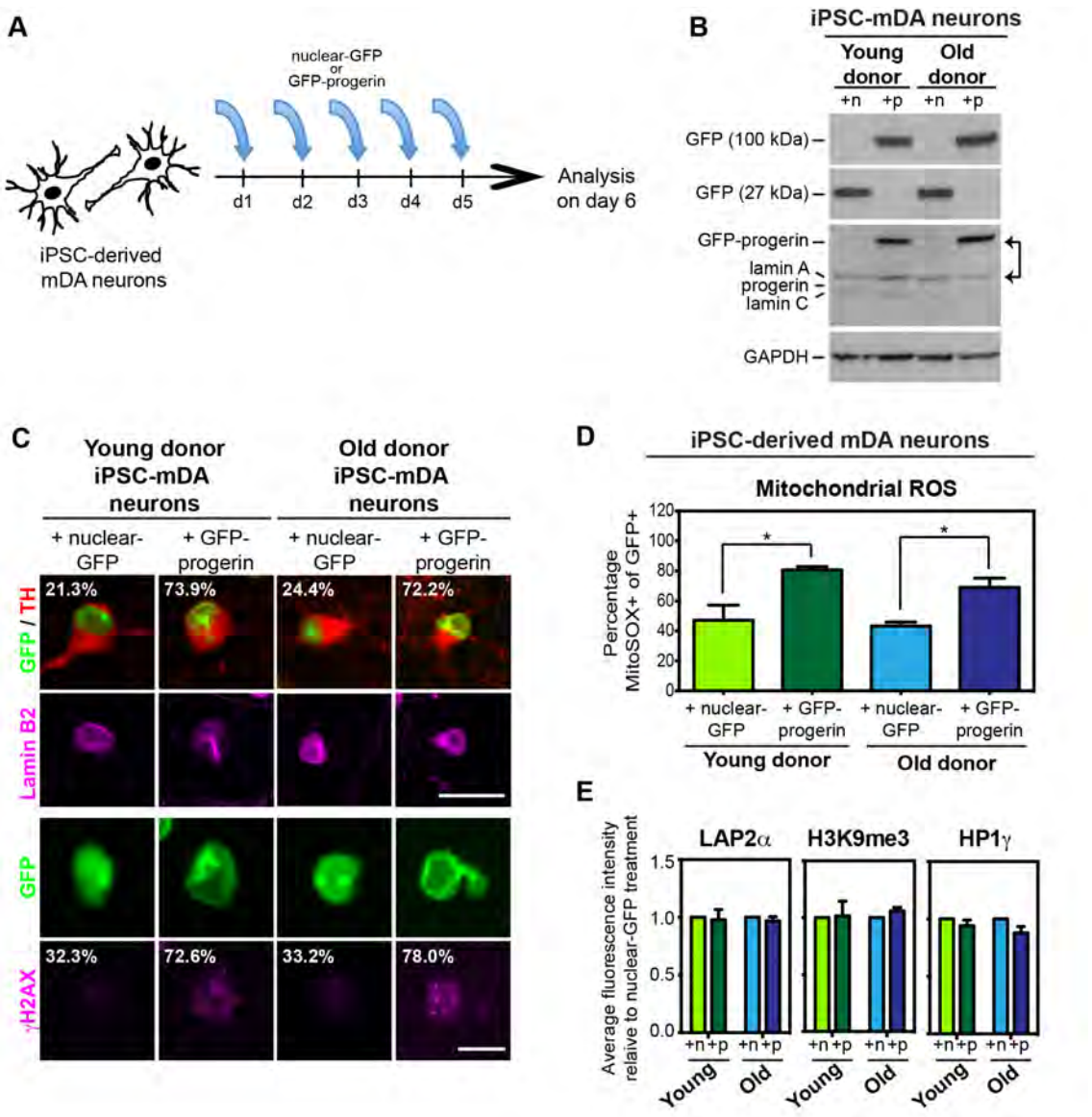

Figure 6.4 <u>Progerin overexpression induces a subset of the fibroblast age-associated signature in iPSC-mDA neurons derived from both young and old donors.</u> (A) Modified-RNA was transfected into iPSC-derived mDA neurons (iPSC-mDA neurons) on five consecutive days prior to analysis on day 6. (B) Western blot analysis of transgene expression. A GFP band at 100 kDA denotes the GFP-progerin fusion protein while a GFP band at 27 kDA represents the nuclear-GFP transgene. All lamin A isoforms including the transgene were recognized by a single antibody. Note that progerin overexpression levels exceed endogenous lamin A levels (arrows). iPSC-mDA neurons do not appear to express detectable levels of progerin protein endogenously. n, nuclear-GFP; p, GFP-progerin. (C) Progerin overexpression enhances nuclear folding and blebbing (as seen by lamin B2, pink) and increases DNA damage accumulation (γH2AX) in both young and old donor-derived iPSC-mDA neurons. Percentages indicate the proportion of cells with enhanced nuclear folding and/or blebbing or the proportion of

cells with >3 enlarged γH2AX foci. (D) Flow cytometry analysis of mitochondrial superoxide levels (MitoSOX) demonstrates increased mitochondrial dysfunction with progerin overexpression. n= 3 independent RNA transfections of iPSC-mDA neurons derived from independent iPSC clones (E) Quantification of immunocytochemistry for LAP2α, H3K9me3 and HP1γ shows no difference between iPSC-mDA neurons transfected with GFP-progerin or nuclear-GFP, unlike the phenotype observed in iPSC-fibroblasts (see **Figure 5.2**). Fluorescence intensities were normalized to the intensities observed in nuclear-GFP-treated cells. *$p<0.05$ according to Student's t tests (D). Bar graphs represent mean ± SEM. Scale bars: 10 μm (C, bottom), 25 μm (C, top).

cell type-specific responses of iPSC-fibroblasts and iPSC-mDA neurons to our in vitro aging paradigm.

Evaluation of Neuron-Specific Age-Related Markers

To examine cell-type specific responses to progerin exposure, we investigated parameters associated with in vivo neuronal aging such as degenerative changes in dendrite branching (Hof and Morrison, 2004). Remarkably, 5 days of progerin exposure in differentiated (day 65) mDA neurons was sufficient to induce a degenerative phenotype resulting in the breakdown of established neurites (**Figure 6.5A**). Degeneration was not observed in cells transfected with control nuclear-GFP mRNA. We next assessed expression of MAP2, which specifically labels dendrites (Bernhardt, 1984). Quantitative analysis showed a marked reduction in average dendrite length following progerin exposure in mDA neurons derived from either young or old donor iPSCs (**Figure 6.5B**). Importantly, the percentages of iPSC-mDA neurons expressing the dopamine neuron markers NURR1 and TH remained unchanged, suggesting that the addition of progerin did not simply induce toxicity (**Figure 6.6A and B**). Furthermore, the progression of events following progerin treatment (**Figure 6.6C**) were analogous to the classical “dying-back” response previously described (Finn et al., 2000; Ikegami and Koike, 2003; Raff et al., 2002; Song et al., 2006), which involves the shortening of dendrites prior to cell soma demise and to activation of programmed cell death in the nucleus. These findings are in contrast to observations made following treatment of iPSC-mDA neurons with

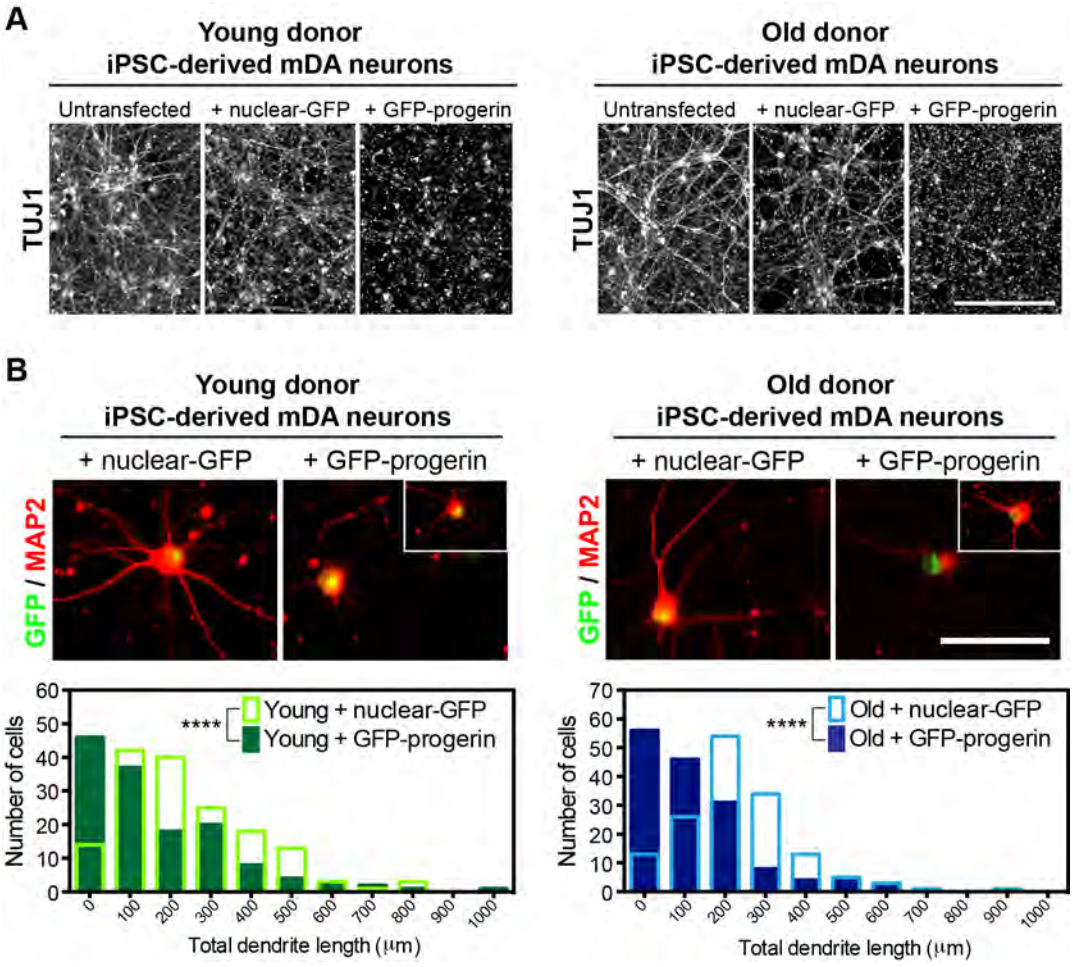

Figure 6.5 Progerin overexpression neurite degeneration in iPSC-mDA neurons. (A) Immunocytochemistry for the pan-neuronal marker TUJ1 shows a loss of the established neuronal network in day 70 iPSC-mDA neurons overexpressing progerin but not in iPSC-mDA neurons overexpressing nuclear-GFP. (B) MAP2 immunocytochemistry reveals reduced intact dendrite lengths following overexpression of progerin in most but not all (inset) iPSC-mDA neurons derived from both young and old donors. Frequency distributions display total dendrite length measurements from 3 independent RNA transfections (50 cells each, non-apoptotic nuclei only). ****p<0.0001 according to Kolmogorov-Smirnov tests. Scale bars: 200 μm (A), 50 μm (B).

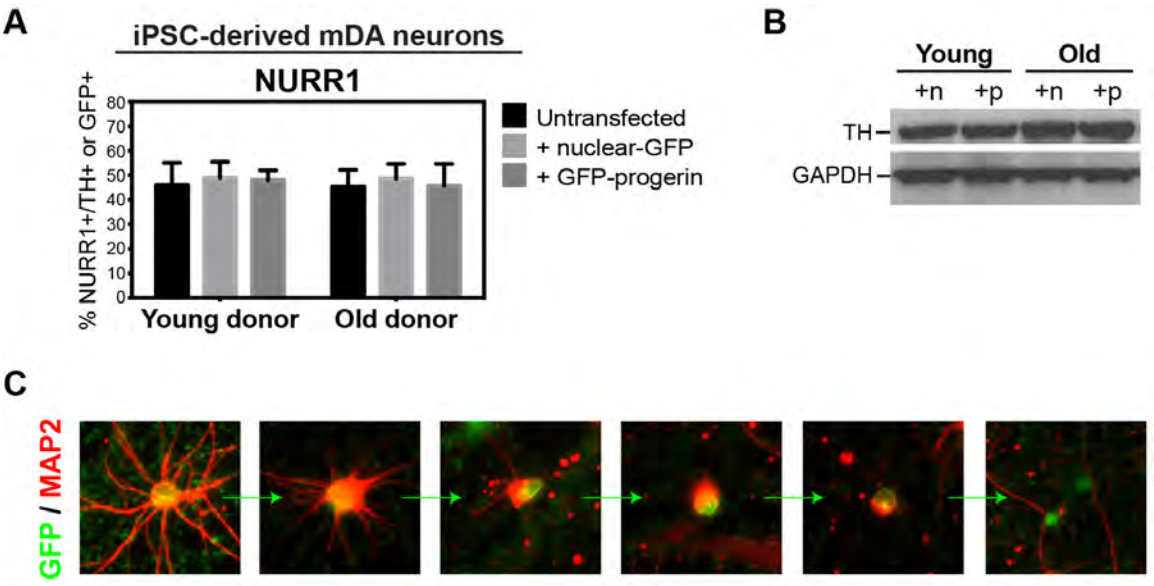

Figure 6.6 <u>Progerin overexpression induces a neurodegeneration-like phenotype not indicative of acute toxicity.</u> (A and B) The percentage of NURR1^{+} iPSC-derived mDA neurons (A) and the protein expression levels of TH (B) remain unchanged with transfection, indicating that progerin overexpression does not downregulate key mDA neuron proteins (a typical sign of acute toxicity). Bar graph represents mean ± SEM. n, nuclear-GFP; p, GFP-progerin. (C) Representative iPSC-mDA neurons overexpressing progerin at various stages in the degeneration process (*not* a time course). Note that dendrite shortening and loss of MAP2 occur prior to nuclear condensation (i.e. induction of apoptosis).

mitochondrial toxins such as carbonyl cyanide M-chlorophenyl hydrazine (CCCP) that rapidly induce mDA neuron marker loss and nuclear condensation prior to neurite shortening (data not shown).

To further characterize the age-like phenotype in iPSC-mDA neurons following progerin overexpression, we performed gene expression analysis by RNA-seq. Principle component analysis confirmed a reset in gene expression following reprogramming and illustrated the similarity between iPSC-mDA neurons derived from donors of different ages (**Figure 6.7A**). Analysis of the differentially expressed transcripts between treatment groups also revealed that progerin overexpression induced highly similar ($p<2.93 \times 10\text{-}321$) changes in young and old donor iPSC-mDA neurons (**Figure 6.7A and B**). Importantly, many of the overlapping progerin-induced expression changes have been previously associated with changes that occur during normal neuronal aging, including neurite degeneration, oxidative stress, dysfunctional proteostasis, and cell cycle reactivation (**Table 6.2**). Induction of transcripts associated with age-like processes was confirmed by analysis of gene ontology (**Figure 6.8A**). Furthermore, progerin mimicked gene expression changes which have been associated with PD (Lauridsen et al., 2011; Potashkin et al., 2012; Ryu et al., 2005) (**Table 6.2**), indicating a mDA neuron-specific response. Surprisingly, progerin may also be influencing maturation of iPSC-mDA neurons as indicated by the downregulation of *FOXD2* and *PDGFRA*. Finally, progerin overexpression in iPSC-mDA neurons induced differential expression of many uncharacterized

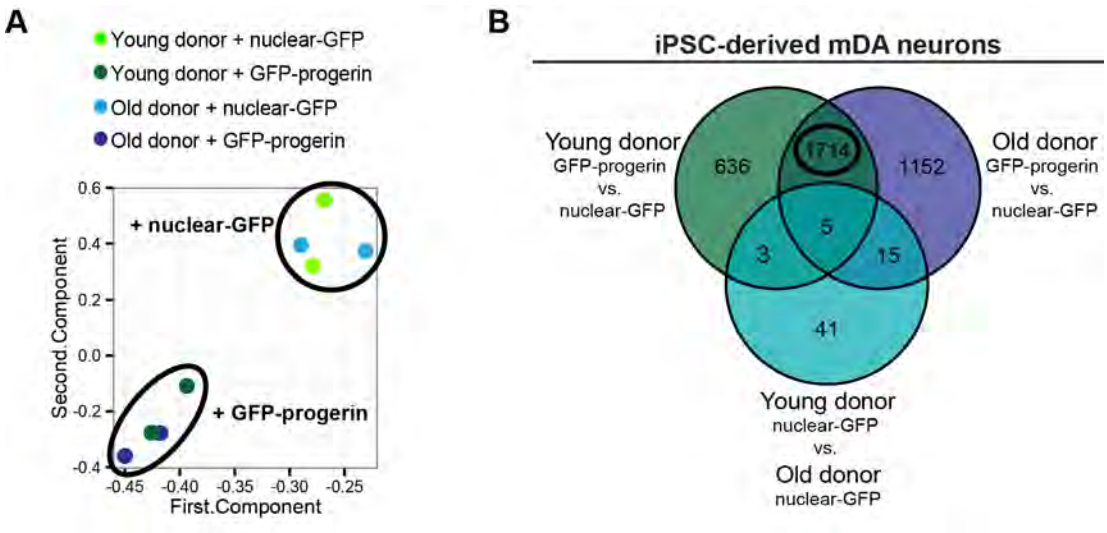

Figure 6.7 <u>Global gene expression analysis by RNA-seq reveals progerin-induced changes.</u> (A) Principal component analysis of RNA-seq gene expression data further corroborates the reprogramming-induced reset of age that results in the high similarity of iPSC-mDA neurons from both young and old donors. Progerin overexpression induces similar changes in mDA neurons independent of donor age. (B) Venn diagram where each colored circle indicates the number of differentially expressed genes (Fold change +/- 2, $p<0.05$) between two groups. The heavy black circle indicates the overlapping "aging signature" that was further analyzed.

Neuronal Age-Related Processes	Top 55 Up/Downregulated Genes* Induced by Progerin Overexpression
Oxidative stress	*ENHO; NDUFB6; ATP5L; PRDX4; FTL; ATOX1; NDUFA5; COX14; RPL12; ARL6IP5; TFAM; PRDX1; MT3; UQCR10; NDUFB11; TNIP3; DISC1*
Neurite degeneration	*TMSB10; TMSB4X; CCDC126; TSNAX; SCOC; PFN1; MT3; BEX1; NOSTRIN; LAMC3; FLI1; LEP; VIT; DISC1; GJA5; MYH1*
Dysfunctional proteostasis	*NEDD8; PPIB; PSMB3; UBC; UBE2T; SVIP; UBL5; SEC11C; VPS25; ABHD10; DNAJC8; LAMTOR1; LIPJ*
Chromatin modification/Active gene transcription	*TCEB2; TCEAL8; RMRP; RPPH1; PRDM1; BHMT2; SNORA53*
Cell cycle/Apoptosis	*PCNA; EAPP; YPEL5; RGS2; MIR663A; SGOL1*
Stress response	*SNHG15; SUMO2; MARCO; PEAR1; STAB2; SEC14L4*
DNA damage response	*NOP10; TCEAL7; UBE2T*
Neurodegeneration	*TBXA2R; GLI1; COL6A6*
Parkinson's disease-associated	*ZNHIT3; SEC11C; BCAS1*
Maturation	*FOXD2; PDGFRA*

Table 6.2 Gene expression changes with progerin overexpression represent neuronal age-related processes. The top 55 upregulated and the top 55 downregulated genes (Fold change +/- 2, $p<0.05$) were categorized for their potential relation to processes associated with neuronal aging. Genes representing uncharacterized coding genes and noncoding RNAs were excluded.

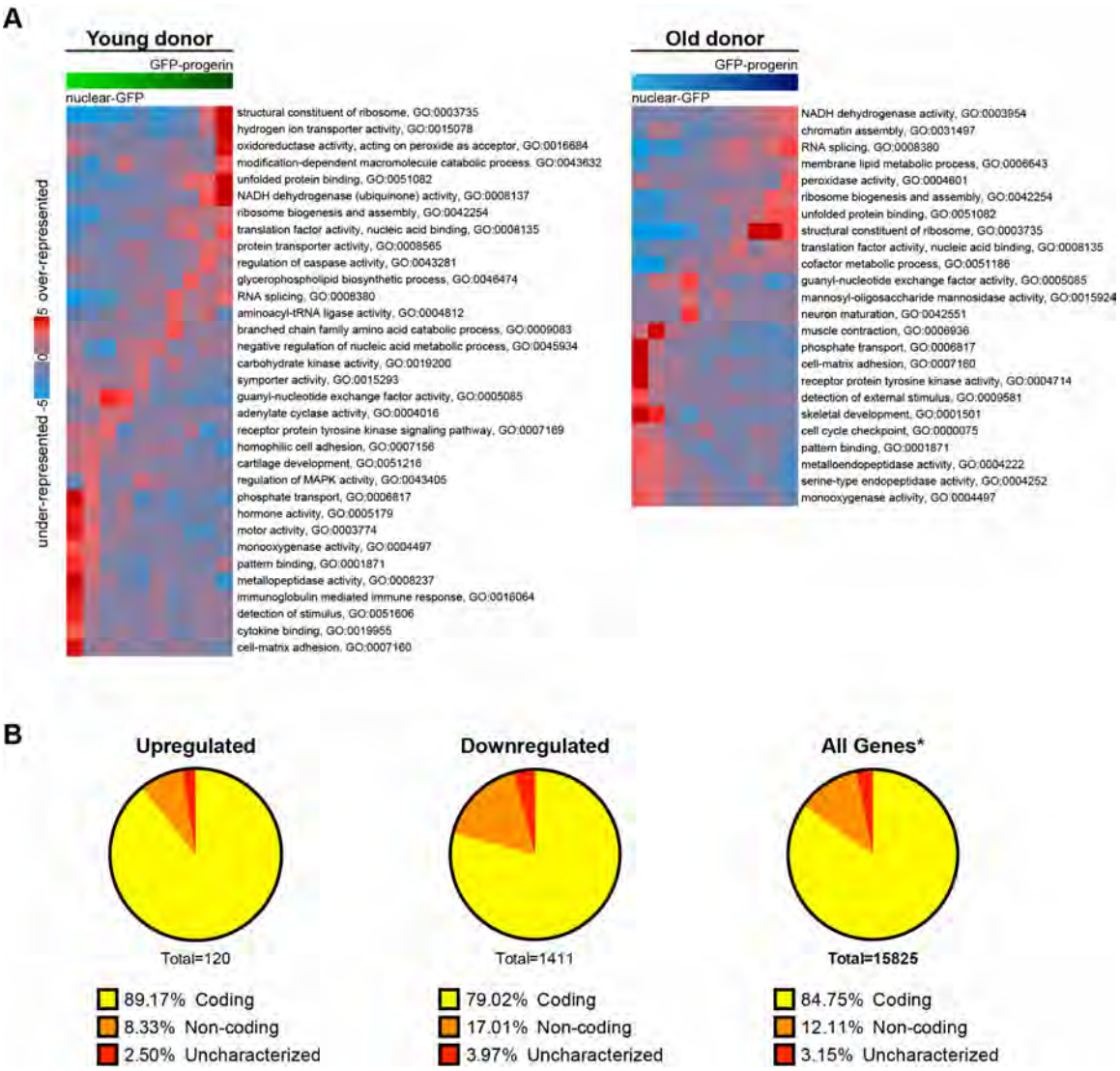

Figure 6.8 <u>Further analysis of gene expression changes following progerin expression in iPSC-mDA neurons.</u> (A) The significant gene ontology terms that are enriched in nuclear-GFP-treated or GFPprogerin-treated iPSC-derived mDA neurons (left to right). (B) Pie charts representing the proportion of the significantly differentially expressed transcripts compared to all genes that are coding, non-coding, or uncharacterized. “All genes” represents those that were reliably measured by RNA-seq.

genes as well as a significant downregulation of non-coding RNAs (**Figure 6.8B**) similar to recent observations in the aging rat brain (Wood et al., 2013). Taken together, these data suggest that progerin induces not only cellular but also molecular changes indicative of an age-related response in iPSC-mDA neurons.

Discussion

We have validated our induced aging strategy as a suitable tool for use in multiple iPSC-derived cell types, including post-mitotic neurons. We have established that progerin overexpression in iPSC-derived mDA neurons induces a cell type-specific response, triggering neurodegenerative-related processes.

HGPS and Progerin in the Human Brain

HGPS is a segmental syndrome that does not affect all tissues equally, suggesting that some tissues may be protected. While it was recently established that the absence of a severe neurological defect in HGPS may be due to miR-9 regulation of lamin A and progerin (Jung et al., 2012; Nissan et al., 2012), we suspect that HGPS patients may just not live long enough to develop a neurological phenotype. It is also still not clear whether this means that progerin does not accumulate to a significant level in the brains of apparently healthy individuals of old age. In fact, human brain aging is largely not understood, and it remains to be determined whether different neuronal subtypes have distinct aging programs (that could be differently affected by progerin).

Unfortunately, human brain tissue as used herein represents a mixture of cell types that confound questions of aging. Furthermore, the data that has been previously derived from mouse (or possibly even rat and monkey, for that matter) is not as informative as once thought (Loerch et al., 2008). In order to better understand human brain aging, future studies will benefit from laser-capture techniques to obtain specific populations from human brain tissue that can then be profiled and analyzed for expression of progerin with age. Regulation of alternative splicing should also be further studied because it may be that the upregulation of lamin A and progerin without changes in lamin C or miR-9 could reflect an age-dependent change in alternative splicing machinery as has been reported in the aging brain (Tollervey et al., 2011).

Future Analysis of the Progerin-Induced Phenotype

It is worth noting that our in vitro induced aging strategy bypasses the differential progerin levels found across various tissues in HGPS patients by using modified-RNAs to express progerin. This technique allowed for the study of the effects of high levels of progerin in iPSC-mDA neurons, which may not be possible by simply differentiating HGPS iPSCs.

While our study addressed several age-associated phenotypes in iPSC-mDA neurons, it was not exhaustive. It will be interesting in future studies to more completely analyze the progerin-induced response by looking at additional characteristics such as electrophysiology and dopamine release, which would

speak to the functionality of the iPSC-mDA neurons. Furthermore, profiling of laser-captured mDA neurons from human postmortem brain tissue as mentioned above would also help to determine how closely progerin overexpression mimics the normal aging process for this cell type.

CHAPTER SEVEN

Progerin-Induced Aging Enables Modeling of Late-Onset PD Features In Vitro and In Vivo

Introduction

A key motivation for manipulating age in iPSC-mDA neurons is the need for developing faithful models of late-onset neurodegenerative disorders such as PD. Several groups have established iPSC-based disease models of PD. However, those studies reported phenotypes in cell types of uncertain relevance for PD such as neural stem cells (Liu et al., 2012b) or early biochemical phenotypes in mDA neurons without modeling the severe neurodegenerative features of the disease (Cooper et al., 2012; Nguyen et al., 2011; Seibler et al., 2011). We hypothesized that the lack of a neurodegenerative phenotype in those studies may be a result of the age-reset during reprogramming. Similar to PD patients who do not exhibit disease symptoms until later in life, PD iPSC-mDA neurons may be too "young" to mimic the degenerative phase of the disease.

Results

Differentiation of PD iPSCs to mDA Neurons

In order to study the combinatorial effect of age and genetic susceptibility in PD, we obtained iPSCs derived from PD patients (provided by the D. Krainc lab, Cambridge, MA) as well as iPSCs derived from apparently healthy individuals

(controls, also referred to as C1 and C2) (provided by the K. Eggan lab, Cambridge, MA). PD iPSCs were sequenced for their respective homozygous mutations in either PINK1 (Q456X) or Parkin (V324A), demonstrating that reprogramming did not select against the mutation (**Figure 7.1A**). PINK1 and Parkin are thought to act in a common pathway to promote the autophagic degradation of damaged mitochondria (Dodson and Guo, 2007) in addition to the unique functions of Parkin in the ubiquitin-proteasome pathway (Shimura et al., 2000). Despite the mutations, PINK1-Q456X and Parkin-V324A iPSCs differentiated into mDA neurons with similar efficiencies as C1 and C2 iPSCs and maintained mDA neuron markers after several week of maturation (**Figure 7.1B and C**).

Progerin Overexpression in PD iPSC-mDA Neurons: In Vitro

We sought to test whether progerin overexpression would reveal disease-associated phenotypes that cannot be currently modeled in PD iPSC studies. Therefore, we were particularly interested in defining PD-related phenotypes that depend on induced in vitro aging and thereby mimic the late-onset nature of the disease. PD and control iPSC-mDA neurons (day 65) transfected with GFP-progerin or nuclear-GFP for 5 days did not show changes in NURR1 (**Figure 7.2A**) or TH (**Figure 7.2B**) expression. Dendrite length was also identical in PD versus control iPSC-mDA neurons under untreated (data not shown) or nuclear-GFP-treated conditions (**Figure 7.3A and B**); however, progerin overexpression revealed a loss of dendrite length that was significantly enhanced in mDA neurons derived from PINK1-Q456X and Parkin-V324A iPSCs (**Figure 7.3A**

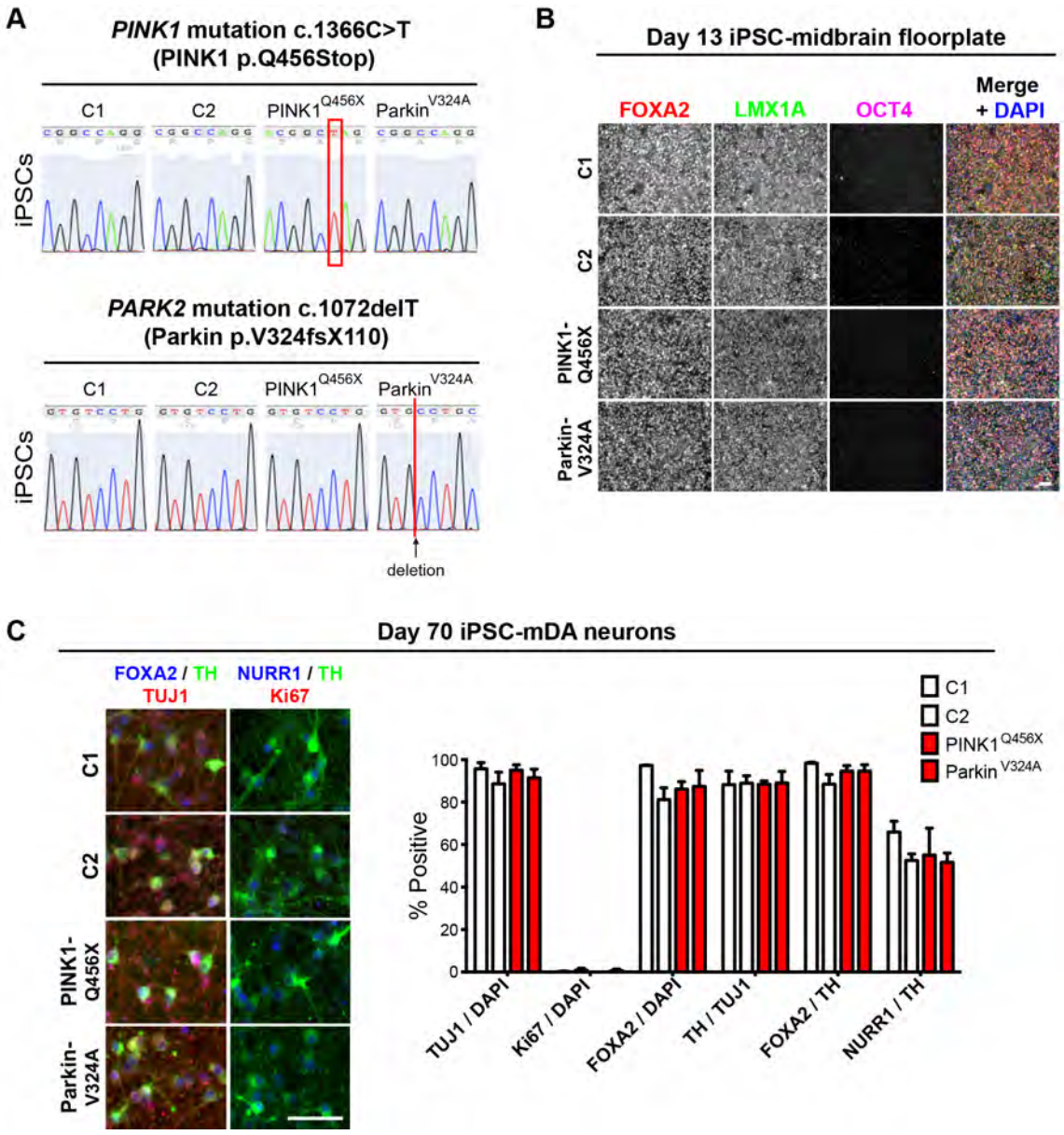

Figure 7.1 **Differentiation of PD mutant iPSCs into mDA neurons.** (A) Sequencing for the homozygous PINK1 c.1366C>T and PARK2 c.1072delT mutations found in the PD mutant iPSCs but not in apparently healthy control iPSCs. (B) Immunocytochemistry at day 13 of differentiation demonstrated no differences between healthy donors and PD patients in the conversion of $OCT4^{+}$ iPSCs to $FOXA2^{+}/LMX1A^{+}$ midbrain floorplate precursors. (C) Further differentiation of precursors to post-mitotic mDA neurons was unaffected in PD mutant cells. n= at least 3 independent differentiations. Bar graph represents mean ± SEM. Scale bars: 50 µm.

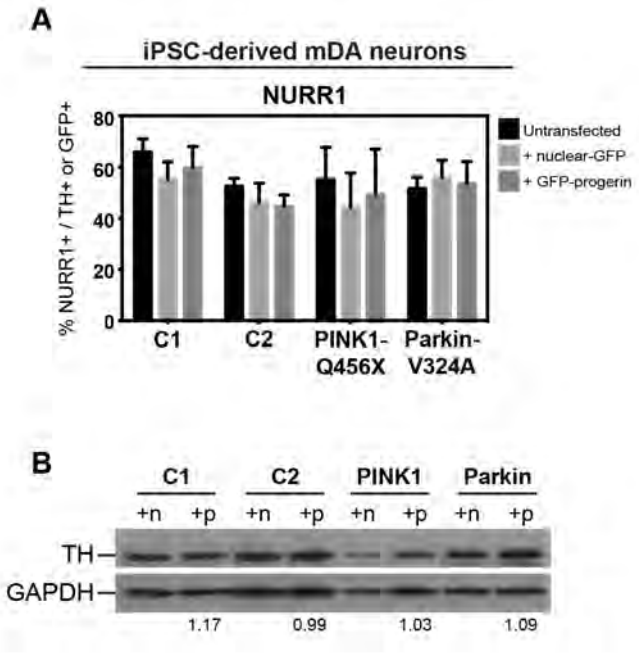

Figure 7.2 Progerin overexpression does not induce loss of mDA neuron-specific markers. (A and B) Quantification of NURR1+ cells (A) and western blot analysis of TH protein levels (B) do not reveal significant differences with transfection of GFP-progerin modified-RNA. n, nuclear-GFP; p, GFP-progerin. Numbers below the western blot indicate the ratio of GFPprogerin: nuclear-GFP expression of TH normalized to GAPDH. Bar graph represents mean ± SEM.

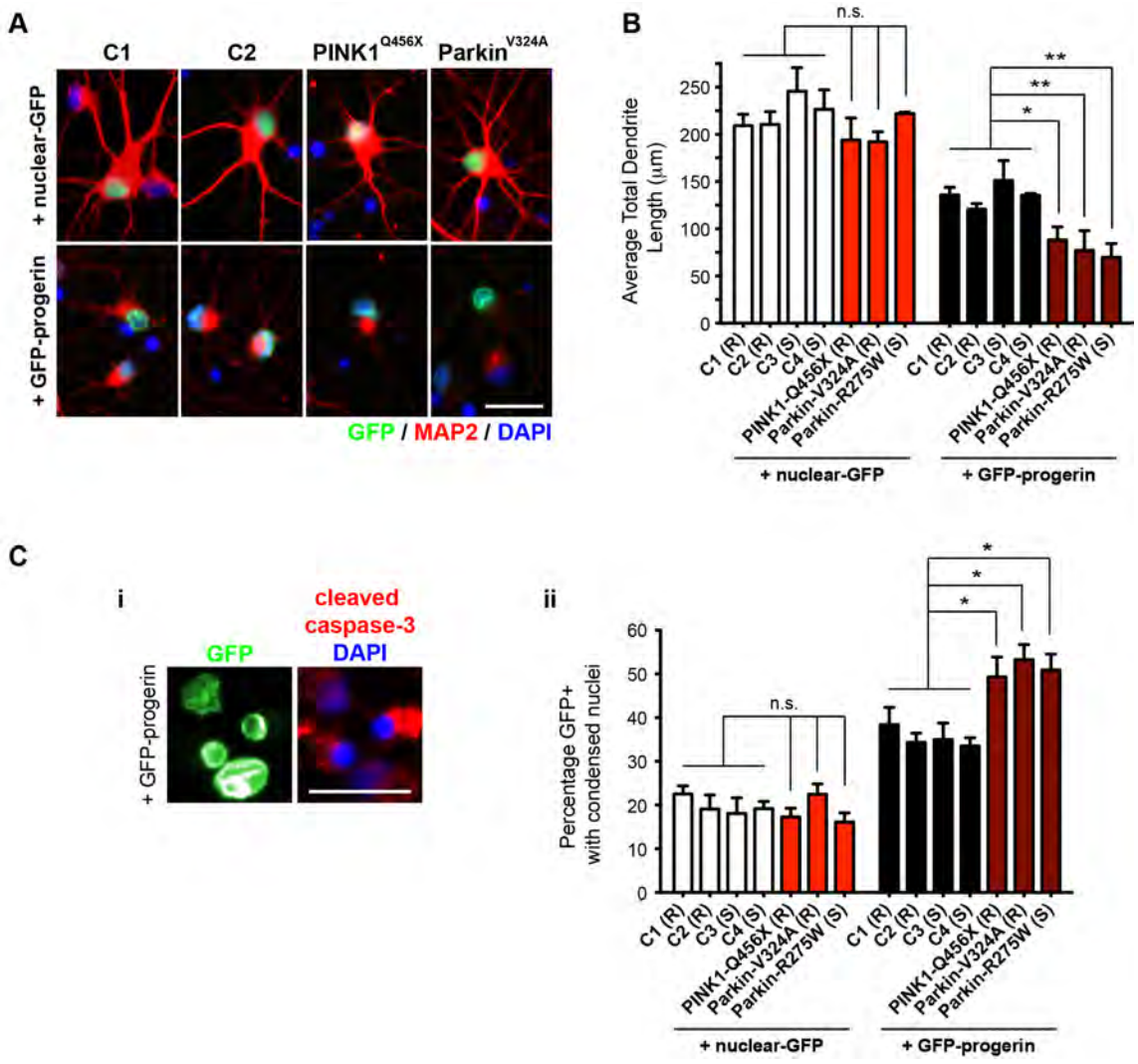

Figure 7.3 Progerin Overexpression Reveals Disease-Specific Phenotypes In Vitro in iPSC-Based Models of Genetic PD. (A) Immunocytochemistry for the dendrite marker MAP2. (B) Quantification of average total dendrite length per GFP+ neuron shows accelerated dendrite shortening in PD mutant iPSC-mDA neurons compared to apparently healthy controls (C1-4) in response to progerin overexpression. (Ci) A representative example of cleaved caspase-3 immunocytochemistry in cells treated with progerin. (Cii) Analysis of GFP+ cells undergoing cell death following RNA transfection as identified by condensed nuclear morphologies. n.s., not significant, *p<0.05, ** p<0.01, *** p<0.001 according to one-way ANOVA with Dunnett's tests (n= 3 independent differentiations and modified-RNA transfections in all cases). Bar graphs represent mean ± SEM. n, nuclear-GFP; p, GFP-progerin; C1-4, lines derived from apparently healthy donors; (R), iPSC derived using retroviral factors; (S), iPSC derived using Sendai viral factors. Scale bars: 25 μm.

and B). Furthermore, we investigated the incidence of cell death in the iPSC-mDA neurons, which could be monitored by condensation of the nucleus and an expression of cleaved caspase-3 (**Figure 7.3Ci**) suggestive of apoptosis. PD iPSC-mDA neurons demonstrated an increased susceptibility to nuclear condensation compared to control iPSC-mDA neurons following progerin overexpression (**Figure 7.3Cii**). Similar to dendrite length, this difference was not observed with nuclear-GFP treatment (**Figure 7.3ii**), indicating that PD mutant mDA neurons are more prone to activating a cell death program upon induced aging. GFP-progerin-positive condensed nuclei were not detected until day 4 or day 5 of progerin transfection, suggesting a progressive decline (similar to that observed in **Figure 6.6C**) rather than an acute toxicity.

It has been suggested that decreased neuronal survival in PD is in part caused by diminished levels of phosphorylated S473 AKT (p-AKT) based on studies in PD models (Tain et al., 2009) and in brain tissue from PD patients (Malagelada et al., 2008; Timmons et al., 2009). Interestingly, PINK1-Q456X and Parkin-V324A mutant iPSC-mDA neurons showed a significant reduction in p-AKT in response to progerin while C1 and C2 iPSC-mDA neurons showed a slight increase in p-AKT (**Figure 7.4A and B**). The deregulation of AKT signaling also resulted in the corresponding changes in the phosphorylation of the downstream signaling targets ULK1 and 4EBP1 (**Figure 7.4A and B**). Of note, there was considerable variability in the basal levels of AKT, ULK1 and 4EBP1 across

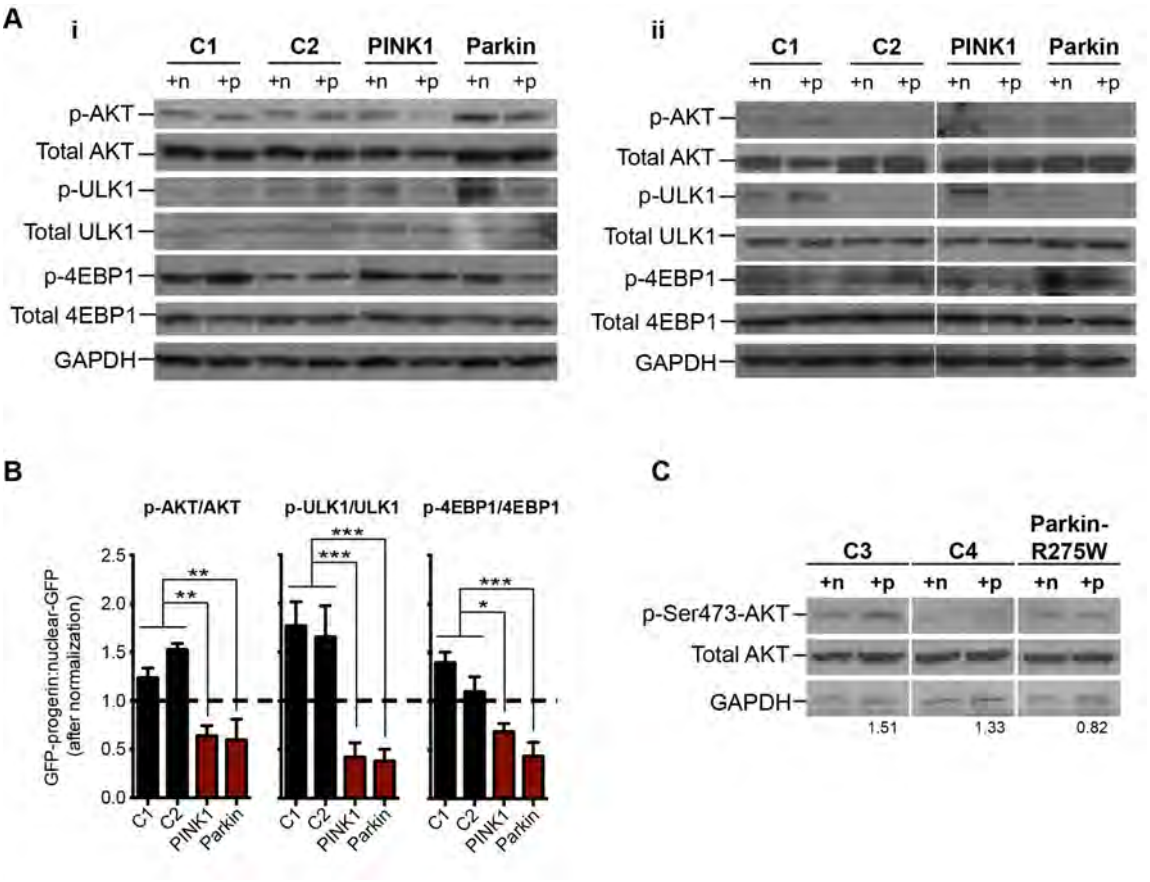

Figure 7.4 PD-specific AKT dysregulation in response to progerin. (A) Western blot analysis of AKT pathway signaling demonstrates genotype-specific responses to progerin overexpression. Blots in (Ai) and (Aii) represent results from replicate experiments demonstrating the variability in basal p-AKT levels with each differentiation. (B) Quantification of phospho-specific bands which were normalized to total protein before calculating the ratio of the levels expressed following progerin or nuclear-GFP treatment. Dotted line indicates an equal amount of phosphorylated protein in both treatment conditions. Quantification represents 3 independent cell experiments/isolates for each genotype. (C) Western blot analysis of AKT pathway signaling in an additional PD patient with a heterozygous mutation in Parkin (p.R275W). Numbers below the blots indicate the ratio of p-AKT (GFP-progerin) to p-AKT (nuclear-GFP). n, nuclear-GFP; p, GFP-progerin; C1-4, lines derived from apparently healthy donors. *p<0.05, ** p<0.01, *** p<0.001 according to one-way ANOVA with Dunnett's tests (n= 3 independent differentiations and modified-RNA transfections in all cases). Bar graphs represent mean ± SEM.

replicate differentiations independent of genotype and treatment (**Figure 7.4A**). However, the progerin-induced reduction in the activation status of AKT signaling components was consistent (independent of basal levels) and mimicked the reported signaling changes in PD.

To further confirm the progerin-induced differences between PD and healthy donor control iPSC-mDA neurons, we reprogrammed additional fibroblasts from a PD patient with a heterozygous R275W Parkin mutation using Sendai virus-based reprogramming (data not shown). Similar to the progerin-induced phenotype in PINK1-Q456X and Parkin-V324A, progerin overexpression drove enhanced dendrite shortening (**Figure 7.3B**), increased apoptosis (**Figure 7.3Cii**), and reduced AKT activation (**Figure 7.4C**) in Parkin-R275W iPSC-mDA neurons compared to C3 and C4 iPSC-mDA neurons. This data demonstrates the robust effect of progerin overexpression in PD iPSC-mDA neurons irrespective of reprogramming technique.

Progerin Overexpression in PD iPSC-mDA Neurons: In Vivo

In order to assess the long-term effects of progerin exposure, day 22 mDA neurons derived from PD (PINK1-Q456X and Parkin-V324A) and control (C1) iPSCs were transduced with lentiviral vectors expressing GFP-progerin or nuclear-GFP under the control of the neuron-specific human synapsin (hSyn) promoter. Onset of hSyn-driven transgene expression was detectable within 7 days in vitro and expression was maintained in cultured cells for at least 90 days (latest time point tested), demonstrating the utility of the hSyn promoter which

supports continuous expression in mDA neurons in contrast to the ubiquitous CMV or CAG promoters which are typically silenced in this cell type. The iPSC-mDA neurons were grafted 8 days later into the striatum of 6-hydroxydopamine (6-OHDA) lesioned NOD-SCID IL2Rgc-null mice (**Figure 7.5A**) when the cells had been differentiated to a stage ideal for survival in vivo (Ganat et al., 2012). In vitro analysis of matched aliquots of cells 3 days after transplantation confirmed similar differentiation capacity between PD and control iPSCs as well as expression of NURR1 and TH in GFP-positive cells (**Figure 7.5B**).

The unilateral 6-OHDA lesion animal model rotates following administration of amphetamine due to the loss of dopamine in the striatum (Fibiger et al., 1973). As a result, it allows for functional analysis of the human iPSC-derived mDA neuron graft where recovery of ipsilateral rotational behavior following transplantation indicates iPSC-mDA neuron survival and innervation of the host striatum. In vivo analysis 3 months after grafting resulted in a reduction of amphetamine-induced rotation scores in most animals (**Figure 7.6**), signifying mDA neuron survival at least above the threshold required for behavioral improvement. Interestingly, there was a small subset of animals that did not recover (**Figure 7.6,** *pink symbols*) which had received either PINK1-Q456X or Parkin-V324A iPSC-mDA neurons expressing progerin. Although the low number of animals analyzed was inadequate to determine significance, lack of recovery was surprising considering that survival of only a few hundred mDA neurons is sufficient to rescue behavior.

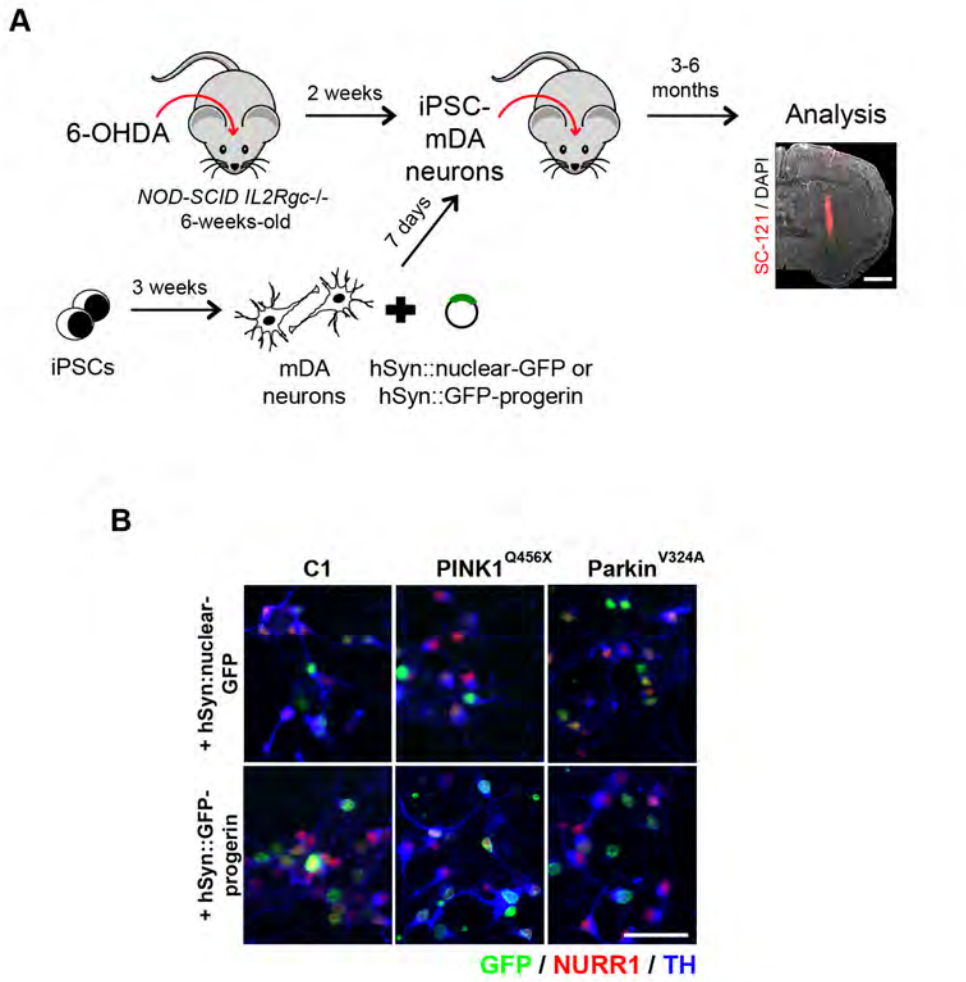

Figure 7.5 Transplantation of PD iPSC-mDA neurons into the 6-OHDA lesion model. (A) Schematic illustration of the transplantation studies into 6-OHDA lesioned parkinsonian mice. Immunofluorescence image depicts a representative iPSC-mDA neuron graft indicated in the striatum by expression of the human-specific marker SC-121. (B) Immunocytochemistry for NURR1 and TH in iPSC-mDA neurons replated in vitro and fixed 3 days post transplant. At least 50% of cells already expressed the synapsin-driven transgene at this time point. Scale bars: 1 mm (A), 50 µm (B).

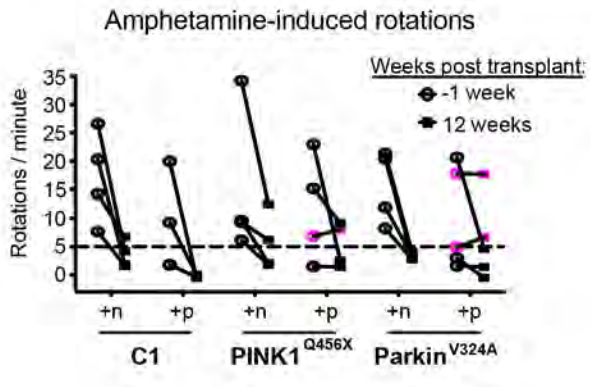

Figure 7.6 <u>Behavioral analysis of 6-OHDA 3 months post transplant.</u> Number of rotations induced by amphetamine in lesioned mice transplanted with control or PD mutant iPSC-mDA neurons expressing hSyn::nuclear-GFP or hSyn::GFP-progerin. Analysis was performed prior to transplantation to determine efficacy of lesioning as well as 3 months following engraftment. Dotted line indicates threshold for successful lesioning. Pink symbols identify successfully lesioned animals that did not show recovery. n= 3-5 animals per treatment group.

To address whether incomplete behavioral recovery in the animals was due to a smaller number of surviving mDA neurons, we performed stereological quantification of the grafts. While graft volume was not significantly affected in progerin-treated versus nuclear-GFP-treated groups (data not shown), progerin-expressing mDA neuron grafts showed a dramatic reduction in TH^+ cell numbers (**Figure 7.7A and B**) that was not observed at the time of transplantation (**Figure 7.5A**) or 1 month post-grafting (data not shown). Strikingly, the reduction in TH^+ cells was particularly pronounced in progerin-expressing mDA neuron grafts from PINK1-Q456X and Parkin-V324A iPSCs and minimal in C1 iPSC-mDA neuron grafts (**Figure 7.7A and B**). Analysis of the rare serotonergic and GABAergic neuron contaminants produced during the mDA neuron differentiation did not show a similar progerin-induced deficit (**Figure 7.7C and D**), suggesting that the significant loss of TH in PINK1-Q456X and Parkin-V324A iPSC-mDA neuron grafts expressing progerin was cell type-specific. Of note, progerin did not reduce the number of iPSC-mDA neurons expressing the transgene (**Figure 7.7E**) or induce loss of FOXA2 (**Figure 7.7F**), indicating a gradual degeneration at 3 months that has not yet advanced to the complete absence of mDA neuron markers and cell death. These results support the ability of progerin to mimic the progressive decline observed in PD patients.

To further assess biomarkers of age and disease status of the iPSC-mDA neurons, we performed ultrastructural analysis of the grafts 6 months after transplantation by transmission electron microscopy (TEM). Although not

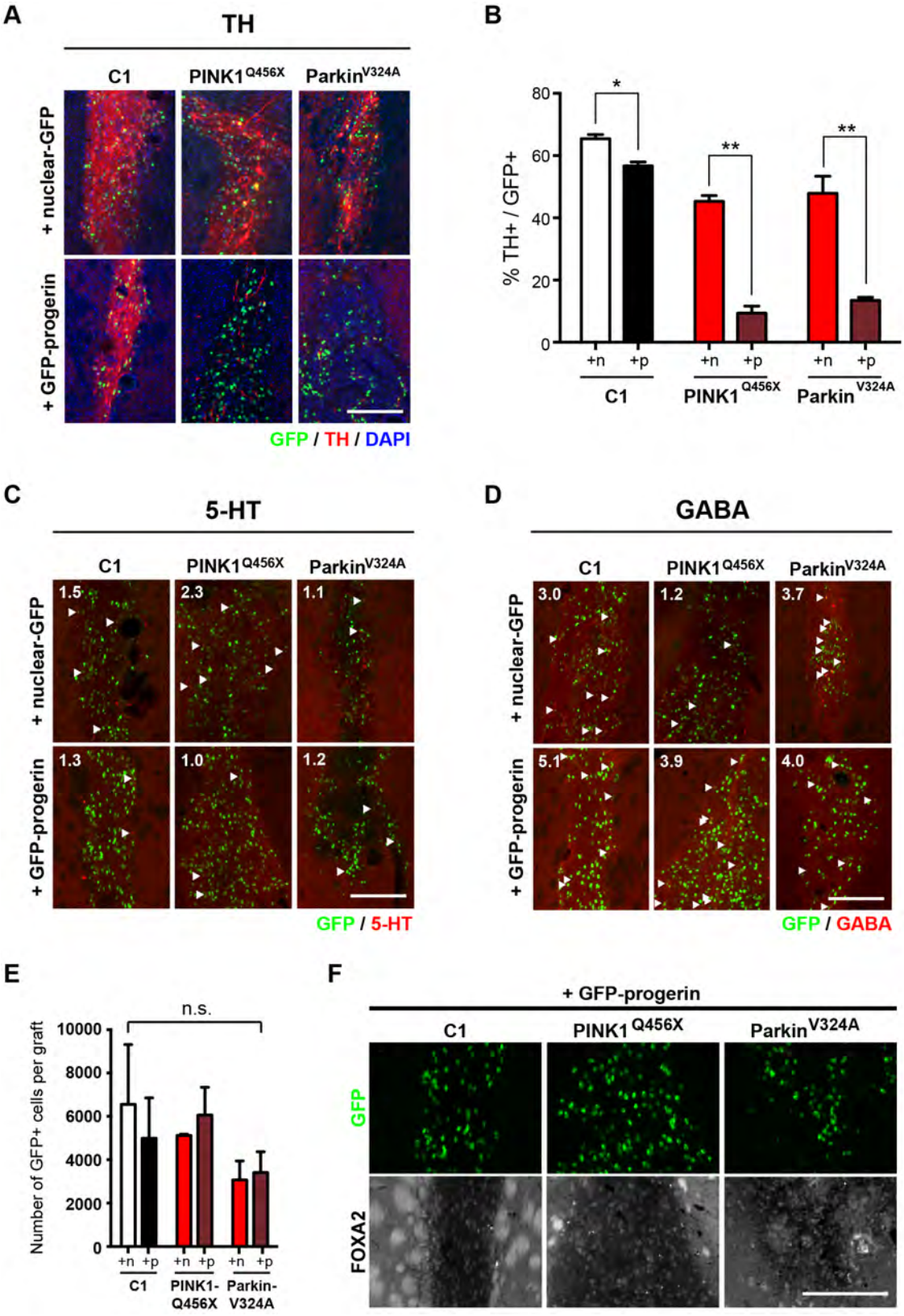
A
TH
C1
PINK1Q456X
ParkinV324A
+ nuclear-GFP
+ GFP-progerin
GFP / TH / DAPI
B
% TH+ / GFP+
80
60
40
20
0
*
**
**
+n
+p
C1
PINK1Q456X
ParkinV324A
C
5-HT
1.5
2.3
1.1
1.3
1.0
1.2
GFP / 5-HT
D
GABA
3.0
1.2
3.7
5.1
3.9
4.0
GFP / GABA
E
n.s.
Number of GFP+ cells per graft
10000
8000
6000
4000
2000
0
C1
PINK1-Q456X
Parkin-V324A
F
+ GFP-progerin
GFP
FOXA2

Figure 7.7 Analysis of iPSC-mDA neuron grafts reveals progerin-induced progressive PD phenotype. (A) Immunohistochemical assessment at 3 months post transplant reveals a dramatic loss of TH in PD mutant mDA neurons overexpressing progerin. (B) Stereological quantification of the percentage of GFP^+ cells that are TH^+. Cells in the graft that were not expressing the transgene were not analyzed. (C and D) Immunohistochemistry of the same grafts shown in (A) for 5-HT labeling serotonergic neurons (C) and for GABA labeling GABAergic neurons (D). Numbers represent the percentage of GFP^+ cells also positive for the respective marker (using ImageJ). Arrowheads indicate positive cells. (E) Stereological quantification of the number of GFP^+ cells per graft. (F) Immunohistochemistry of the same grafts shown in (A) for GFP and FOXA2. Bar graphs represent mean ± SEM. n.s., not significant, *$p<0.05$, ** $p<0.01$ according to Student's t-tests (B) or two-way ANOVA with Tukey tests. n.s., not significant. n= 3 mice per condition. Scale bars: 200 μm.

quantifiable, initial observations of the embedded tissue by light microscopy demonstrated a continued, progressive loss of TH immunoreactivity and only a few remaining GFP^+ cells in grafts overexpressing progerin (**Figure 7.8A**). Analysis by TEM confirmed the progerin-induced reduction of TH expression in iPSC-mDA neuron dendrites (**Figure 7.8B**) as well as the folded nuclear morphologies in surviving $progerin^+$ cells (**Figure 7.8C**).

To determine the age status of the grafted neurons we focused on the intracellular accumulation of neuromelanin. Neuromelanin is an electron-dense pigment present in adult mDA neurons but absent in fetal or neonatal stages including iPSC-mDA neurons (Mann and Yates, 1974; Sulzer et al., 2008). In human fetal tissue transplantation studies, neuromelanin was detected in grafts 4 to 14 years after intrastriatal injection, a time course similar to normal development (Loh et al., 2010). In just 6 months, we observed robust accumulation of neuromelanin with lipofuscin deposits (Barden, 1969) selectively in grafts overexpressing progerin (an average of 8 deposits per 55 μm^2 versus 0.5 deposits in nuclear-GFP expressing grafts, **Figure 7.9**) and regardless of genetic background. The melanin granules appeared very similar to those observed previously in substantia nigra neurons of both PD and healthy brains (Roy and Wolman, 1969).

In addition, progerin overexpression revealed genotype-specific effects in PD iPSC-derived grafts, phenotypes not observed in PD grafts overexpressing

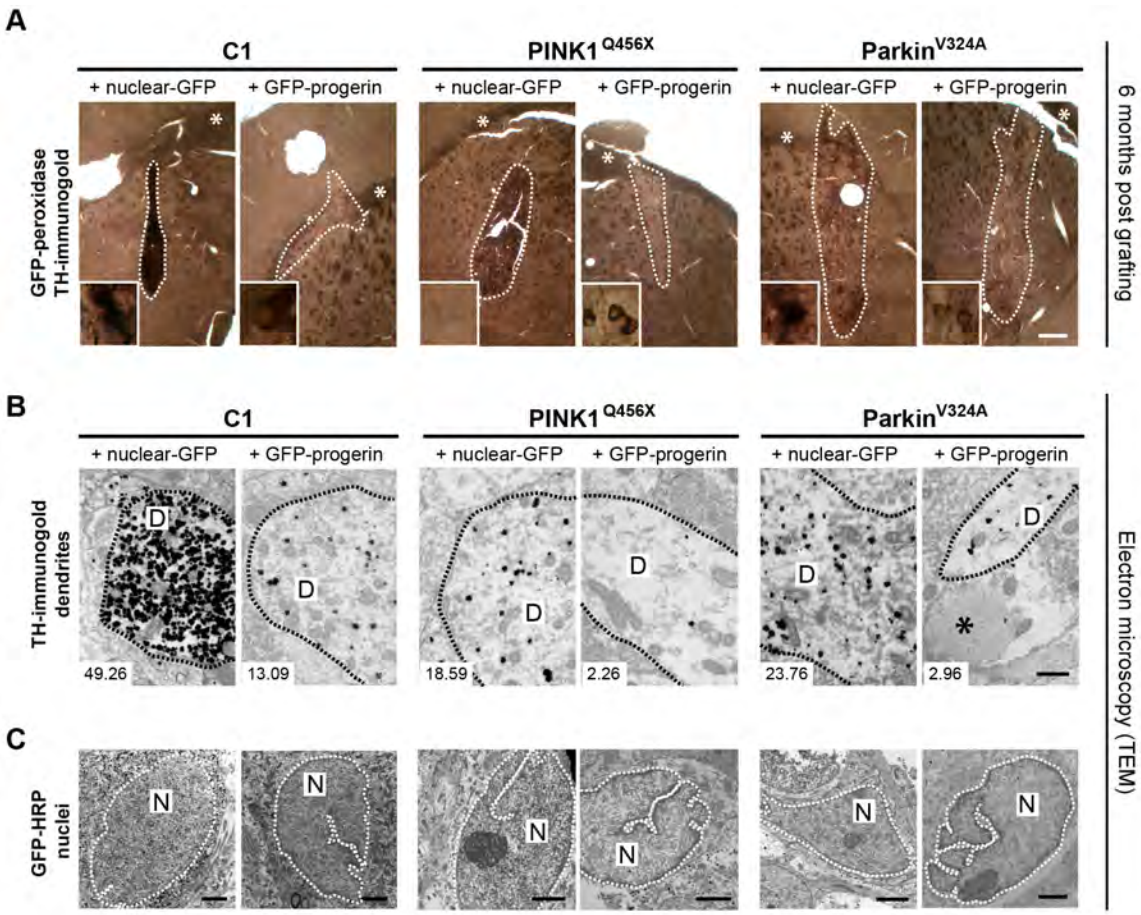

Figure 7.8 **Ultrastructural analysis of xenografts.** (A) Images of graft area in embedded tissue immunostained for TH (immunogold) and GFP (HRP) at 6 months post transplant demonstrate a dramatic loss of TH^+ when progerin is overexpressed. This pattern of TH loss in controls and PD mutants is consistent with what was observed at 3 months post transplant (see Figure 7.7). White dotted line defines the graft. Asterisks denote the corpus callosum. Insets show representative GFP^+ nuclei and the respective TH level. (B and C) Ultrastructural analysis by transmission electron microscopy (TEM). Representative TH^+ dendrites (B) and GFP^+ nuclei (C) are outlined and each labeled with a D or an N, respectively. Number at bottom left represents the average number of TH-immunogold particles per μm^2. Asterisk identifies a fibrillar body of broken-down microtubules. Scale bars: 400 μm (A), 500 nm (B), 2 μm (C).

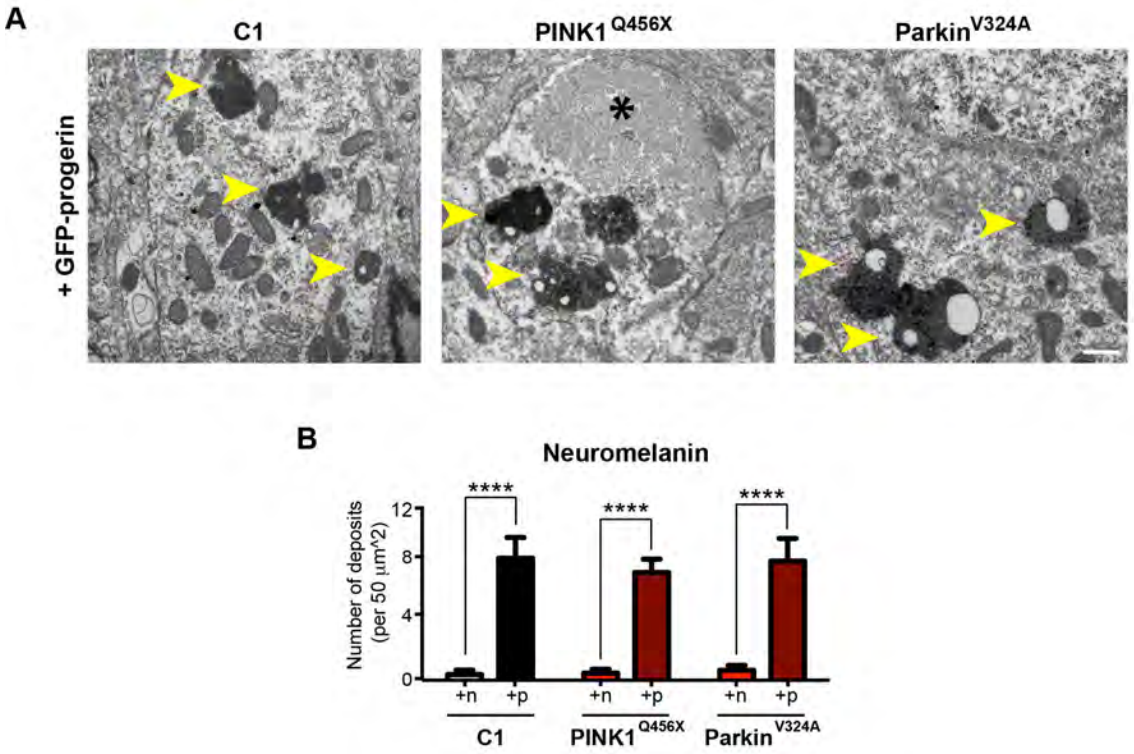

Figure 7.9 <u>Progerin induces neuromelanin accumulation in iPSC-mDA neuron xenografts.</u> (A) Ultrastructural analysis 6 months after transplantation revealed accumulation of neuromelanin with lipofuscin deposits (*yellow arrowheads*) in mDA neuron grafts transduced with progerin. Asterisk in (A) indicates a fibrillar body. Black dots represent TH-immunogold staining. (B) Quantification of neuromelanin deposits from EM analysis. Ten 50-µm^2 regions were analyzed per animal. Bar graph represents mean ± SEM. Scale bar: 500 nm.

nuclear-GFP or in any non-PD control grafts. For instance, signs of neurite degeneration such as the appearance of fibrillar bodies were prominent in PD-derived grafts overexpressing progerin (*asterisks* in **Figure 7.8B**, **Figure 7.9A**, and **Figure 7.10C**), indicating a breakdown of microtubules (Jaworski et al., 2011). Furthermore, PINK1-Q456X grafts contained cells with enlarged mitochondria, a phenotype much more pronounced in progerin overexpressing cells (area = 0.167 μm^2 compared to 0.0387 μm^2 for PINK1 iPSC-mDA overexpressing nuclear-GFP, p=0.0005; **Figure 7.10A and B**). The presence of enlarged mitochondria under progerin-treated conditions may indicate an increase in mitochondrial biogenesis, which was noted by Krainc and colleagues at the level of increased expression of PGC-1α (Seibler et al., 2011). This phenomenon may be compensating for the loss of mitochondrial function as suggested for the enlarged mitochondria found in MitoPark mice (Sterky et al., 2011). In contrast, Parkin mutant grafts showed less dramatic mitochondrial defects (such as abnormal mitochondrial fusion; data not shown) but strikingly, exhibited large multilamellar inclusions (**Figure 7.10C**). Multilamellar inclusions such as these have been observed in various neurodegenerative models (Cheng et al., 2011; Phillips et al., 2008) and in PD brain tissue (Roy and Wolman, 1969). While these inclusions differ from the classical Lewy body morphology found in surviving mDA neurons in brains from Parkinson's patients, they may be an alternative form or simply an early aggregate that will progress to the classical form (Fornai et al., 2004). The presence of these neuronal inclusions suggests decreased function of the ubiquitin-proteasome pathway, which could be related

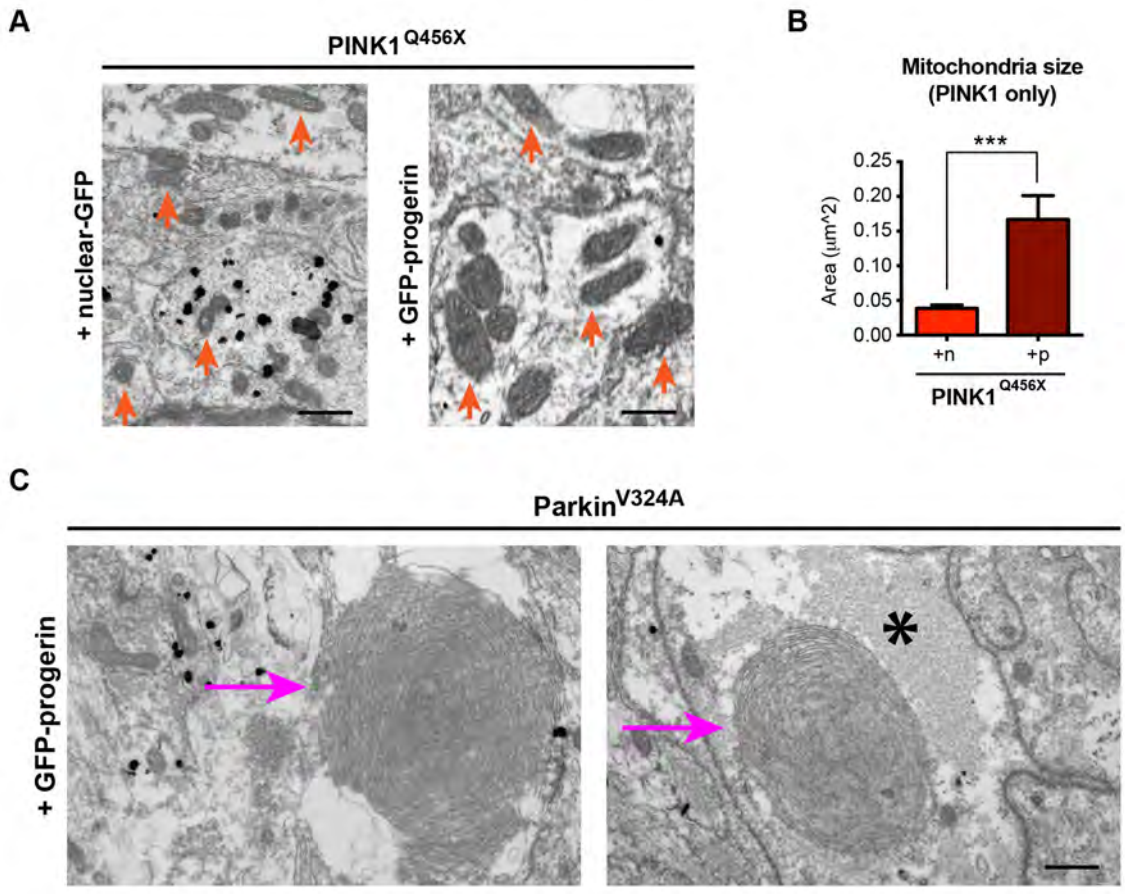

Figure 7.10 Progerin reveals disease phenotypes in PD iPSC-mDA neurons that require age. (A) PINK1 mutant graft with progerin displays enlarged mitochondria (compare representative mitochondria indicated by *orange arrows* in nuclear-GFP and GFP-progerin groups). (C) Large multilamellar inclusions present in Parkin mutant graft with progerin (*pink arrows*). This phenotype was not observed in any other treatment group. Asterisk in (C) indicates a fibrillar body. Black dots in (A) and (C) represent TH-immunogold staining. Scale bars: 500 nm.

in this case to the loss of normal Parkin function. The dependence of the phenotype on progerin expression in both the PINK1-Q456X and Parkin-V324A grafts suggests that age-related factors contribute to the dysfunction.

Discussion

Our in vivo results corroborate the in vitro data that the age of iPSC-mDA neurons is reset to a "young" state not conducive to modeling late-onset features of PD. In contrast, progerin-induced neuronal aging reveals phenotypes consistent with normal aging as well as disease-associated phenotypes that reflect the synergistic interaction of genotype and age in modeling late-onset degenerative aspects of PD. To our knowledge, our study is the first to incorporate an age-like component into an iPSC-based model of a late-onset disease to better phenocopy the true disease state. While progerin exposure may not capture all aspects of normal aging, our study demonstrates that the induced aging strategy triggers an aged-like state suitable for modeling at least some late-onset aspects in a manner not previously possible in the iPSC field.

We observed a robust degenerative phenotype in two genetic PD iPSC models. In future studies it will be interesting to mechanistically dissect the separate contribution of genetic and age-related disease susceptibility such as the differences observed in grafted PINK1 versus Parkin mutant iPSC-mDA neurons using isogenic, gene-corrected lines. These isogenic lines will also further the investigation into the ultrastructural inclusions observed in Parkin-derived mDA

neurons in vivo which may be compatible with precursor lesions to Lewy body formation. As Lewy bodies are less frequently observed in PD patients with Parkin or PINK1 mutations (Nuytemans et al., 2010), it will be intriguing to test our strategy in additional PD subpopulations such as patients with mutations in alpha-synuclein or LRRK2 or in sporadic PD.

The mechanism of TH^+ cell loss in the current study remains to be determined. In the future it will be important to perform time course experiments to further examine the progressive reduction in TH^+ neurons upon long-term exposure in vivo despite our preliminary observations that there are comparable TH^+ neuron numbers in the in vitro system and at early time points after grafting. These studies will also aid in understanding differences in the acquisition of age- and disease-associated phenotypes using modified-RNA versus the hSyn-driven lentivirus to overexpress progerin, which appear to give rise to phenotypes at different rates.

Finally, our technology could be integrated into a drug discovery pipeline aimed at counteracting the increased disease susceptibility of aged cells, a target which cannot be pursued using current PD-iPSC models where the symptom-relevant cells appear "young" and resistant to the degenerative aspect of the disease.

CHAPTER EIGHT

Discussion and Future Directions

The current study represents a first attempt at manipulating age in iPSC-derived somatic cell types. We define a set of cellular markers that correlate with the chronological age of donor fibroblasts, including markers of nuclear organization, heterochromatin, DNA damage and mitochondrial stress. We demonstrate a loss of these age-associated markers upon reprogramming and report that iPSC-derived lineages do not reacquire features of aging upon differentiation. We further show that in apparently healthy, non-HGPS fibroblasts progerin exposure is sufficient to induce the same set of age-associated markers that define the original old donor fibroblast population prior to iPSC induction. Importantly, we present an induced aging strategy that mimics several aspects of normal aging in an iPSC-derived lineage beyond fibroblasts and demonstrate the utility of our approach for modeling late-onset disorders such as PD (**Figure 8.1** and **Table 8.1**. The induced aging platform established here will allow for a broad range of applications and future investigations, which are discussed below.

Applications in Defining and Programming Cellular Age

While our study presents several age-associated markers that are erased by reprogramming, it remains to be determined whether *all* aspects of age are reset in cells derived from old donors. It will be interesting in the future to define a more

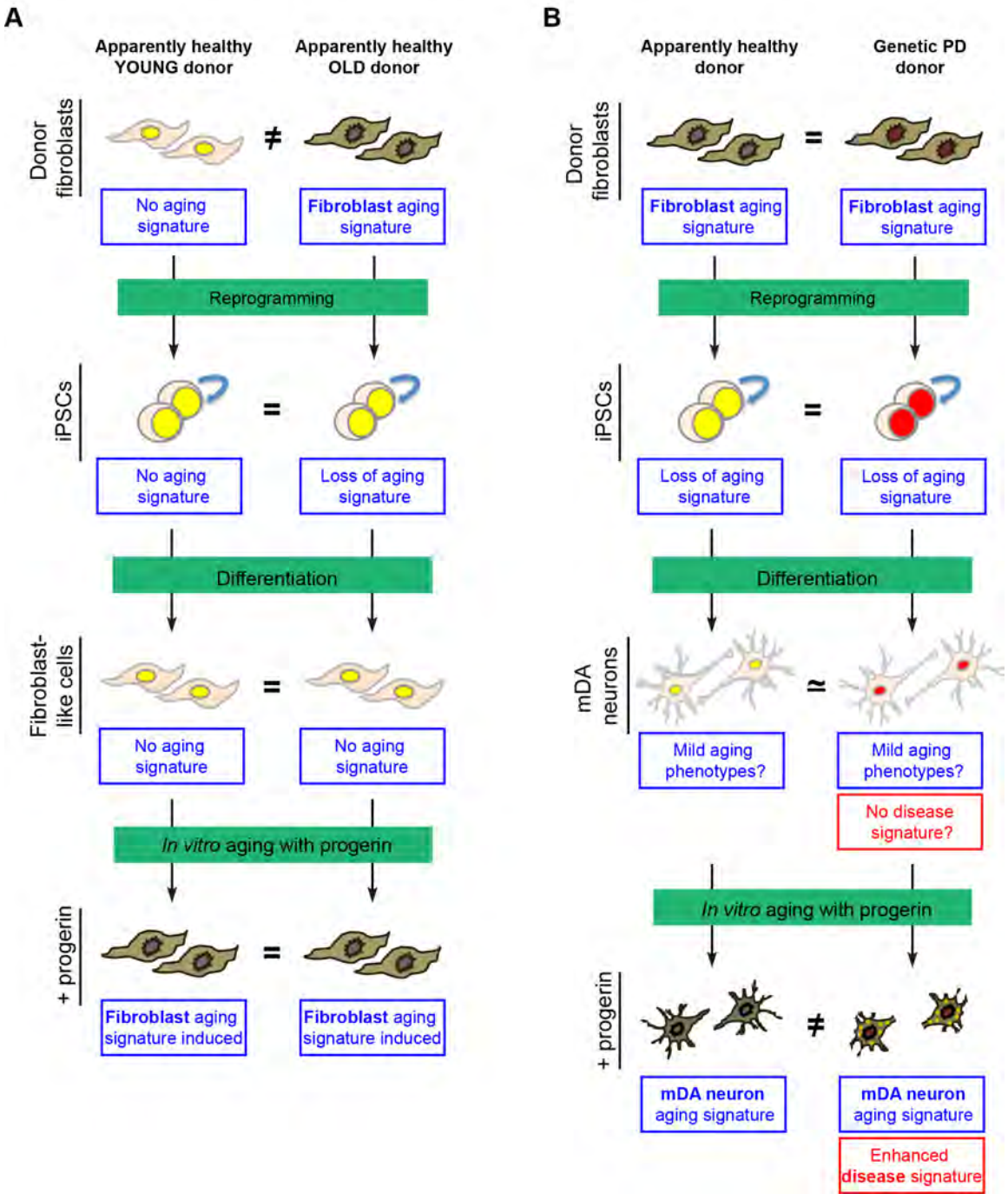

Figure 8.1 **Summary diagram.** (A) A set of age-associated markers found in primary fibroblasts derived from old donors are lost during reprogramming to iPSCs and are not regained upon differentiation of iPSCs to fibroblast-like cells or mDA neurons. As a result, the reprogramming/differentiation paradigm generates cells with a "young" phenotype regardless of donor age. However, age-associated markers can be reestablished upon overexpression of progerin, giving rise to "old" iPSC-derived cells. (B) iPSCs derived from PD patients and apparently healthy donors appear to be

phenotypically identical despite their genotypic differences. Upon differentiation into mDA neurons only minor differences are observed between PD versus control cells (no/mild disease signature). However, progerin overexpression triggers an mDA aging-like signature and reveals multiple disease-associated phenotypes that require the interaction between genotype and phenotype in PD iPSC-derived mDA neurons (enhanced disease signature).

Fibroblast aging signature	**Associated marker**
Nuclear folding and blebbing	Lamin A/C
Loss of nuclear organization proteins	LAP2α
Loss of heterochromatin	H3K9me3, HP1γ
Accumulation of DNA damage	γH2AX
Increased mitochondrial ROS generation	MitoSOX
Telomere shortening	Telomeric repeats Q-FISH probe
Upregulation of senescence markers	SA-β-Gal
mDA neuron aging signature	**Associated marker**
Enhanced nuclear folding and blebbing	Lamin A/C
Accumulation of DNA damage	γH2AX
Increased mitochondrial ROS generation	MitoSOX
Dendrite shortening	MAP2ab
Neurodegeneration gene expression signature	RNA-seq
Hyperactivation of p-AKT	p-AKT, p-4EBP1, p-ULK1
Mild decrease of TH^+ neurons	TH *in vivo*
Accumulation of neuromelanin	Electron microscopy *in vivo*
PD disease signature	**Associated marker**
Enhanced susceptibility to cell death activation	Cleaved caspase-3
Accelerated dendrite shortening	MAP2ab
Loss of p-AKT	p-AKT, p-4EBP1, p-ULK1
Pronounced/progressive loss of TH^+ neurons	TH *in vivo*
Enlarged mitochondria	Electron microscopy *in vivo* – PINK1 only
Multilamellar inclusions	Electron microscopy *in vivo* – Parkin only

Table 8.1 Summary of phenotypes and associated markers. Cell type-specific markers are listed for healthy iPSC-derived fibroblasts and mDA neurons as well as PD iPSC-derived neurons following progerin expression.

comprehensive aging signature using many more fibroblast lines from young and old donors. In addition to assessing candidate age-associated markers like nucleolar morphology (Sinclair et al., 1997) and p16 expression levels (Tsygankov et al., 2009), gene expression and methylation profiling would allow for measuring the extent of rejuvenation on a genome-wide scale. However, in contrast to previous studies that have claimed that iPSCs possess epigenetic memory of the cell of origin (Kim et al., 2010), it will be important to compare populations where the iPSCs are of sufficient passage number (as discussed in Chapter 1) and where the fibroblasts are from multiple young and multiple old donors to eliminate individual/derivation/in vitro culture biases. With this in mind, the genome-wide techniques could uncover lasting age-related markers that co-occur in multiple donors or could more firmly verify the reprogramming reset of age.

Our results indicate that progerin levels may affect the timing by which age-related phenotypes appear. The use of modified-RNAs rapidly induced very high levels of expression and triggered age-related markers within just 3 days in iPSC-derived fibroblasts and 5 days in iPSC-derived neurons. In contrast, lentiviral expression under the control of a neuronal-specific promoter led to a gradual accumulation of progerin that produced a more progressive phenotype. In the future, it will be interesting to further dissect these different observations by titrating the amount of modified-RNA and following the phenotype over time. These experiments would better determine whether there is a threshold level of

progerin that is necessary to trigger particular phenotypes and whether there is a consistent order to these events, which we did not address here. Furthermore, these experiments would help to establish whether our induced aging paradigm will also be amenable for deriving cells of intermediate ages. Lower doses or shorter courses of progerin modified-RNA may result in iPSC-fibroblasts that are 40-years-old instead of 80-years old, for instance. Using a more comprehensive list of aging biomarkers (as discussed in the previous paragraph), iPSC-fibroblasts with various progerin treatments could be compared to primary fibroblasts that represent the aging spectrum to determine the amount of progerin required to achieve a particular chronological age. Data obtained in this manner would also help to elucidate whether age-related marker expression increases gradually or occurs as a binary “off/on” switch between young and old age. Finally, the characterization of additional biomarkers of aging will aid in our understanding of how closely progerin exposure in iPSC-derived somatic cells truly mimics normal aging. It may be that progerin overexpression does not trigger key pathways involved in aging, necessitating complementary and/or replacement strategies that could be identified from such studies.

In addition to facilitating the programming of cellular age, progerin may also be able to induce maturation in iPSC-derived somatic cells. As discussed in Chapter 1, the directed differentiation of pluripotent stem cells gives rise to immature, embryonic-like cell types that require months of in vitro or in vivo maturation to establish robust functional properties (reviewed in (Liu et al., 2012a; Saha and

Jaenisch, 2009)). This phenomenon has been reported in iPSC-derived cardiomyocytes, hematopoietic stem cells, pancreatic beta cells, and neurons. While the analyses that were addressed in this study focused on markers of aging, it may well be that progerin can also induce markers related to functional maturity. In fact, we observed changes in gene expression in young and old donor iPSC-derived mDA neurons that may indicate the loss of immature features following progerin treatment (**Table 6.2** and **Figure 6.8A**). However, our iPSC-derived mDA neurons or fibroblasts may simply be old *embryonic* cells rather than old *adult* cells. Although it is still unclear whether triggers of aging can also play a role in maturation, it will be interesting in the future, for instance, to titrate progerin levels over long time frames and look for accelerated upregulation of the dopamine transporter DAT, dopamine release, or electrophysiological properties that do not normally arise until after 100 days of in vitro differentiation of iPSCs toward mDA neurons (unpublished data from our lab). It will also be interesting to apply progerin to other embryonic/fetal-like iPSC-derived somatic cell types and look for maturation properties that could improve these cells for use in replacement therapy.

Another interesting aspect of our induced aging paradigm is the ability to address the reversibility of age-related markers. Using a doxycycline (dox)-inducible GFP-progerin fibroblast line (kindly provided by T. Misteli), we have observed rapid induction of progerin expression upon dox removal, which triggers abnormal nuclear morphologies. Subsequent re-addition of dox results in reversal of

nuclear folding and blebbing upon progerin turnover (**Figure 8.2**). Similarly, iPSC-derived somatic cells could be treated with progerin modified-RNA for a given time and then further cultured in its absence. Assessment of age-related markers at each stage would determine whether particular markers are dependent on progerin or whether progerin induces lasting effects. For instance, following programming of iPSC-derived somatic cells from age 10 to age 80, do the cells return to age 10? Are they still age 80? Or are they reverted only part way to age 40? Furthermore, do all of the markers follow the same chronological pattern upon loss of progerin? Exposure of various iPSC-derived lineages to progerin would also elucidate whether different cell types respond in the same manner. In addition, strategies to rescue single progerin-induced phenotypes, such as oxidative damage with antioxidants or telomere shortening with hTERT overexpression, could be explored to determine whether there is a downstream master regulator of the progerin-induced phenotype. Conversely, single phenotypes could be triggered using pro-oxidants or telomerase inhibitors, for instance, to determine whether a single hit is sufficient to cause the other age-related phenotypes. Ultimately, understanding reversibility of age and the primary culprit(s) may also get us closer to new strategies for extending healthspan and/or lifespan.

Applications in Disease Modeling

We present a strategy for revealing robust late-onset phenotypes in mDA neurons derived from multiple iPSC-based models of genetic PD. Prior to this study, reports of PD iPSC models focused on cell types and phenotypes of

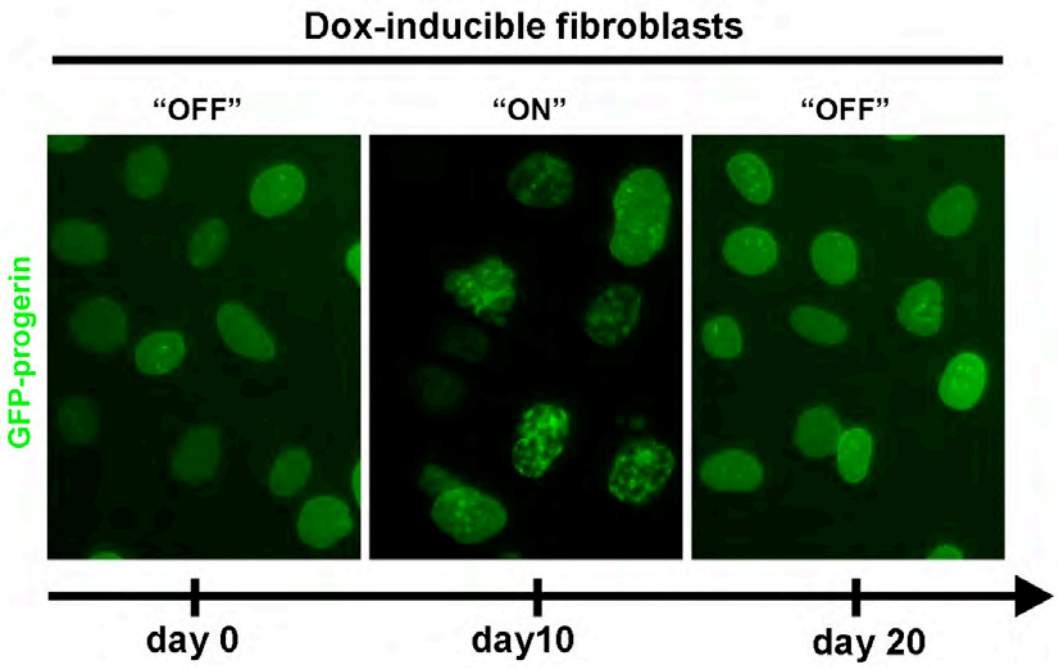

Figure 8.2 Reversibility of nuclear morphology abnormalities upon removal of progerin. A tet-inducible fibroblast line (Scaffidi and Misteli, 2008) acquires GFP-progerin expression and nuclear morphology abnormalities upon removal of doxycycline over a 10-day time course. Nuclear abnormalities are reversed upon re-addition of doxycycline and silencing of the transgene. Some leaky expression is observed in the "OFF" state.

questionable relevance to the disease. For instance, a recent study suggests that reduced primary fiber outgrowth in LRRK2-G2019S neurons may reflect a "neurodegeneration" phenotype (Sánchez-Danés et al., 2012). However, earlier time points were not assessed; therefore, it is unclear whether this phenotype manifested during development, which would be unlikely in PD, or upon terminal differentiation. Because disease-relevant cells affected in late-onset diseases typically appear healthy until later in life, we chose to treat our iPSC-mDA neurons with progerin *after* a very extensive fiber network was established. Thus, we interpret the progerin-mediated changes as a degenerative response given the breakdown of neurites and the progressive nature of the phenotype, which more faithfully recapitulates PD.

Although we established several PD-specific phenotypes upon induced aging, the mechanism of mDA neuron loss is still unclear. In the future it will be interesting to take a closer look at the progerin-induced events. For example, it will be important to determine whether the inclusions formed in Parkin-mutant iPSC-mDA neurons overexpressing progerin (Figure 7.10**C**) are comprised of ubiquitinated alpha-synuclein as reported for typical Lewy bodies (Spillantini et al., 1997) and whether they progress to a more classical morphology at later points (>6 months) post grafting. Furthermore, analysis at various time points following progerin treatment should elucidate the correlation between progerin accumulation and the onset of each disease phenotype. These data will also reveal the timing of degeneration (shortened dendrite lengths, loss of TH, etc.)

and cell death in relation to the timing of inclusion formation, which remains controversial (reviewed in (Cookson, 2009)). In fact, the evidence that alpha-synuclein aggregation plays a causal role in PD comes from engineered models where it is artificially induced as the primary event. The finding that aggregation occurs prior to cell death would support these studies. Conversely, aggregation only present in the rare surviving neurons would indicate that inclusion formation might simply be a byproduct of the degeneration process. It will also be important to investigate the mechanism of cell death in PD, which has been suggested to occur via apoptosis, necrosis, autophagy, or a combination thereof (reviewed in ((Venderova and Park, 2012)). In our study, we observed the activation of apoptosis in progerin-treated iPSC-mDA neurons in vitro as evidenced by nuclear condensation and caspase-3 cleavage. However, in vivo we observed evidence of autophagic cell death (data not shown). In order to dissect the mechanism, it will be advantageous in the future to define differentiation protocols that distinguish between mDA neurons of the substantia nigra, which are susceptible in PD, and mDA neurons of the ventral tegmental area, which are relatively protected in PD (Chung et al., 2005). It may also be beneficial to consider co-culture with astrocytes or an organoid culture system like the recently described “mini brains” (Lancaster et al., 2013) in order to incorporate potential non-cell autonomous aspects of PD. Furthermore, as mentioned in Chapter 7, isogenic iPSC lines would greatly aid in these endeavors by limiting the inherent noise in comparing cells from individuals with different backgrounds. Finally, these strategies in combination with progerin overexpression could be

used to characterize additional PD iPSC models bearing other PINK1 or Parkin mutations or the more common LRRK2 or alpha-synuclein mutations, aiding in our understanding of the relationship between different causes of PD. Ultimately, these data could all inform the development of a more relevant drug-screening platform using PD iPSC-derived mDA neurons to find candidate therapeutics for PD that actually target the degenerative phase of the disease. Because there is also a progressive loss of mDA neurons with age in healthy individuals (Chu and Kordower, 2007), therapeutics aimed at treating PD could even be relevant to the aging population as a whole.

Beyond PD, progerin-induced aging could be applied to iPSC-based models of other late-onset diseases, including additional neurodegenerative disorders such as ALS and AD, cardiovascular disease, macular degeneration, and cancer, where the iPSC-derived somatic cells are similarly too “young”. Including an age-like component in these models will hopefully allow us to examine the unique contributions of age and genetic susceptibility in these diseases and to determine why a particular disease is late-onset. We may even one day be able to use the complementary strategies of reprogramming and induced aging to predict a young donor’s susceptibility to a variety of age-related diseases.

BIBLIOGRAPHY

Agarwal, S., Loh, Y.-H., Mcloughlin, E.M., Huang, J., Park, I.-H., Miller, J.D., Huo, H., Okuka, M., Dos Reis, R.M., Loewer, S.*, et al.* (2010). Telomere elongation in induced pluripotent stem cells from dyskeratosis congenita patients. Nature *464*, 292-296.

Albin, R.L., Young, A.B., and Penney, J.B. (1989). The functional anatomy of basal ganglia disorders. Trends Neurosci *12*, 366-375.

Angot, E., Steiner, J.A., Lema Tome, C.M., Ekstrom, P., Mattsson, B., Bjorklund, A., and Brundin, P. (2012). Alpha-synuclein cell-to-cell transfer and seeding in grafted dopaminergic neurons in vivo. PLoS One *7*, e39465.

Anokye-Danso, F., Trivedi, C.M., Juhr, D., Gupta, M., Cui, Z., Tian, Y., Zhang, Y., Yang, W., Gruber, P.J., Epstein, J.A.*, et al.* (2011). Highly efficient miRNA-mediated reprogramming of mouse and human somatic cells to pluripotency. Cell Stem Cell *8*, 376-388.

Bahar, R., Hartmann, C.H., Rodriguez, K.A., Denny, A.D., Busuttil, R.A., Dolle, M.E., Calder, R.B., Chisholm, G.B., Pollock, B.H., Klein, C.A.*, et al.* (2006). Increased cell-to-cell variation in gene expression in ageing mouse heart. Nature *441*, 1011-1014.

Baker, D.J., Dawlaty, M.M., Wijshake, T., Jeganathan, K.B., Malureanu, L., van Ree, J.H., Crespo-Diaz, R., Reyes, S., Seaburg, L., Shapiro, V.*, et al.* (2013). Increased expression of BubR1 protects against aneuploidy and cancer and extends healthy lifespan. Nat Cell Biol *15*, 96-102.

Barbeau, A., Roy, M., Bernier, G., Campanella, G., and Paris, S. (1987). Ecogenetics of Parkinson's disease: prevalence and environmental aspects in rural areas. The Canadian journal of neurological sciences Le journal canadien des sciences neurologiques *14*, 36-41.

Barden, H. (1969). The histochemical relationship of neuromelanin and lipofuscin. J Neuropathol Exp Neurol *28*, 419-441.

Benabid, A.L., Pollak, P., Gross, C., Hoffmann, D., Benazzouz, A., Gao, D.M., Laurent, A., Gentil, M., and Perret, J. (1994). Acute and long-term effects of subthalamic nucleus stimulation in Parkinson's disease. Stereotactic and functional neurosurgery *62*, 76-84.

Benson, E.K., Lee, S.W., and Aaronson, S.A. (2010). Role of progerin-induced telomere dysfunction in HGPS premature cellular senescence. Journal of Cell Science *123*, 2605-2612.

Bergo, M.O., Gavino, B., Ross, J., Schmidt, W.K., Hong, C., Kendall, L.V., Mohr, A., Meta, M., Genant, H., Jiang, Y.*, et al.* (2002). Zmpste24 deficiency in mice causes spontaneous bone fractures, muscle weakness, and a prelamin A processing defect. Proc Natl Acad Sci U S A *99*, 13049-13054.

Bernardes de Jesus, B., Vera, E., Schneeberger, K., Tejera, A.M., Ayuso, E., Bosch, F., and Blasco, M.A. (2012). Telomerase gene therapy in adult and old mice delays aging and increases longevity without increasing cancer. EMBO Mol Med *4*, 691-704.

Bernhardt, R. (1984). Light and electron microscopic studies of the distribution of microtubule-associated protein 2 in rat brain: a difference between dendritic and axonal cytoskeletons. Journal of comparative neurology (1911) *226*, 203-221.

Betarbet, R., Sherer, T.B., MacKenzie, G., Garcia-Osuna, M., Panov, A.V., and Greenamyre, J.T. (2000). Chronic systemic pesticide exposure reproduces features of Parkinson's disease. Nat Neurosci *3*, 1301-1306.

Bilican, B., Serio, A., Barmada, S.J., Nishimura, A.L., Sullivan, G.J., Carrasco, M., Phatnani, H.P., Puddifoot, C.A., Story, D., Fletcher, J.*, et al.* (2012). Mutant induced pluripotent stem cell lines recapitulate aspects of TDP-43 proteinopathies and reveal cell-specific vulnerability. Proceedings of the National Academy of Sciences *109*, 5803-5808.

Birkmayer, W., and Hornykiewicz, O. (1961). [The L-3,4-dioxyphenylalanine (DOPA)-effect in Parkinson-akinesia]. Wiener klinische Wochenschrift *73*, 787-788.

Bjedov, I., Toivonen, J.M., Kerr, F., Slack, C., Jacobson, J., Foley, A., and Partridge, L. (2010). Mechanisms of life span extension by rapamycin in the fruit fly Drosophila melanogaster. Cell Metab *11*, 35-46.

Blackburn, E.H., Greider, C.W., and Szostak, J.W. (2006). Telomeres and telomerase: the path from maize, Tetrahymena and yeast to human cancer and aging. Nat Med *12*, 1133-1138.

Blasco, M.A. (2007). The epigenetic regulation of mammalian telomeres. Nature reviews Genetics *8*, 299-309.

Blum, B., Hrvatin, S.S., Schuetz, C., Bonal, C., Rezania, A., and Melton, D.A. (2012). Functional beta-cell maturation is marked by an increased glucose threshold and by expression of urocortin 3. Nat Biotechnol *30*, 261-264.

Bodnar, A.G., Ouellette, M., Frolkis, M., Holt, S.E., Chiu, C.P., Morin, G.B., Harley, C.B., Shay, J.W., Lichtsteiner, S., and Wright, W.E. (1998). Extension of life-span by introduction of telomerase into normal human cells. Science *279*, 349-352.

Bonifati, V., Rizzu, P., van Baren, M.J., Schaap, O., Breedveld, G.J., Krieger, E., Dekker, M.C., Squitieri, F., Ibanez, P., Joosse, M.*, et al.* (2003). Mutations in the DJ-1 gene associated with autosomal recessive early-onset parkinsonism. Science *299*, 256-259.

Braak, H., Del Tredici, K., Rub, U., de Vos, R.A., Jansen Steur, E.N., and Braak, E. (2003). Staging of brain pathology related to sporadic Parkinson's disease. Neurobiol Aging *24*, 197-211.

Bradley, A., Evans, M., Kaufman, M.H., and Robertson, E. (1984). Formation of germ-line chimaeras from embryo-derived teratocarcinoma cell lines. Nature *309*, 255-256.

Bridger, J.M., and Kill, I.R. (2004). Aging of Hutchinson-Gilford progeria syndrome fibroblasts is characterised by hyperproliferation and increased apoptosis. Exp Gerontol *39*, 717-724.

Briggs, R., and King, T.J. (1952). Transplantation of Living Nuclei From Blastula Cells into Enucleated Frogs' Eggs. Proc Natl Acad Sci U S A *38*, 455-463.

Brinster, R.L. (1974). The effect of cells transferred into the mouse blastocyst on subsequent development. The Journal of experimental medicine *140*, 1049-1056.

Brons, I.G., Smithers, L.E., Trotter, M.W., Rugg-Gunn, P., Sun, B., Chuva de Sousa Lopes, S.M., Howlett, S.K., Clarkson, A., Ahrlund-Richter, L., Pedersen, R.A.*, et al.* (2007). Derivation of pluripotent epiblast stem cells from mammalian embryos. Nature *448*, 191-195.

Burke, R.E., Dauer, W.T., and Vonsattel, J.P. (2008). A critical evaluation of the Braak staging scheme for Parkinson's disease. Ann Neurol *64*, 485-491.

Burkhardt, M.F., Martinez, F.J., Wright, S., Ramos, C., Volfson, D., Mason, M., Garnes, J., Dang, V., Lievers, J., Shoukat-Mumtaz, U.*, et al.* (2013). A cellular model for sporadic ALS using patient-derived induced pluripotent stem cells. Molecular and cellular neurosciences *56*, 355-364.

Caboni, P., Sherer, T.B., Zhang, N., Taylor, G., Na, H.M., Greenamyre, J.T., and Casida, J.E. (2004). Rotenone, deguelin, their metabolites, and the rat model of Parkinson's disease. Chemical research in toxicology *17*, 1540-1548.

Calne, D.B., Teychenne, P.F., Claveria, L.E., Eastman, R., Greenacre, J.K., and Petrie, A. (1974). Bromocriptine in Parkinsonism. British medical journal *4*, 442-444.

Canela, A., Vera, E., Klatt, P., and Blasco, M.A. (2007). High-throughput telomere length quantification by FISH and its application to human population studies. Proc Natl Acad Sci U S A *104*, 5300-5305.

Cao, K., Blair, C.D., Faddah, D.A., Kieckhaefer, J.E., Olive, M., Erdos, M.R., Nabel, E.G., and Collins, F.S. (2011a). Progerin and telomere dysfunction collaborate to trigger cellular senescence in normal human fibroblasts. The Journal of Clinical Investigation *121*, 2833-2844.

Cao, K., Capell, B.C., Erdos, M.R., Djabali, K., and Collins, F.S. (2007). A lamin A protein isoform overexpressed in Hutchinson-Gilford progeria syndrome interferes with mitosis in progeria and normal cells. Proceedings of the National Academy of Sciences of the United States of America *104*, 4949-4954.

Cao, K., Graziotto, J.J., Blair, C.D., Mazzulli, J.R., Erdos, M.R., Krainc, D., and Collins, F.S. (2011b). Rapamycin reverses cellular phenotypes and enhances mutant protein clearance in Hutchinson-Gilford progeria syndrome cells. Science translational medicine *3*, 89ra58.

Capell, B.C., Erdos, M.R., Madigan, J.P., Fiordalisi, J.J., Varga, R., Conneely, K.N., Gordon, L.B., Der, C.J., Cox, A.D., and Collins, F.S. (2005). Inhibiting farnesylation of progerin prevents the characteristic nuclear blebbing of Hutchinson-Gilford progeria syndrome. Proc Natl Acad Sci U S A *102*, 12879-12884.

Carlsson, A., Lindqvist, M., and Magnusson, T. (1957). 3,4-Dihydroxyphenylalanine and 5-hydroxytryptophan as reserpine antagonists. Nature *180*, 1200.

Cenci, M.A., and Konradi, C. (2010). Maladaptive striatal plasticity in L-DOPA-induced dyskinesia. Progress in brain research *183*, 209-233.

Chambers, S.M., Shaw, C.A., Gatza, C., Fisk, C.J., Donehower, L.A., and Goodell, M.A. (2007). Aging hematopoietic stem cells decline in function and exhibit epigenetic dysregulation. PLoS Biol *5*, e201.

Cheng, H.C., Kim, S.R., Oo, T.F., Kareva, T., Yarygina, O., Rzhetskaya, M., Wang, C., During, M., Talloczy, Z., Tanaka, K.*, et al.* (2011). Akt suppresses retrograde degeneration of dopaminergic axons by inhibition of macroautophagy. J Neurosci *31*, 2125-2135.

Cheng, H.C., Ulane, C.M., and Burke, R.E. (2010). Clinical progression in Parkinson disease and the neurobiology of axons. Ann Neurol *67*, 715-725.

Chu, Y., and Kordower, J.H. (2007). Age-associated increases of alpha-synuclein in monkeys and humans are associated with nigrostriatal dopamine depletion: Is this the target for Parkinson's disease? Neurobiol Dis *25*, 134-149.

Chung, C.Y., Khurana, V., Auluck, P.K., Tardiff, D.F., Mazzulli, J.R., Soldner, F., Baru, V., Lou, Y., Freyzon, Y., Cho, S.*, et al.* (2013). Identification and rescue of alpha-synuclein toxicity in Parkinson patient-derived neurons. Science *342*, 983-987.

Chung, C.Y., Seo, H., Sonntag, K.C., Brooks, A., Lin, L., and Isacson, O. (2005). Cell type-specific gene expression of midbrain dopaminergic neurons reveals molecules involved in their vulnerability and protection. Hum Mol Genet *14*, 1709-1725.

Cong, L., Ran, F.A., Cox, D., Lin, S., Barretto, R., Habib, N., Hsu, P.D., Wu, X., Jiang, W., Marraffini, L.A.*, et al.* (2013). Multiplex genome engineering using CRISPR/Cas systems. Science *339*, 819-823.

Constantinescu, D., Gray, H.L., Sammak, P.J., Schatten, G.P., and Csoka, A.B. (2006). Lamin A/C expression is a marker of mouse and human embryonic stem cell differentiation. STEM CELLS *24*, 177-185.

Cookson, M.R. (2009). alpha-Synuclein and neuronal cell death. Molecular neurodegeneration *4*, 9.

Cooper, O., Seo, H., Andrabi, S., Guardia-Laguarta, C., Graziotto, J., Sundberg, M., McLean, J.R., Carrillo-Reid, L., Xie, Z., Osborn, T.*, et al.* (2012). Pharmacological rescue of mitochondrial deficits in iPSC-derived neural cells from patients with familial Parkinson's disease. Science translational medicine *4*, 141ra190.

Corasaniti, M.T., Strongoli, M.C., Pisanelli, A., Bruno, P., Rotiroti, D., Nappi, G., and Nistico, G. (1992). Distribution of paraquat into the brain after its systemic injection in rats. Functional neurology *7*, 51-56.

Corrodi, H., Fuxe, K., Hokfelt, T., Lidbrink, P., and Ungerstedt, U. (1973). Effect of ergot drugs on central catecholamine neurons: evidence for a stimulation of central dopamine neurons. The Journal of pharmacy and pharmacology *25*, 409-412.

Cotzias, G.C., Papavasiliou, P.S., and Gellene, R. (1969). Modification of Parkinsonism--chronic treatment with L-dopa. N Engl J Med *280*, 337-345.

D'Amour, K.A., Bang, A.G., Eliazer, S., Kelly, O.G., Agulnick, A.D., Smart, N.G., Moorman, M.A., Kroon, E., Carpenter, M.K., and Baetge, E.E. (2006). Production of pancreatic hormone-expressing endocrine cells from human embryonic stem cells. Nat Biotechnol *24*, 1392-1401.

Davis, R.L., Weintraub, H., and Lassar, A.B. (1987). Expression of a single transfected cDNA converts fibroblasts to myoblasts. Cell *51*, 987-1000.

de Wert, G., and Mummery, C. (2003). Human embryonic stem cells: research, ethics and policy. Human reproduction (Oxford, England) *18*, 672-682.

Dechat, T., Pfleghaar, K., Sengupta, K., Shimi, T., Shumaker, D.K., Solimando, L., and Goldman, R.D. (2008). Nuclear lamins: major factors in the structural

organization and function of the nucleus and chromatin. Genes & Development *22*, 832-853.

Desplats, P., Lee, H.J., Bae, E.J., Patrick, C., Rockenstein, E., Crews, L., Spencer, B., Masliah, E., and Lee, S.J. (2009). Inclusion formation and neuronal cell death through neuron-to-neuron transmission of alpha-synuclein. Proc Natl Acad Sci U S A *106*, 13010-13015.

Dimos, J.T., Rodolfa, K.T., Niakan, K.K., Weisenthal, L.M., Mitsumoto, H., Chung, W., Croft, G.F., Saphier, G., Leibel, R., Goland, R.*, et al.* (2008). Induced pluripotent stem cells generated from patients with ALS can be differentiated into motor neurons. Science *321*, 1218-1221.

Dobin, A., Davis, C.A., Schlesinger, F., Drenkow, J., Zaleski, C., Jha, S., Batut, P., Chaisson, M., and Gingeras, T.R. (2013). STAR: ultrafast universal RNA-seq aligner. Bioinformatics *29*, 15-21.

Dodson, M.W., and Guo, M. (2007). Pink1, Parkin, DJ-1 and mitochondrial dysfunction in Parkinson's disease. Current opinion in neurobiology *17*, 331-337.

Doetschman, T.C., Eistetter, H., Katz, M., Schmidt, W., and Kemler, R. (1985). The in vitro development of blastocyst-derived embryonic stem cell lines: formation of visceral yolk sac, blood islands and myocardium. Journal of embryology and experimental morphology *87*, 27-45.

Doi, A., Park, I.H., Wen, B., Murakami, P., Aryee, M.J., Irizarry, R., Herb, B., Ladd-Acosta, C., Rho, J., Loewer, S.*, et al.* (2009). Differential methylation of tissue- and cancer-specific CpG island shores distinguishes human induced pluripotent stem cells, embryonic stem cells and fibroblasts. Nat Genet *41*, 1350-1353.

Dolnikov, K., Shilkrut, M., Zeevi-Levin, N., Gerecht-Nir, S., Amit, M., Danon, A., Itskovitz-Eldor, J., and Binah, O. (2006). Functional properties of human embryonic stem cell-derived cardiomyocytes: intracellular Ca2+ handling and the role of sarcoplasmic reticulum in the contraction. Stem Cells *24*, 236-245.

Doonan, R., McElwee, J.J., Matthijssens, F., Walker, G.A., Houthoofd, K., Back, P., Matscheski, A., Vanfleteren, J.R., and Gems, D. (2008). Against the oxidative damage theory of aging: superoxide dismutases protect against oxidative stress but have little or no effect on life span in Caenorhabditis elegans. Genes & development *22*, 3236-3241.

Eakin, G.S., Hadjantonakis, A.K., Papaioannou, V.E., and Behringer, R.R. (2005). Developmental potential and behavior of tetraploid cells in the mouse embryo. Developmental biology *288*, 150-159.

Ebert, A.D., Yu, J., Rose, F.F., Jr., Mattis, V.B., Lorson, C.L., Thomson, J.A., and Svendsen, C.N. (2009). Induced pluripotent stem cells from a spinal muscular atrophy patient. Nature *457*, 277-280.

Edgar, D., Shabalina, I., Camara, Y., Wredenberg, A., Calvaruso, M.A., Nijtmans, L., Nedergaard, J., Cannon, B., Larsson, N.G., and Trifunovic, A. (2009). Random point mutations with major effects on protein-coding genes are the driving force behind premature aging in mtDNA mutator mice. Cell Metab *10*, 131-138.

Egawa, N., Kitaoka, S., Tsukita, K., Naitoh, M., Takahashi, K., Yamamoto, T., Adachi, F., Kondo, T., Okita, K., Asaka, I.*, et al.* (2012). Drug screening for ALS using patient-specific induced pluripotent stem cells. Sci Transl Med *4*, 145ra104.

Eriksson, M., Brown, W.T., Gordon, L.B., Glynn, M.W., Singer, J., Scott, L., Erdos, M.R., Robbins, C.M., Moses, T.Y., Berglund, P.*, et al.* (2003). Recurrent de novo point mutations in lamin A cause Hutchinson-Gilford progeria syndrome. Nature *423*, 293-298.

Evans, M.J., and Kaufman, M.H. (1981). Establishment in culture of pluripotential cells from mouse embryos. Nature *292*, 154-156.

Fibiger, H.C., Phillips, A.G., and Clouston, R.A. (1973). Regulatory deficits after unilateral electrolytic or 6-OHDA lesions of the substantia nigra. The American journal of physiology *225*, 1282-1287.

Finch, B.W., and Ephrussi, B. (1967). RETENTION OF MULTIPLE DEVELOPMENTAL POTENTIALITIES BY CELLS OF A MOUSE TESTICULAR TERATOCARCINOMA DURING PROLONGED CULTURE in vitro AND THEIR EXTINCTION UPON HYBRIDIZATION WITH CELLS OF PERMANENT LINES. Proc Natl Acad Sci U S A *57*, 615-621.

Finn, J.T., Weil, M., Archer, F., Siman, R., Srinivasan, A., and Raff, M.C. (2000). Evidence that Wallerian degeneration and localized axon degeneration induced by local neurotrophin deprivation do not involve caspases. J Neurosci *20*, 1333-1341.

Fornai, F., Lenzi, P., Gesi, M., Soldani, P., Ferrucci, M., Lazzeri, G., Capobianco, L., Battaglia, G., De Blasi, A., Nicoletti, F.*, et al.* (2004). Methamphetamine produces neuronal inclusions in the nigrostriatal system and in PC12 cells. Journal of neurochemistry *88*, 114-123.

Fraga, M.F., and Esteller, M. (2007). Epigenetics and aging: the targets and the marks. Trends in genetics : TIG *23*, 413-418.

Freije, J.M., Blay, P., Pendas, A.M., Cadinanos, J., Crespo, P., and Lopez-Otin, C. (1999). Identification and chromosomal location of two human genes encoding

enzymes potentially involved in proteolytic maturation of farnesylated proteins. Genomics *58*, 270-280.

Freije, J.M., and López-Otín, C. (2012). Reprogramming aging and progeria. Current Opinion in Cell Biology *24*, 757-764.

Funayama, M., Hasegawa, K., Ohta, E., Kawashima, N., Komiyama, M., Kowa, H., Tsuji, S., and Obata, F. (2005). An LRRK2 mutation as a cause for the parkinsonism in the original PARK8 family. Ann Neurol *57*, 918-921.

Fusaki, N., Ban, H., Nishiyama, A., Saeki, K., and Hasegawa, M. (2009). Efficient induction of transgene-free human pluripotent stem cells using a vector based on Sendai virus, an RNA virus that does not integrate into the host genome. Proceedings of the Japan Academy, Series B *85*, 348-362.

Gafni, O., Weinberger, L., Mansour, A.A., Manor, Y.S., Chomsky, E., Ben-Yosef, D., Kalma, Y., Viukov, S., Maza, I., Zviran, A.*, et al.* (2013). Derivation of novel human ground state naive pluripotent stem cells. Nature *504*, 282-286.

Ganat, Y.M., Calder, E.L., Kriks, S., Nelander, J., Tu, E.Y., Jia, F., Battista, D., Harrison, N., Parmar, M., Tomishima, M.J.*, et al.* (2012). Identification of embryonic stem cell-derived midbrain dopaminergic neurons for engraftment. J Clin Invest *122*, 2928-2939.

Gardner, R.L. (1968). Mouse chimeras obtained by the injection of cells into the blastocyst. Nature *220*, 596-597.

Gautier, C.A., Kitada, T., and Shen, J. (2008). Loss of PINK1 causes mitochondrial functional defects and increased sensitivity to oxidative stress. Proc Natl Acad Sci U S A *105*, 11364-11369.

Glynn, M.W., and Glover, T.W. (2005). Incomplete processing of mutant lamin A in Hutchinson-Gilford progeria leads to nuclear abnormalities, which are reversed by farnesyltransferase inhibition. Human molecular genetics *14*, 2959-2969.

Goldman, R.D., Shumaker, D.K., Erdos, M.R., Eriksson, M., Goldman, A.E., Gordon, L.B., Gruenbaum, Y., Khuon, S., Mendez, M., Varga, R.*, et al.* (2004). Accumulation of mutant lamin A causes progressive changes in nuclear architecture in Hutchinson-Gilford progeria syndrome. Proc Natl Acad Sci U S A *101*, 8963-8968.

Gonon, F., and Bloch, B. (1998). Kinetics and geometry of the excitatory dopaminergic transmission in the rat striatum in vivo. Advances in pharmacology (San Diego, Calif) *42*, 140-144.

Goodarzi, H., Elemento, O., and Tavazoie, S. (2009). Revealing global regulatory perturbations across human cancers. Mol Cell *36*, 900-911.

Gordon, L.B., Kleinman, M.E., Miller, D.T., Neuberg, D.S., Giobbie-Hurder, A., Gerhard-Herman, M., Smoot, L.B., Gordon, C.M., Cleveland, R., Snyder, B.D.*, et al.* (2012). Clinical trial of a farnesyltransferase inhibitor in children with Hutchinson-Gilford progeria syndrome. Proc Natl Acad Sci U S A *109*, 16666-16671.

Gorrell, J.M., DiMonte, D., and Graham, D. (1996). The role of the environment in Parkinson's disease. Environmental health perspectives *104*, 652-654.

Greer, E.L., Maures, T.J., Hauswirth, A.G., Green, E.M., Leeman, D.S., Maro, G.S., Han, S., Banko, M.R., Gozani, O., and Brunet, A. (2010). Members of the H3K4 trimethylation complex regulate lifespan in a germline-dependent manner in C. elegans. Nature *466*, 383-387.

Guenther, M.G., Frampton, G.M., Soldner, F., Hockemeyer, D., Mitalipova, M., Jaenisch, R., and Young, R.A. (2010). Chromatin structure and gene expression programs of human embryonic and induced pluripotent stem cells. Cell Stem Cell *7*, 249-257.

Guo, G., Yang, J., Nichols, J., Hall, J.S., Eyres, I., Mansfield, W., and Smith, A. (2009). Klf4 reverts developmentally programmed restriction of ground state pluripotency. Development *136*, 1063-1069.

Gurdon, J.B. (1962). The developmental capacity of nuclei taken from intestinal epithelium cells of feeding tadpoles. Journal of embryology and experimental morphology *10*, 622-640.

Halje, P., Tamte, M., Richter, U., Mohammed, M., Cenci, M.A., and Petersson, P. (2012). Levodopa-induced dyskinesia is strongly associated with resonant cortical oscillations. J Neurosci *32*, 16541-16551.

Hanna, J., Cheng, A.W., Saha, K., Kim, J., Lengner, C.J., Soldner, F., Cassady, J.P., Muffat, J., Carey, B.W., and Jaenisch, R. (2010). Human embryonic stem cells with biological and epigenetic characteristics similar to those of mouse ESCs. Proc Natl Acad Sci U S A *107*, 9222-9227.

Hanna, J., Wernig, M., Markoulaki, S., Sun, C.W., Meissner, A., Cassady, J.P., Beard, C., Brambrink, T., Wu, L.C., Townes, T.M.*, et al.* (2007). Treatment of sickle cell anemia mouse model with iPS cells generated from autologous skin. Science *318*, 1920-1923.

Hannum, G., Guinney, J., Zhao, L., Zhang, L., Hughes, G., Sadda, S., Klotzle, B., Bibikova, M., Fan, J.B., Gao, Y.*, et al.* (2013). Genome-wide methylation profiles reveal quantitative views of human aging rates. Mol Cell *49*, 359-367.

Hansen, C., Angot, E., Bergstrom, A.L., Steiner, J.A., Pieri, L., Paul, G., Outeiro, T.F., Melki, R., Kallunki, P., Fog, K.*, et al.* (2011). alpha-Synuclein propagates

from mouse brain to grafted dopaminergic neurons and seeds aggregation in cultured human cells. J Clin Invest *121*, 715-725.

Hargus, G., Cooper, O., Deleidi, M., Levy, A., Lee, K., Marlow, E., Yow, A., Soldner, F., Hockemeyer, D., Hallett, P.J.*, et al.* (2010). Differentiated Parkinson patient-derived induced pluripotent stem cells grow in the adult rodent brain and reduce motor asymmetry in Parkinsonian rats. Proceedings of the National Academy of Sciences *107*, 15921-15926.

Harman, D. (1960). The free radical theory of aging: the effect of age on serum mercaptan levels. Journal of gerontology *15*, 38-40.

Harrison, D.E., Strong, R., Sharp, Z.D., Nelson, J.F., Astle, C.M., Flurkey, K., Nadon, N.L., Wilkinson, J.E., Frenkel, K., Carter, C.S.*, et al.* (2009). Rapamycin fed late in life extends lifespan in genetically heterogeneous mice. Nature *460*, 392-395.

Hassler, R. (1938). Zur Pathologie der Paralysis agitans und des postenzephalitischen Parkinsonism. J Psychol Neurol *48*, 387–476.

Hayflick, L. (1965). THE LIMITED IN VITRO LIFETIME OF HUMAN DIPLOID CELL STRAINS. Exp Cell Res *37*, 614-636.

Hennekam, R.C.M. (2006). Hutchinson-Gilford progeria syndrome: review of the phenotype. American Journal of Medical Genetics Part A *140*, 2603-2624.

Herranz, D., Munoz-Martin, M., Canamero, M., Mulero, F., Martinez-Pastor, B., Fernandez-Capetillo, O., and Serrano, M. (2010). Sirt1 improves healthy ageing and protects from metabolic syndrome-associated cancer. Nature communications *1*, 3.

Herrera, E., Samper, E., Martin-Caballero, J., Flores, J.M., Lee, H.W., and Blasco, M.A. (1999). Disease states associated with telomerase deficiency appear earlier in mice with short telomeres. EMBO J *18*, 2950-2960.

Hirsch, E., Graybiel, A.M., and Agid, Y.A. (1988). Melanized dopaminergic neurons are differentially susceptible to degeneration in Parkinson's disease. Nature *334*, 345-348.

Hockemeyer, D., Soldner, F., Beard, C., Gao, Q., Mitalipova, M., DeKelver, R.C., Katibah, G.E., Amora, R., Boydston, E.A., Zeitler, B.*, et al.* (2009). Efficient targeting of expressed and silent genes in human ESCs and iPSCs using zinc-finger nucleases. Nat Biotechnol *27*, 851-857.

Hockemeyer, D., Wang, H., Kiani, S., Lai, C.S., Gao, Q., Cassady, J.P., Cost, G.J., Zhang, L., Santiago, Y., Miller, J.C.*, et al.* (2011). Genetic engineering of human pluripotent cells using TALE nucleases. Nat Biotechnol *29*, 731-734.

Hoeijmakers, J.H. (2009). DNA damage, aging, and cancer. N Engl J Med *361*, 1475-1485.

Hof, P.R., and Morrison, J.H. (2004). The aging brain: morphomolecular senescence of cortical circuits. Trends Neurosci *27*, 607-613.

Huangfu, D., Maehr, R., Guo, W., Eijkelenboom, A., Snitow, M., Chen, A.E., and Melton, D.A. (2008). Induction of pluripotent stem cells by defined factors is greatly improved by small-molecule compounds. Nature Biotechnology *26*, 795-797.

Hussein, S.M., Batada, N.N., Vuoristo, S., Ching, R.W., Autio, R., Narva, E., Ng, S., Sourour, M., Hamalainen, R., Olsson, C.*, et al.* (2011). Copy number variation and selection during reprogramming to pluripotency. Nature *471*, 58-62.

Ichida, J.K., Blanchard, J., Lam, K., Son, E.Y., Chung, J.E., Egli, D., Loh, K.M., Carter, A.C., Di Giorgio, F.P., Koszka, K.*, et al.* (2009). A small-molecule inhibitor of tgf-Beta signaling replaces sox2 in reprogramming by inducing nanog. Cell Stem Cell *5*, 491-503.

Ikegami, K., and Koike, T. (2003). Non-apoptotic neurite degeneration in apoptotic neuronal death: pivotal role of mitochondrial function in neurites. Neuroscience *122*, 617-626.

Isacson, O., and Deacon, T. (1997). Neural transplantation studies reveal the brain's capacity for continuous reconstruction. Trends Neurosci *20*, 477-482.

Israel, M.A., Yuan, S.H., Bardy, C., Reyna, S.M., Mu, Y., Herrera, C., Hefferan, M.P., Van Gorp, S., Nazor, K.L., Boscolo, F.S.*, et al.* (2012). Probing sporadic and familial Alzheimer's disease using induced pluripotent stem cells. Nature *482*, 216-220.

Itskovitz-Eldor, J., Schuldiner, M., Karsenti, D., Eden, A., Yanuka, O., Amit, M., Soreq, H., and Benvenisty, N. (2000). Differentiation of human embryonic stem cells into embryoid bodies compromising the three embryonic germ layers. Molecular medicine (Cambridge, Mass) *6*, 88-95.

Jaworski, T., Lechat, B., Demedts, D., Gielis, L., Devijver, H., Borghgraef, P., Duimel, H., Verheyen, F., Kugler, S., and Van Leuven, F. (2011). Dendritic degeneration, neurovascular defects, and inflammation precede neuronal loss in a mouse model for tau-mediated neurodegeneration. Am J Pathol *179*, 2001-2015.

Jones, P.A., and Taylor, S.M. (1980). Cellular differentiation, cytidine analogs and DNA methylation. Cell *20*, 85-93.

Jung, H.-J., Coffinier, C., Choe, Y., Beigneux, A.P., Davies, B.S.J., Yang, S.H., Barnes, R.H., Hong, J., Sun, T., Pleasure, S.J.*, et al.* (2012). Regulation of

prelamin A but not lamin C by miR-9, a brain-specific microRNA. Proceedings of the National Academy of Sciences *109*, E423-431.

Kaeberlein, M., McVey, M., and Guarente, L. (1999). The SIR2/3/4 complex and SIR2 alone promote longevity in Saccharomyces cerevisiae by two different mechanisms. Genes & development *13*, 2570-2580.

Kariko, K., Buckstein, M., Ni, H., and Weissman, D. (2005). Suppression of RNA recognition by Toll-like receptors: the impact of nucleoside modification and the evolutionary origin of RNA. Immunity *23*, 165-175.

Keller, G. (2005). Embryonic stem cell differentiation: emergence of a new era in biology and medicine. Genes & development *19*, 1129-1155.

Kemmerer, D., Miller, L., Macpherson, M.K., Huber, J., and Tranel, D. (2013). An investigation of semantic similarity judgments about action and non-action verbs in Parkinson's disease: implications for the Embodied Cognition Framework. Frontiers in human neuroscience *7*, 146.

Kennedy, B.K., Austriaco, N.R., Jr., Zhang, J., and Guarente, L. (1995). Mutation in the silencing gene SIR4 can delay aging in S. cerevisiae. Cell *80*, 485-496.

Khan, J.M., Lyon, A.R., and Harding, S.E. (2013). The case for induced pluripotent stem cell-derived cardiomyocytes in pharmacological screening. British journal of pharmacology *169*, 304-317.

Kim, K., Doi, A., Wen, B., Ng, K., Zhao, R., Cahan, P., Kim, J., Aryee, M.J., Ji, H., Ehrlich, L.I.R.*, et al.* (2010). Epigenetic memory in induced pluripotent stem cells. Nature *467*, 285-290.

Kim, R.H., Smith, P.D., Aleyasin, H., Hayley, S., Mount, M.P., Pownall, S., Wakeham, A., You-Ten, A.J., Kalia, S.K., Horne, P.*, et al.* (2005). Hypersensitivity of DJ-1-deficient mice to 1-methyl-4-phenyl-1,2,3,6-tetrahydropyrindine (MPTP) and oxidative stress. Proc Natl Acad Sci U S A *102*, 5215-5220.

Kitada, T., Asakawa, S., Hattori, N., Matsumine, H., Yamamura, Y., Minoshima, S., Yokochi, M., Mizuno, Y., and Shimizu, N. (1998). Mutations in the parkin gene cause autosomal recessive juvenile parkinsonism. Nature *392*, 605-608.

Kleinsmith, L.J., and Pierce, G.B., Jr. (1964). MULTIPOTENTIALITY OF SINGLE EMBRYONAL CARCINOMA CELLS. Cancer research *24*, 1544-1551.

Koch, C.M., and Wagner, W. (2011). Epigenetic-aging-signature to determine age in different tissues. Aging (Albany NY) *3*, 1018-1027.

Koch, P., Tamboli, I.Y., Mertens, J., Wunderlich, P., Ladewig, J., Stuber, K., Esselmann, H., Wiltfang, J., Brustle, O., and Walter, J. (2012). Presenilin-1

L166P mutant human pluripotent stem cell-derived neurons exhibit partial loss of gamma-secretase activity in endogenous amyloid-beta generation. Am J Pathol *180*, 2404-2416.

Kono, T., Tsunoda, Y., and Nakahara, T. (1991). Production of identical twin and triplet mice by nuclear transplantation. The Journal of experimental zoology *257*, 214-219.

Kordower, J.H., Chu, Y., Hauser, R.A., Freeman, T.B., and Olanow, C.W. (2008a). Lewy body-like pathology in long-term embryonic nigral transplants in Parkinson's disease. Nat Med *14*, 504-506.

Kordower, J.H., Chu, Y., Hauser, R.A., Olanow, C.W., and Freeman, T.B. (2008b). Transplanted dopaminergic neurons develop PD pathologic changes: a second case report. Movement disorders : official journal of the Movement Disorder Society *23*, 2303-2306.

Kriks, S., Shim, J.-W., Piao, J., Ganat, Y.M., Wakeman, D.R., Xie, Z., Carrillo-Reid, L., Auyeung, G., Antonacci, C., Buch, A.*, et al.* (2011). Dopamine neurons derived from human ES cells efficiently engraft in animal models of Parkinson's disease. Nature *480*, 547-551.

Kroon, E., Martinson, L.A., Kadoya, K., Bang, A.G., Kelly, O.G., Eliazer, S., Young, H., Richardson, M., Smart, N.G., Cunningham, J.*, et al.* (2008). Pancreatic endoderm derived from human embryonic stem cells generates glucose-responsive insulin-secreting cells in vivo. Nat Biotechnol *26*, 443-452.

Kruegel, U., Robison, B., Dange, T., Kahlert, G., Delaney, J.R., Kotireddy, S., Tsuchiya, M., Tsuchiyama, S., Murakami, C.J., Schleit, J.*, et al.* (2011). Elevated proteasome capacity extends replicative lifespan in Saccharomyces cerevisiae. PLoS Genet *7*, e1002253.

Kulessa, H., Frampton, J., and Graf, T. (1995). GATA-1 reprograms avian myelomonocytic cell lines into eosinophils, thromboblasts, and erythroblasts. Genes and Development *9*, 1250-1262.

Lafaille, F.G., Pessach, I.M., Zhang, S.Y., Ciancanelli, M.J., Herman, M., Abhyankar, A., Ying, S.W., Keros, S., Goldstein, P.A., Mostoslavsky, G.*, et al.* (2012). Impaired intrinsic immunity to HSV-1 in human iPSC-derived TLR3-deficient CNS cells. Nature *491*, 769-773.

Lagouge, M., Argmann, C., Gerhart-Hines, Z., Meziane, H., Lerin, C., Daussin, F., Messadeq, N., Milne, J., Lambert, P., Elliott, P.*, et al.* (2006). Resveratrol improves mitochondrial function and protects against metabolic disease by activating SIRT1 and PGC-1alpha. Cell *127*, 1109-1122.

Lancaster, M.A., Renner, M., Martin, C.A., Wenzel, D., Bicknell, L.S., Hurles, M.E., Homfray, T., Penninger, J.M., Jackson, A.P., and Knoblich, J.A. (2013).

Cerebral organoids model human brain development and microcephaly. Nature *501*, 373-379.

Langston, J.W., Ballard, P., Tetrud, J.W., and Irwin, I. (1983). Chronic Parkinsonism in humans due to a product of meperidine-analog synthesis. Science *219*, 979-980.

Lapasset, L., Milhavet, O., Prieur, A., Besnard, E., Babled, A., Aït-Hamou, N., Leschik, J., Pellestor, F., Ramirez, J.-M., De Vos, J.*, et al.* (2011). Rejuvenating senescent and centenarian human cells by reprogramming through the pluripotent state. Genes & Development *25*, 2248-2253.

Larson, K., Yan, S.J., Tsurumi, A., Liu, J., Zhou, J., Gaur, K., Guo, D., Eickbush, T.H., and Li, W.X. (2012). Heterochromatin formation promotes longevity and represses ribosomal RNA synthesis. PLoS Genet *8*, e1002473.

Laurent, L.C., Ulitsky, I., Slavin, I., Tran, H., Schork, A., Morey, R., Lynch, C., Harness, J.V., Lee, S., Barrero, M.J.*, et al.* (2011). Dynamic changes in the copy number of pluripotency and cell proliferation genes in human ESCs and iPSCs during reprogramming and time in culture. Cell Stem Cell *8*, 106-118.

Lauridsen, J.B., Johansen, J.L., Rekling, J.C., Thirstrup, K., Moerk, A., and Sager, T.N. (2011). Regulation of the Bcas1 and Baiap3 transcripts in the subthalamic nucleus in mice recovering from MPTP toxicity. Neuroscience research *70*, 269-276.

Lee, B.H., Lee, M.J., Park, S., Oh, D.C., Elsasser, S., Chen, P.C., Gartner, C., Dimova, N., Hanna, J., Gygi, S.P.*, et al.* (2010). Enhancement of proteasome activity by a small-molecule inhibitor of USP14. Nature *467*, 179-184.

Lee, G., Papapetrou, E.P., Kim, H., Chambers, S.M., Tomishima, M.J., Fasano, C.A., Ganat, Y.M., Menon, J., Shimizu, F., Viale, A.*, et al.* (2009). Modelling pathogenesis and treatment of familial dysautonomia using patient-specific iPSCs. Nature *461*, 402-406.

Lee, G., Ramirez, C.N., Kim, H., Zeltner, N., Liu, B., Radu, C., Bhinder, B., Kim, Y.J., Choi, I.Y., Mukherjee-Clavin, B.*, et al.* (2012). Large-scale screening using familial dysautonomia induced pluripotent stem cells identifies compounds that rescue IKBKAP expression. Nat Biotechnol *30*, 1244-1248.

Li, J.Y., Englund, E., Holton, J.L., Soulet, D., Hagell, P., Lees, A.J., Lashley, T., Quinn, N.P., Rehncrona, S., Bjorklund, A.*, et al.* (2008). Lewy bodies in grafted neurons in subjects with Parkinson's disease suggest host-to-graft disease propagation. Nat Med *14*, 501-503.

Li, X., Patel, J.C., Wang, J., Avshalumov, M.V., Nicholson, C., Buxbaum, J.D., Elder, G.A., Rice, M.E., and Yue, Z. (2010). Enhanced striatal dopamine transmission and motor performance with LRRK2 overexpression in mice is

eliminated by familial Parkinson's disease mutation G2019S. J Neurosci *30*, 1788-1797.

Limousin, P., Pollak, P., Benazzouz, A., Hoffmann, D., Le Bas, J.F., Broussolle, E., Perret, J.E., and Benabid, A.L. (1995). Effect of parkinsonian signs and symptoms of bilateral subthalamic nucleus stimulation. Lancet *345*, 91-95.

Lin, F., and Worman, H.J. (1997). Expression of nuclear lamins in human tissues and cancer cell lines and transcription from the promoters of the lamin A/C and B1 genes. Experimental Cell Research *236*, 378-384.

Lindvall, O., Rehncrona, S., Brundin, P., Gustavii, B., Astedt, B., Widner, H., Lindholm, T., Bjorklund, A., Leenders, K.L., Rothwell, J.C.*, et al.* (1989). Human fetal dopamine neurons grafted into the striatum in two patients with severe Parkinson's disease. A detailed account of methodology and a 6-month follow-up. Archives of neurology *46*, 615-631.

Liu, B., Wang, J., Chan, K.M., Tjia, W.M., Deng, W., Guan, X., Huang, J.D., Li, K.M., Chau, P.Y., Chen, D.J.*, et al.* (2005). Genomic instability in laminopathy-based premature aging. Nat Med *11*, 780-785.

Liu, G., Rogers, J., Murphy, C.T., and Rongo, C. (2011a). EGF signalling activates the ubiquitin proteasome system to modulate C. elegans lifespan. EMBO J *30*, 2990-3003.

Liu, G.-H., Barkho, B.Z., Ruiz, S., Diep, D., Qu, J., Yang, S.-L., Panopoulos, A.D., Suzuki, K., Kurian, L., Walsh, C.*, et al.* (2011b). Recapitulation of premature ageing with iPSCs from Hutchinson-Gilford progeria syndrome. Nature *472*, 221-225.

Liu, G.-H., Ding, Z., and Izpisua Belmonte, J.C. (2012a). iPSC technology to study human aging and aging-related disorders. Current Opinion in Cell Biology *24*, 765-774.

Liu, G.-H., Qu, J., Suzuki, K., Nivet, E., Li, M., Montserrat, N., Yi, F., Xu, X., Ruiz, S., Zhang, W.*, et al.* (2012b). Progressive degeneration of human neural stem cells caused by pathogenic LRRK2. Nature *491*, 603-607.

Loerch, P.M., Lu, T., Dakin, K.A., Vann, J.M., Isaacs, A., Geula, C., Wang, J., Pan, Y., Gabuzda, D.H., Li, C.*, et al.* (2008). Evolution of the aging brain transcriptome and synaptic regulation. PloS one *3*, e3329.

Loh, Y.-H., Hartung, O., Li, H., Guo, C., Sahalie, J.M., Manos, P.D., Urbach, A., Heffner, G.C., Grskovic, M., Vigneault, F.*, et al.* (2010). Reprogramming of T cells from human peripheral blood. Cell Stem Cell *7*, 15-19.

Lopez-Otin, C., Blasco, M.A., Partridge, L., Serrano, M., and Kroemer, G. (2013). The hallmarks of aging. Cell *153*, 1194-1217.

Low, P. (2011). The role of ubiquitin-proteasome system in ageing. General and comparative endocrinology *172*, 39-43.

Lowry, W.E., Richter, L., Yachechko, R., Pyle, A.D., Tchieu, J., Sridharan, R., Clark, A.T., and Plath, K. (2008). Generation of human induced pluripotent stem cells from dermal fibroblasts. Proc Natl Acad Sci U S A *105*, 2883-2888.

Luk, K.C., Kehm, V., Carroll, J., Zhang, B., O'Brien, P., Trojanowski, J.Q., and Lee, V.M. (2012a). Pathological alpha-synuclein transmission initiates Parkinson-like neurodegeneration in nontransgenic mice. Science *338*, 949-953.

Luk, K.C., Kehm, V.M., Zhang, B., O'Brien, P., Trojanowski, J.Q., and Lee, V.M. (2012b). Intracerebral inoculation of pathological alpha-synuclein initiates a rapidly progressive neurodegenerative alpha-synucleinopathy in mice. The Journal of experimental medicine *209*, 975-986.

Luk, K.C., Song, C., O'Brien, P., Stieber, A., Branch, J.R., Brunden, K.R., Trojanowski, J.Q., and Lee, V.M. (2009). Exogenous alpha-synuclein fibrils seed the formation of Lewy body-like intracellular inclusions in cultured cells. Proc Natl Acad Sci U S A *106*, 20051-20056.

Lutz, W., Sanderson, W., and Scherbov, S. (2008). The coming acceleration of global population ageing. Nature *451*, 716-719.

Mackay, G.E., and West, J.D. (2005). Fate of tetraploid cells in 4n<-->2n chimeric mouse blastocysts. Mechanisms of development *122*, 1266-1281.

Madrazo, I., Leon, V., Torres, C., Aguilera, M.C., Varela, G., Alvarez, F., Fraga, A., Drucker-Colin, R., Ostrosky, F., Skurovich, M.*, et al.* (1988). Transplantation of fetal substantia nigra and adrenal medulla to the caudate nucleus in two patients with Parkinson's disease. N Engl J Med *318*, 51.

Mahmoudi, S., and Brunet, A. (2012). Aging and reprogramming: a two-way street. Current Opinion in Cell Biology *24*, 744-756.

Malagelada, C., Jin, Z.H., and Greene, L.A. (2008). RTP801 is induced in Parkinson's disease and mediates neuron death by inhibiting Akt phosphorylation/activation. Journal of Neuroscience *28*, 14363-14371.

Mali, P., Yang, L., Esvelt, K.M., Aach, J., Guell, M., DiCarlo, J.E., Norville, J.E., and Church, G.M. (2013). RNA-guided human genome engineering via Cas9. Science *339*, 823-826.

Mandal, P.K., and Rossi, D.J. (2013). Reprogramming human fibroblasts to pluripotency using modified mRNA. Nat Protoc *8*, 568-582.

Mann, D.M., and Yates, P.O. (1974). Lipoprotein pigments--their relationship to ageing in the human nervous system. II. The melanin content of pigmented nerve cells. Brain *97*, 489-498.

Manning-Bog, A.B., McCormack, A.L., Li, J., Uversky, V.N., Fink, A.L., and Di Monte, D.A. (2002). The herbicide paraquat causes up-regulation and aggregation of alpha-synuclein in mice: paraquat and alpha-synuclein. J Biol Chem *277*, 1641-1644.

Marion, R.M., Strati, K., Li, H., Tejera, A., Schoeftner, S., Ortega, S., Serrano, M., and Blasco, M.A. (2009). Telomeres acquire embryonic stem cell characteristics in induced pluripotent stem cells. Cell Stem Cell *4*, 141-154.

Martin, G.R. (1981). Isolation of a pluripotent cell line from early mouse embryos cultured in medium conditioned by teratocarcinoma stem cells. Proc Natl Acad Sci U S A *78*, 7634-7638.

Mayshar, Y., Ben-David, U., Lavon, N., Biancotti, J.C., Yakir, B., Clark, A.T., Plath, K., Lowry, W.E., and Benvenisty, N. (2010). Identification and classification of chromosomal aberrations in human induced pluripotent stem cells. Cell Stem Cell *7*, 521-531.

Mazereeuw-Hautier, J., Wilson, L.C., Mohammed, S., Smallwood, D., Shackleton, S., Atherton, D.J., and Harper, J.I. (2007). Hutchinson–Gilford progeria syndrome: clinical findings in three patients carrying the G608G mutation in LMNA and review of the literature. British Journal of Dermatology *156*, 1308-1314.

Mcclintock, D., Ratner, D., Lokuge, M., Owens, D.M., Gordon, L.B., Collins, F.S., and Djabali, K. (2007). The mutant form of lamin A that causes Hutchinson-Gilford progeria is a biomarker of cellular aging in human skin. PloS one *2*, e1269.

McKinney-Freeman, S., Cahan, P., Li, H., Lacadie, S.A., Huang, H.T., Curran, M., Loewer, S., Naveiras, O., Kathrein, K.L., Konantz, M.*, et al.* (2012). The transcriptional landscape of hematopoietic stem cell ontogeny. Cell Stem Cell *11*, 701-714.

Medvedik, O., Lamming, D.W., Kim, K.D., and Sinclair, D.A. (2007). MSN2 and MSN4 link calorie restriction and TOR to sirtuin-mediated lifespan extension in Saccharomyces cerevisiae. PLoS Biol *5*, e261.

Mesquita, A., Weinberger, M., Silva, A., Sampaio-Marques, B., Almeida, B., Leao, C., Costa, V., Rodrigues, F., Burhans, W.C., and Ludovico, P. (2010). Caloric restriction or catalase inactivation extends yeast chronological lifespan by inducing H2O2 and superoxide dismutase activity. Proc Natl Acad Sci U S A *107*, 15123-15128.

Milner, T.A., Waters, E.M., Robinson, D.C., and Pierce, J.P. (2011). Degenerating processes identified by electron microscopic immunocytochemical methods. Methods in molecular biology *793*, 23-59.

Min, J.N., Whaley, R.A., Sharpless, N.E., Lockyer, P., Portbury, A.L., and Patterson, C. (2008). CHIP deficiency decreases longevity, with accelerated aging phenotypes accompanied by altered protein quality control. Molecular and cellular biology *28*, 4018-4025.

Mitne-Neto, M., Machado-Costa, M., Marchetto, M.C., Bengtson, M.H., Joazeiro, C.A., Tsuda, H., Bellen, H.J., Silva, H.C., Oliveira, A.S., Lazar, M.*, et al.* (2011). Downregulation of VAPB expression in motor neurons derived from induced pluripotent stem cells of ALS8 patients. Hum Mol Genet *20*, 3642-3652.

Mummery, C., Ward-van Oostwaard, D., Doevendans, P., Spijker, R., van den Brink, S., Hassink, R., van der Heyden, M., Opthof, T., Pera, M., de la Riviere, A.B.*, et al.* (2003). Differentiation of human embryonic stem cells to cardiomyocytes: role of coculture with visceral endoderm-like cells. Circulation *107*, 2733-2740.

Murga, M., Bunting, S., Montana, M.F., Soria, R., Mulero, F., Canamero, M., Lee, Y., McKinnon, P.J., Nussenzweig, A., and Fernandez-Capetillo, O. (2009). A mouse model of ATR-Seckel shows embryonic replicative stress and accelerated aging. Nat Genet *41*, 891-898.

Nagy, A., Gocza, E., Diaz, E.M., Prideaux, V.R., Ivanyi, E., Markkula, M., and Rossant, J. (1990). Embryonic stem cells alone are able to support fetal development in the mouse. Development *110*, 815-821.

Newman, A.M., and Cooper, J.B. (2010). Lab-specific gene expression signatures in pluripotent stem cells. Cell Stem Cell *7*, 258-262.

Nguyen, H.N., Byers, B., Cord, B., Shcheglovitov, A., Byrne, J., Gujar, P., Kee, K., Schüle, B., Dolmetsch, R.E., Langston, W.*, et al.* (2011). LRRK2 mutant iPSC-derived DA neurons demonstrate increased susceptibility to oxidative stress. Cell Stem Cell *8*, 267-280.

Nichols, J., and Smith, A. (2009). Naive and primed pluripotent states. Cell Stem Cell *4*, 487-492.

Niedernhofer, L.J., Glorioso, J.C., and Robbins, P.D. (2011). Dedifferentiation rescues senescence of progeria cells but only while pluripotent. Stem Cell Research & Therapy *2*, 28.

Nissan, X., Blondel, S., Navarro, C., Maury, Y., Denis, C., Girard, M., Martinat, C., De Sandre-Giovannoli, A., Levy, N., and Peschanski, M. (2012). Unique preservation of neural cells in Hutchinson- Gilford progeria syndrome is due to the expression of the neural-specific miR-9 microRNA. CellReports *2*, 1-9.

Okita, K., Nakagawa, M., Hyenjong, H., Ichisaka, T., and Yamanaka, S. (2008). Generation of mouse induced pluripotent stem cells without viral vectors. Science *322*, 949-953.

Olanow, C.W., and Prusiner, S.B. (2009). Is Parkinson's disease a prion disorder? Proc Natl Acad Sci U S A *106*, 12571-12572.

Osorio, F.G., Navarro, C.L., Cadinanos, J., Lopez-Mejia, I.C., Quiros, P.M., Bartoli, C., Rivera, J., Tazi, J., Guzman, G., Varela, I.*, et al.* (2011). Splicing-directed therapy in a new mouse model of human accelerated aging. Sci Transl Med *3*, 106ra107.

Paisan-Ruiz, C., Jain, S., Evans, E.W., Gilks, W.P., Simon, J., van der Brug, M., Lopez de Munain, A., Aparicio, S., Gil, A.M., Khan, N.*, et al.* (2004). Cloning of the gene containing mutations that cause PARK8-linked Parkinson's disease. Neuron *44*, 595-600.

Palacino, J.J., Sagi, D., Goldberg, M.S., Krauss, S., Motz, C., Wacker, M., Klose, J., and Shen, J. (2004). Mitochondrial dysfunction and oxidative damage in parkin-deficient mice. J Biol Chem *279*, 18614-18622.

Papapetrou, E.P., Tomishima, M.J., Chambers, S.M., Mica, Y., Reed, E., Menon, J., Tabar, V., Mo, Q., Studer, L., and Sadelain, M. (2009). Stoichiometric and temporal requirements of Oct4, Sox2, Klf4, and c-Myc expression for efficient human iPSC induction and differentiation. Proceedings of the National Academy of Sciences *106*, 12759-12764.

Park, I.-H., Arora, N., Huo, H., Maherali, N., Ahfeldt, T., Shimamura, A., Lensch, M.W., Cowan, C., Hochedlinger, K., and Daley, G.Q. (2008a). Disease-specific induced pluripotent stem cells. Cell *134*, 877-886.

Park, I.-H., Zhao, R., West, J.A., Yabuuchi, A., Huo, H., Ince, T.A., Lerou, P.H., Lensch, M.W., and Daley, G.Q. (2008b). Reprogramming of human somatic cells to pluripotency with defined factors. Nature *451*, 141-146.

Parkinson, J. (1817). An essay on the shaking palsy. Whitingham and Rowland, London.

Payami, H., Larsen, K., Bernard, S., and Nutt, J. (1994). Increased risk of Parkinson's disease in parents and siblings of patients. Ann Neurol *36*, 659-661.

Pendas, A.M., Zhou, Z., Cadinanos, J., Freije, J.M., Wang, J., Hultenby, K., Astudillo, A., Wernerson, A., Rodriguez, F., Tryggvason, K.*, et al.* (2002). Defective prelamin A processing and muscular and adipocyte alterations in Zmpste24 metalloproteinase-deficient mice. Nat Genet *31*, 94-99.

Penner, M.R., Roth, T.L., Barnes, C.A., and Sweatt, J.D. (2010). An epigenetic hypothesis of aging-related cognitive dysfunction. Front Aging Neurosci *2*, 9.

Phillips, S.E., Woodruff, E.A., 3rd, Liang, P., Patten, M., and Broadie, K. (2008). Neuronal loss of Drosophila NPC1a causes cholesterol aggregation and age-progressive neurodegeneration. J Neurosci *28*, 6569-6582.

Polo, J.M., Liu, S., Figueroa, M.E., Kulalert, W., Eminli, S., Tan, K.Y., Apostolou, E., Stadtfeld, M., Li, Y., Shioda, T.*, et al.* (2010). Cell type of origin influences the molecular and functional properties of mouse induced pluripotent stem cells. Nature Biotechnology *28*, 848-855.

Polymeropoulos, M.H., Lavedan, C., Leroy, E., Ide, S.E., Dehejia, A., Dutra, A., Pike, B., Root, H., Rubenstein, J., Boyer, R.*, et al.* (1997). Mutation in the alpha-synuclein gene identified in families with Parkinson's disease. Science *276*, 2045-2047.

Potashkin, J.A., Santiago, J.A., Ravina, B.M., Watts, A., and Leontovich, A.A. (2012). Biosignatures for Parkinson's disease and atypical parkinsonian disorders patients. PLoS One *7*, e43595.

Powers, R.W., 3rd, Kaeberlein, M., Caldwell, S.D., Kennedy, B.K., and Fields, S. (2006). Extension of chronological life span in yeast by decreased TOR pathway signaling. Genes & development *20*, 174-184.

Prather, R.S., Barnes, F.L., Sims, M.M., Robl, J.M., Eyestone, W.H., and First, N.L. (1987). Nuclear transplantation in the bovine embryo: assessment of donor nuclei and recipient oocyte. Biology of reproduction *37*, 859-866.

Prather, R.S., Sims, M.M., and First, N.L. (1989). Nuclear transplantation in early pig embryos. Biology of reproduction *41*, 414-418.

Prigione, A., Fauler, B., Lurz, R., Lehrach, H., and Adjaye, J. (2010). The senescence-related mitochondrial/oxidative stress pathway is repressed in human induced pluripotent stem cells. STEM CELLS *28*, 721-733.

Prigione, A., Hossini, A.M., Lichtner, B., Serin, A., Fauler, B., Megges, M., Lurz, R., Lehrach, H., Makrantonaki, E., Zouboulis, C.C.*, et al.* (2011). Mitochondrial-associated cell death mechanisms are reset to an embryonic-like state in aged donor-derived iPS cells harboring chromosomal aberrations. PloS one *6*, e27352.

Raff, M.C., Whitmore, A.V., and Finn, J.T. (2002). Axonal self-destruction and neurodegeneration. Science *296*, 868-871.

Rais, Y., Zviran, A., Geula, S., Gafni, O., Chomsky, E., Viukov, S., Mansour, A.A., Caspi, I., Krupalnik, V., Zerbib, M.*, et al.* (2013). Deterministic direct reprogramming of somatic cells to pluripotency. Nature *502*, 65-70.

Röber, R.A., Weber, K., and Osborn, M. (1989). Differential timing of nuclear lamin A/C expression in the various organs of the mouse embryo and the young

animal: a developmental study. Development (Cambridge, England) *105*, 365-378.

Rodriguez, S., Coppede, F., Sagelius, H., and Eriksson, M. (2009). Increased expression of the Hutchinson-Gilford progeria syndrome truncated lamin A transcript during cell aging. European journal of human genetics : EJHG *17*, 928-937.

Rogina, B., and Helfand, S.L. (2004). Sir2 mediates longevity in the fly through a pathway related to calorie restriction. Proc Natl Acad Sci U S A *101*, 15998-16003.

Roy, S., and Wolman, L. (1969). Ultrastructural observations in Parkinsonism. The Journal of pathology *99*, 39-44.

Rubinsztein, D.C., Marino, G., and Kroemer, G. (2011). Autophagy and aging. Cell *146*, 682-695.

Rudolph, K.L., Chang, S., Lee, H.W., Blasco, M., Gottlieb, G.J., Greider, C., and DePinho, R.A. (1999). Longevity, stress response, and cancer in aging telomerase-deficient mice. Cell *96*, 701-712.

Rusinol, A.E., and Sinensky, M.S. (2006). Farnesylated lamins, progeroid syndromes and farnesyl transferase inhibitors. J Cell Sci *119*, 3265-3272.

Ryu, E.J., Angelastro, J.M., and Greene, L.A. (2005). Analysis of gene expression changes in a cellular model of Parkinson disease. Neurobiol Dis *18*, 54-74.

Saha, K., and Jaenisch, R. (2009). Technical Challenges in Using Human Induced Pluripotent Stem Cells to Model Disease. Cell Stem Cell *5*, 584-595.

Sánchez-Danés, A., Richaud-Patin, Y., Carballo-Carbajal, I., Jiménez-Delgado, S., Caig, C., Mora, S., Di Guglielmo, C., Ezquerra, M., Patel, B., Giralt, A.*, et al.* (2012). Disease-specific phenotypes in dopamine neurons from human iPS-based models of genetic and sporadic Parkinson's disease. EMBO Molecular Medicine *4*, 380-395.

Sazani, P., and Kole, R. (2003). Therapeutic potential of antisense oligonucleotides as modulators of alternative splicing. J Clin Invest *112*, 481-486.

Scaffidi, P., and Misteli, T. (2005). Reversal of the cellular phenotype in the premature aging disease Hutchinson-Gilford progeria syndrome. Nature Medicine *11*, 440-445.

Scaffidi, P., and Misteli, T. (2006). Lamin A-dependent nuclear defects in human aging. Science *312*, 1059-1063.

Scaffidi, P., and Misteli, T. (2008). Lamin A-dependent misregulation of adult stem cells associated with accelerated ageing. Nature Cell Biology *10*, 452-459.

Schrerer, H.J. (1939). Melanin pigmentation of the substantia nigra in primates. The Journal of comparative neurology *71*, 91.

Seibler, P., Graziotto, J., Jeong, H., Simunovic, F., Klein, C., and Krainc, D. (2011). Mitochondrial Parkin recruitment is impaired in neurons derived from mutant PINK1 induced pluripotent stem cells. The Journal of neuroscience : the official journal of the Society for Neuroscience *31*, 5970-5976.

Sheng, X., Reppel, M., Nguemo, F., Mohammad, F.I., Kuzmenkin, A., Hescheler, J., and Pfannkuche, K. (2012). Human pluripotent stem cell-derived cardiomyocytes: response to TTX and lidocain reveals strong cell to cell variability. PLoS One *7*, e45963.

Shimura, H., Hattori, N., Kubo, S., Mizuno, Y., Asakawa, S., Minoshima, S., Shimizu, N., Iwai, K., Chiba, T., Tanaka, K.*, et al.* (2000). Familial Parkinson disease gene product, parkin, is a ubiquitin-protein ligase. Nat Genet *25*, 302-305.

Shults, C.W. (2006). Lewy bodies. Proc Natl Acad Sci U S A *103*, 1661-1668.

Siebold, A.P., Banerjee, R., Tie, F., Kiss, D.L., Moskowitz, J., and Harte, P.J. (2010). Polycomb Repressive Complex 2 and Trithorax modulate Drosophila longevity and stress resistance. Proc Natl Acad Sci U S A *107*, 169-174.

Siegfried, J., and Lippitz, B. (1994). Bilateral chronic electrostimulation of ventroposterolateral pallidum: a new therapeutic approach for alleviating all parkinsonian symptoms. Neurosurgery *35*, 1126-1129; discussion 1129-1130.

Sinclair, D.A., Mills, K., and Guarente, L. (1997). Accelerated aging and nucleolar fragmentation in yeast sgs1 mutants. Science *277*, 1313-1316.

Smith, Y., Wichmann, T., Factor, S.A., and DeLong, M.R. (2012). Parkinson's disease therapeutics: new developments and challenges since the introduction of levodopa. Neuropsychopharmacology *37*, 213-246.

Smyth, G.K. (2004). Linear models and empirical bayes methods for assessing differential expression in microarray experiments. Statistical applications in genetics and molecular biology *3*, Article3.

Soldner, F., Hockemeyer, D., Beard, C., Gao, Q., Bell, G.W., Cook, E.G., Hargus, G., Blak, A., Cooper, O., Mitalipova, M.*, et al.* (2009). Parkinson's disease patient-derived induced pluripotent stem cells free of viral reprogramming factors. Cell *136*, 964-977.

Sommer, B., Barbieri, S., Hofele, K., Wiederhold, K., Probst, A., Mistl, C., Danner, S., Kauffmann, S., Spooren, W., Tolnay, M.*, et al.* (2000). Mouse models of alpha-synucleinopathy and Lewy pathology. Exp Gerontol *35*, 1389-1403.

Sommer, C.A., Stadtfeld, M., Murphy, G.J., Hochedlinger, K., Kotton, D.N., and Mostoslavsky, G. (2009). Induced pluripotent stem cell generation using a single lentiviral stem cell cassette. Stem Cells *27*, 543-549.

Song, M.S., Saavedra, L., and de Chaves, E.I. (2006). Apoptosis is secondary to non-apoptotic axonal degeneration in neurons exposed to Abeta in distal axons. Neurobiol Aging *27*, 1224-1238.

Spillantini, M.G., Schmidt, M.L., Lee, V.M., Trojanowski, J.Q., Jakes, R., and Goedert, M. (1997). Alpha-synuclein in Lewy bodies. Nature *388*, 839-840.

Stadtfeld, M., Nagaya, M., Utikal, J., Weir, G., and Hochedlinger, K. (2008). Induced pluripotent stem cells generated without viral integration. Science *322*, 945-949.

Sterky, F.H., Lee, S., Wibom, R., Olson, L., and Larsson, N.G. (2011). Impaired mitochondrial transport and Parkin-independent degeneration of respiratory chain-deficient dopamine neurons in vivo. Proc Natl Acad Sci U S A *108*, 12937-12942.

Stevens, L.C., and Little, C.C. (1954). Spontaneous Testicular Teratomas in an Inbred Strain of Mice. Proc Natl Acad Sci U S A *40*, 1080-1087.

Stice, S.L., and Robl, J.M. (1988). Nuclear reprogramming in nuclear transplant rabbit embryos. Biology of reproduction *39*, 657-664.

Suhr, S.T., Chang, E.A., Tjong, J., Alcasid, N., Perkins, G.A., Goissis, M.D., Ellisman, M.H., Perez, G.I., and Cibelli, J.B. (2010). Mitochondrial rejuvenation after induced pluripotency. PloS one *5*, e14095.

Sulzer, D., Mosharov, E., Talloczy, Z., Zucca, F.A., Simon, J.D., and Zecca, L. (2008). Neuronal pigmented autophagic vacuoles: lipofuscin, neuromelanin, and ceroid as macroautophagic responses during aging and disease. Journal of neurochemistry *106*, 24-36.

Swindell, W.R., Masternak, M.M., Kopchick, J.J., Conover, C.A., Bartke, A., and Miller, R.A. (2009). Endocrine regulation of heat shock protein mRNA levels in long-lived dwarf mice. Mech Ageing Dev *130*, 393-400.

Szilard, L. (1959). ON THE NATURE OF THE AGING PROCESS. Proc Natl Acad Sci U S A *45*, 30-45.

Tabar, V., Panagiotakos, G., Greenberg, E.D., Chan, B.K., Sadelain, M., Gutin, P.H., and Studer, L. (2005). Migration and differentiation of neural precursors

derived from human embryonic stem cells in the rat brain. In Nat Biotechnol, pp. 601-606.

Tachibana, M., Amato, P., Sparman, M., Gutierrez, N.M., Tippner-Hedges, R., Ma, H., Kang, E., Fulati, A., Lee, H.S., Sritanaudomchai, H*., et al.* (2013). Human embryonic stem cells derived by somatic cell nuclear transfer. Cell *153*, 1228-1238.

Tachibana, M., Sparman, M., Sritanaudomchai, H., Ma, H., Clepper, L., Woodward, J., Li, Y., Ramsey, C., Kolotushkina, O., and Mitalipov, S. (2009). Mitochondrial gene replacement in primate offspring and embryonic stem cells. Nature *461*, 367-372.

Tain, L.S., Mortiboys, H., Tao, R.N., Ziviani, E., Bandmann, O., and Whitworth, A.J. (2009). Rapamycin activation of 4E-BP prevents parkinsonian dopaminergic neuron loss. Nature Neuroscience *12*, 1129-1135.

Takahashi, K., Tanabe, K., Ohnuki, M., Narita, M., Ichisaka, T., Tomoda, K., and Yamanaka, S. (2007). Induction of pluripotent stem cells from adult human fibroblasts by defined factors. Cell *131*, 861-872.

Takahashi, K., and Yamanaka, S. (2006). Induction of pluripotent stem cells from mouse embryonic and adult fibroblast cultures by defined factors. Cell *126*, 663-676.

Taylor, S.M., and Jones, P.A. (1979). Multiple new phenotypes induced in 10T 1/2 and 3T3 cells treated with 5-azacytidine. Cell *17*, 771-779.

Tesar, P.J., Chenoweth, J.G., Brook, F.A., Davies, T.J., Evans, E.P., Mack, D.L., Gardner, R.L., and McKay, R.D. (2007). New cell lines from mouse epiblast share defining features with human embryonic stem cells. Nature *448*, 196-199.

Thomson, J.A., Itskovitz-Eldor, J., Shapiro, S.S., Waknitz, M.A., Swiergiel, J.J., Marshall, V.S., and Jones, J.M. (1998). Embryonic stem cell lines derived from human blastocysts. Science *282*, 1145-1147.

Thomson, J.A., Kalishman, J., Golos, T.G., Durning, M., Harris, C.P., Becker, R.A., and Hearn, J.P. (1995). Isolation of a primate embryonic stem cell line. Proc Natl Acad Sci U S A *92*, 7844-7848.

Timmons, S., Coakley, M.F., Moloney, A.M., and O' Neill, C. (2009). Akt signal transduction dysfunction in Parkinson's disease. Neuroscience letters *467*, 30-35.

Tissenbaum, H.A., and Guarente, L. (2001). Increased dosage of a sir-2 gene extends lifespan in Caenorhabditis elegans. Nature *410*, 227-230.

Tollervey, J.R., Wang, Z., Hortobagyi, T., Witten, J.T., Zarnack, K., Kayikci, M., Clark, T.A., Schweitzer, A.C., Rot, G., Curk, T.*, et al.* (2011). Analysis of alternative splicing associated with aging and neurodegeneration in the human brain. Genome Res *21*, 1572-1582.

Toth, J.I., Yang, S.H., Qiao, X., Beigneux, A.P., Gelb, M.H., Moulson, C.L., Miner, J.H., Young, S.G., and Fong, L.G. (2005). Blocking protein farnesyltransferase improves nuclear shape in fibroblasts from humans with progeroid syndromes. Proc Natl Acad Sci U S A *102*, 12873-12878.

Trifunovic, A., Wredenberg, A., Falkenberg, M., Spelbrink, J.N., Rovio, A.T., Bruder, C.E., Bohlooly, Y.M., Gidlof, S., Oldfors, A., Wibom, R.*, et al.* (2004). Premature ageing in mice expressing defective mitochondrial DNA polymerase. Nature *429*, 417-423.

Tsygankov, D., Liu, Y., Sanoff, H.K., Sharpless, N.E., and Elston, T.C. (2009). A quantitative model for age-dependent expression of the p16INK4a tumor suppressor. Proc Natl Acad Sci U S A *106*, 16562-16567.

Ungerstedt, U., Ljungberg, T., and Steg, G. (1974). Behavioral, physiological, and neurochemical changes after 6-hydroxydopamine-induced degeneration of the nigro-striatal dopamine neurons. Advances in neurology *5*, 421-426.

Unternaehrer, J.J., and Daley, G.Q. (2011). Induced pluripotent stem cells for modelling human diseases. Philosophical transactions of the Royal Society of London Series B, Biological sciences *366*, 2274-2285.

Valente, E.M., Abou-Sleiman, P.M., Caputo, V., Muqit, M.M., Harvey, K., Gispert, S., Ali, Z., Del Turco, D., Bentivoglio, A.R., Healy, D.G.*, et al.* (2004). Hereditary early-onset Parkinson's disease caused by mutations in PINK1. Science *304*, 1158-1160.

van der Putten, H., Wiederhold, K.H., Probst, A., Barbieri, S., Mistl, C., Danner, S., Kauffmann, S., Hofele, K., Spooren, W.P., Ruegg, M.A.*, et al.* (2000). Neuropathology in mice expressing human alpha-synuclein. J Neurosci *20*, 6021-6029.

Van Raamsdonk, J.M., and Hekimi, S. (2009). Deletion of the mitochondrial superoxide dismutase sod-2 extends lifespan in Caenorhabditis elegans. PLoS Genet *5*, e1000361.

Van Remmen, H., Ikeno, Y., Hamilton, M., Pahlavani, M., Wolf, N., Thorpe, S.R., Alderson, N.L., Baynes, J.W., Epstein, C.J., Huang, T.T.*, et al.* (2003). Life-long reduction in MnSOD activity results in increased DNA damage and higher incidence of cancer but does not accelerate aging. Physiological genomics *16*, 29-37.

Varela, I., Pereira, S., Ugalde, A.P., Navarro, C.L., Suárez, M.F., Cau, P., Cadiñanos, J., Osorio, F.G., Foray, N., Cobo, J.*, et al.* (2008). Combined treatment with statins and aminobisphosphonates extends longevity in a mouse model of human premature aging. Nature Medicine *14*, 767-772.

Venderova, K., and Park, D.S. (2012). Programmed Cell Death in Parkinson's Disease. Cold Spring Harbor Perspectives in Medicine *2*.

Verlinden, J. (1981). Identification of the human fibroblast surface glycoprotein (FSH) as aminopeptidase M. FEBS letters *123*, 287-290.

Villeponteau, B. (1997). The heterochromatin loss model of aging. Exp Gerontol *32*, 383-394.

Waddington, C.H. (1957). The strategy of the genes: a discussion of some aspects of theoretical biology (New York: Macmillan).

Warren, L., Manos, P.D., Ahfeldt, T., Loh, Y.-H., Li, H., Lau, F., Ebina, W., Mandal, P.K., Smith, Z.D., Meissner, A.*, et al.* (2010). Highly efficient reprogramming to pluripotency and directed differentiation of human cells with synthetic modified mRNA. Cell Stem Cell *7*, 618-630.

Welle, S., Brooks, A., and Thornton, C.A. (2001). Senescence-related changes in gene expression in muscle: similarities and differences between mice and men. Physiological genomics *5*, 67-73.

Whyte, D.B., Kirschmeier, P., Hockenberry, T.N., Nunez-Oliva, I., James, L., Catino, J.J., Bishop, W.R., and Pai, J.K. (1997). K- and N-Ras are geranylgeranylated in cells treated with farnesyl protein transferase inhibitors. J Biol Chem *272*, 14459-14464.

Wickham, H. (2009). ggplot2: elegant graphics for data analysis (Springer New York).

Wilkinson, J.E., Burmeister, L., Brooks, S.V., Chan, C.C., Friedline, S., Harrison, D.E., Hejtmancik, J.F., Nadon, N., Strong, R., Wood, L.K.*, et al.* (2012). Rapamycin slows aging in mice. Aging Cell *11*, 675-682.

Willadsen, S.M. (1986). Nuclear transplantation in sheep embryos. Nature *320*, 63-65.

Wilmut, I., Schnieke, A.E., McWhir, J., Kind, A.J., and Campbell, K.H. (1997). Viable offspring derived from fetal and adult mammalian cells. Nature *385*, 810-813.

Woltjen, K., Michael, I.P., Mohseni, P., Desai, R., Mileikovsky, M., Hamalainen, R., Cowling, R., Wang, W., Liu, P., Gertsenstein, M.*, et al.* (2009). piggyBac

transposition reprograms fibroblasts to induced pluripotent stem cells. Nature *458*, 766-770.

Wood, S.H., Craig, T., Li, Y., Merry, B., and de Magalhaes, J.P. (2013). Whole transcriptome sequencing of the aging rat brain reveals dynamic RNA changes in the dark matter of the genome. Age (Dordrecht, Netherlands) *35*, 763-776.

Wood, S.J., Wypych, J., Steavenson, S., Louis, J.C., Citron, M., and Biere, A.L. (1999). alpha-synuclein fibrillogenesis is nucleation-dependent. Implications for the pathogenesis of Parkinson's disease. J Biol Chem *274*, 19509-19512.

Yang, S.H., Bergo, M.O., Toth, J.I., Qiao, X., Hu, Y., Sandoval, S., Meta, M., Bendale, P., Gelb, M.H., Young, S.G.*, et al.* (2005). Blocking protein farnesyltransferase improves nuclear blebbing in mouse fibroblasts with a targeted Hutchinson-Gilford progeria syndrome mutation. Proc Natl Acad Sci U S A *102*, 10291-10296.

Ye, Z., Zhan, H., Mali, P., Dowey, S., Williams, D.M., Jang, Y.Y., Dang, C.V., Spivak, J.L., Moliterno, A.R., and Cheng, L. (2009). Human-induced pluripotent stem cells from blood cells of healthy donors and patients with acquired blood disorders. Blood *114*, 5473-5480.

Yonetani, M., Nonaka, T., Masuda, M., Inukai, Y., Oikawa, T., Hisanaga, S., and Hasegawa, M. (2009). Conversion of wild-type alpha-synuclein into mutant-type fibrils and its propagation in the presence of A30P mutant. J Biol Chem *284*, 7940-7950.

Yoshida, Y., Takahashi, K., Okita, K., Ichisaka, T., and Yamanaka, S. (2009). Hypoxia enhances the generation of induced pluripotent stem cells. In Cell Stem Cell, pp. 237-241.

Yu, J., Hu, K., Smuga-Otto, K., Tian, S., Stewart, R., Slukvin, II, and Thomson, J.A. (2009). Human induced pluripotent stem cells free of vector and transgene sequences. Science *324*, 797-801.

Yu, J., Vodyanik, M.A., Smuga-Otto, K., Antosiewicz-Bourget, J., Frane, J.L., Tian, S., Nie, J., Jonsdottir, G.A., Ruotti, V., Stewart, R.*, et al.* (2007). Induced pluripotent stem cell lines derived from human somatic cells. Science *318*, 1917-1920.

Zhang, J., Lian, Q., Zhu, G., Zhou, F., Sui, L., Tan, C., Mutalif, R.A., Navasankari, R., Zhang, Y., Tse, H.-F.*, et al.* (2011). A human iPSC model of Hutchinson Gilford Progeria reveals vascular smooth muscle and mesenchymal stem cell defects. Cell Stem Cell *8*, 31-45.

Zhang, Y., Ikeno, Y., Qi, W., Chaudhuri, A., Li, Y., Bokov, A., Thorpe, S.R., Baynes, J.W., Epstein, C., Richardson, A.*, et al.* (2009). Mice deficient in both Mn superoxide dismutase and glutathione peroxidase-1 have increased oxidative

damage and a greater incidence of pathology but no reduction in longevity. The journals of gerontology Series A, Biological sciences and medical sciences *64*, 1212-1220.

Zhang, Y.M., Hartzell, C., Narlow, M., and Dudley, S.C., Jr. (2002). Stem cell-derived cardiomyocytes demonstrate arrhythmic potential. Circulation *106*, 1294-1299.

Zhu, S., Li, W., Zhou, H., Wei, W., Ambasudhan, R., Lin, T., Kim, J., Zhang, K., and Ding, S. (2010). Reprogramming of human primary somatic cells by OCT4 and chemical compounds. Cell Stem Cell *7*, 651-655.

Zimprich, A., Biskup, S., Leitner, P., Lichtner, P., Farrer, M., Lincoln, S., Kachergus, J., Hulihan, M., Uitti, R.J., Calne, D.B.*, et al.* (2004). Mutations in LRRK2 cause autosomal-dominant parkinsonism with pleomorphic pathology. Neuron *44*, 601-607.

Zou, J., Maeder, M.L., Mali, P., Pruett-Miller, S.M., Thibodeau-Beganny, S., Chou, B.K., Chen, G., Ye, Z., Park, I.H., Daley, G.Q.*, et al.* (2009). Gene targeting of a disease-related gene in human induced pluripotent stem and embryonic stem cells. Cell Stem Cell *5*, 97-110.

Zwi, L., Caspi, O., Arbel, G., Huber, I., Gepstein, A., Park, I.H., and Gepstein, L. (2009). Cardiomyocyte differentiation of human induced pluripotent stem cells. Circulation *120*, 1513-1523.